TECHNISCHE UNIVERSITÄT DRESDEN

Analysis of Bacterial Communities Using Droplets Based Millifluidics

Dissertation
zur Erlangung des wissenschaftlichen Grades
Doktoringenieur

vorgelegt von

Xinne Zhao
geboren am 19. August 1990 in Luoyang, China

Institut für Werkstoffwissenschaft
Lehrstuhl Materialwissenschaft und Nanotechnik
Fakultät Maschinenwesen
Technische Universität Dresden
2021

Gutachter: Herr Prof. Dr. G. Cuniberti
Herr Prof. Dr.-Ing. A. Richter
Herr Prof. Dr. rer. medic. H.-P. Wiesmann
Eingereicht am 10.08.2021
Verteidigt am 08.02.2022

Erklärung

a) Hiermit versichere ich, dass ich die vorliegende Arbeit ohne unzulässige Hilfe Dritter und ohne Benutzung anderer als der angegebenen Hilfsmittel angefertigt habe; die aus fremden Quellen direkt oder indirekt übernommenen Gedanken sind als solche kenntlich gemacht.

b) Bei der Auswahl und Auswertung des Materials sowie bei der Herstellung des Manuskripts habe ich Unterstützungsleistungen von folgenden Personen erhalten:

Rico Illing: LabView-Programmcode des Mikrofluidikgeräts (Unterkaptiel 3.4.4)

Tao Huang: Mikroskopie zur Bakterienbeobachtung (Unterkaptiel 3.3.2)

Bergoi Ibarlucea: Betriebsspezifikationen für die Bakterienkultur (Unterkaptiel 3.3.1)

Philip Ruelens: Bakterielle genetische Veränderung und theoretische Anleitung (Unterkaptiel 3.1.1, 5.6 und 6.6)

J. Arjan G. M. de Visser: Anleitung zur Mikrobiologietheorie (Unterkaptiel 4.4, 5.3, und 6.2)

Weitere Personen waren an der geistigen Herstellung der vorliegenden Arbeit nicht beteiligt. Insbesondere habe ich nicht die Hilfe eines kommerziellen Promotionsberaters in Anspruch genommen. Dritte haben von mir keine geldwerten Leistungen für Arbeiten erhalten, die in Zusammenhang mit dem Inhalt der vorgelegten Dissertation stehen.

c) Die Arbeit wurde bisher weder im Inland noch im Ausland in gleicher oder ähnlicher Form einer anderen Prüfungsbehörde vorgelegt und ist auch noch nicht veröffentlicht worden.

d) Diese Promotionsordnung der Fakultät Maschinenwesen an der TU Dresden vom 01.07.2001 wird anerkannt

Abstract

Microbes typically form highly complex and diverse communities that account for a significant portion of life's genetic diversity. Analysis of living systems, *e.g.* bacterial or cell population, plays a significant role in detecting and identifying pathogens, testing antibiotic susceptibility, and the fundamental research of population diversity and evolution. This work focuses on the analysis of bacterial communities using droplets based millifluidics. To monitor the bacteria growth, we designed an optofluidic system, combining the encapsulation of bacteria in numerous emulsion droplets to monitor their long-term behavior and relationship in a co-culture environment using fluorescent signals.

In the first part of this work, we co-encapsulated and cultured two isogenic strains of *Escherichia coli* (*E. coli*) in numerous emulsion droplets to reveal their competition and cooperation relationship. Since two strains of *E. coli* express blue and yellow fluorescent proteins (BFP and YFP, respectively), we quantified their growth by integrating a fluorescence detection system. We analyzed the following parameters: doubling time, population yield, final biomass ratio, correlation map of doubling time and competition coefficient to characterize and compare the bacterial growth kinetics and behavior in mono and co-cultures. In addition, the experimental observations were compared with the predictions from a single growth model.

Finally, we employed the millifluidic device to verify the appearance of cross-protection between antibiotic-sensitive bacteria and antibiotic-resistant bacteria. It is one of the mechanisms by which different bacteria, sharing the same environment, protect each other to survive in the presence of antibiotics. For this purpose, the *E.coli* YFP strain was chosen as an antibiotic-sensitive group. Simultaneously, the *E.coli* BFP strain with β-lactam and its mutations were selected as resistant strains. Combining the millifluidic droplet reactor method with other detection strategies, *e.g.* fluorescence microscopy, fluorescence flow cytometry, and plate reader, we proved the appearance of cross-protection by detecting the filamentary cells, the fluorescence of cell-free media, viable cell rates, cell shape and size, as well as β-lactamase activity.

All these results obtained by millifluidic devices proved that this strategy could be used in a high-throughput bacterial coexistence study. In addition, the research of these general fields, such as bacterial community and antibiotic impact, can help us to reveal the

interaction between microbial species and determine the right dose of antibiotics to inhibit bacterial growth in a co-existent environment efficiently.

Kurzfassung

Mikroben bilden in der Regel hochkomplexe und vielfältige Gemeinschaften, die einen erheblichen Teil der genetischen Vielfalt des Lebens ausmachen. Die Analyse lebender Systeme, z. B. von Bakterien- oder Zellpopulationen, spielt eine wichtige Rolle beim Nachweis und bei der Identifizierung von Krankheitserregern, bei der Prüfung der Empfindlichkeit gegenüber Antibiotika und bei der grundlegenden Erforschung von Populationsvielfalt und Evolution. Diese Arbeit konzentriert sich auf die Analyse bakterieller Gemeinschaften mit Hilfe von Tröpfchen-basierter Millifluidik. Zur Überwachung des Bakterienwachstums haben wir ein optofluidisches System entwickelt, das die Verkapselung von Bakterien in zahlreichen Emulsionströpfchen kombiniert, um ihr langfristiges Verhalten und ihre Beziehung in einer Co-Kultur-Umgebung mithilfe von Fluoreszenzsignalen zu überwachen.

Im ersten Teil dieser Arbeit haben wir zwei isogene Stämme von *Escherichia coli* (*E. coli*) in zahlreichen Emulsionströpfchen co-verkapselt und kultiviert, um ihre Konkurrenz- und Kooperationsbeziehung aufzudecken. Da zwei Stämme von *E. coli* blaue und gelbe Fluoreszenzproteine (BFP bzw. YFP) exprimieren, quantifizierten wir ihr Wachstum durch die Integration eines Fluoreszenz-Detektionssystems. Wir analysierten die folgenden Parameter: Verdopplungszeit, Populationsausbeute, endgültiges Biomasse-Verhältnis, Korrelationskarte der Verdopplungszeit und Konkurrenzkoeffizient, um die bakterielle Wachstumskinetik und das Verhalten in Mono- und Co-Kultur zu charakterisieren und zu vergleichen. Außerdem wurden die experimentellen Beobachtungen mit den Vorhersagen eines einzelnen Wachstumsmodells verglichen.

Schließlich setzten wir das Millifluidik-Gerät ein, um das Auftreten eines Kreuzschutzes zwischen antibiotikaempfindlichen Bakterien und antibiotikaresistenten Bakterien zu überprüfen. Dies ist einer der Mechanismen, durch den verschiedene Bakterien, die sich die gleiche Umgebung teilen, sich gegenseitig schützen, um in Gegenwart von Antibiotika zu überleben. Zu diesem Zweck wurde der *E.coli* YFP-Stamm als antibiotikaempfindliche Gruppe ausgewählt. Gleichzeitig wurden der *E.coli* BFP-Stamm mit β-Lactam und dessen Mutationen als resistente Stämme ausgewählt. In Kombination mit anderen Nachweisstrategien, zum Beispiel Fluoreszenzmikroskopie, Fluoreszenz-Durchflusszytometrie und Plattenlesegerät, wiesen wir das Auftreten des Kreuzschutzes nach, indem wir die filamentären Zellen, die Fluoreszenz des zellfreien Mediums, die Raten lebensfähiger Zellen, die Zellform und -größe sowie die β-Lactamase-Aktivität

nachwiesen.

All diese Ergebnisse, die mit Millifluidik-Geräten erzielt wurden, bewiesen, dass diese Strategie in einer Hochdurchsatzstudie zur bakteriellen Koexistenz eingesetzt werden kann. Außerdem kann die Erforschung dieser allgemeinen Bereiche, wie bakterielle Gemeinschaft und Antibiotikawirkung, uns helfen, die Interaktion zwischen mikrobiellen Spezies aufzudecken und die richtige Dosis des Antibiotika zu bestimmen, um das bakterielle Wachstum in einer koexistenten Umgebung effizient zu hemmen.

Content

Table of Figures

List of Tables

Abbreviations

E. coli	*Escherichia coli*
BFP	Blue fluorescence protein
YFP	Yellow fluorescence protein
LOD	Limit of detection
HFE	Hydrofluoroether
PMT	Photomultiplier tube
FEP	Fluorinated ethylene propylene
MIC	Minimum inhibitory concentration
3D	Three dimensional
2D	Two dimensional
PBS	Phosphate buffered saline
LED	Light-emitting diode
MFDA	Multiple Fluorescence Droplet Analyzer
FDA	Fluorescence Droplet Analyzer
CTX	Cefotaxime solium salt
IPTG	Isopropyl β-D-thiogalactoside
OD_{600}	Optical density at a wavelength of 600 nm
OD_{490}	Optical density at a wavelength of 490 nm
LB broth	Luria-Bertani broth
FSC	Forward scatter
SSC	Side scatter
Galk	Galactokinase
DMSO	Dimethyl sulfoxide
DAQ	Devices data acquisition
FLP	Flippase
rpm	Revolutions per minute

List of Symbols

Millifluidic device

Droplet

V	The volume of a droplet
D	The diameter of a droplet
L	The length of a droplet

Cell number calculation

N	Cell number
C	Cell concentration or cell density
T	Time
a	The point a on log scale cell numbers-time growth curve
b	The point b on log scale cell numbers-time growth curve
c	The slope of calibration curves for FAD
d	The intercept of calibration curves for FAD
τ	Doubling time

Bacteria coexistence

General

Cmax	the maximum cell density
B_0	the initial cell density of *E. coli* BFP
B_1	the final cell density of *E. coli* BFP
Y_0	the initial cell density of *E. coli* YFP
Y_1	the final cell density of *E. coli* YFP
R_0	the ratio between initial cell density of *E. coli* BFP B_0 and *E. coli* YFP Y_0
R_1	the ratio between final cell density of *E. coli* BFP B_1 and *E. coli* YFP Y_1
C_{by}	the effect of *E. coli* BFP on *E. coli* YFP
C_{yb}	the effect of *E. coli* YFP on *E. coli* BFP
N_b	Cell number of *E. coli* BFP after incubating for few hours
N_y	Cell number of *E. coli* YFP after incubating for few hours
N(t)	the cell number at time point t
N_0	the initial cell number
r	the initial per capita growth rate
K	the maximum cell number

ν	the deceleration parameter

1 Introduction

1.1 Motivation

Understanding the functions and dynamics of microbial communities and their competition or cooperation is crucial for human survival and health.[1-4] The human microbiome is made up of approximately 100 trillion cells, 99% of which are bacteria.[5, 6] For example, there are up to 400 species of beneficial, harmful, and neutral bacteria that coexist in the human gut; their balance has a direct impact on the host's health.[7] Recently studies show this balance can not only interact with mood but also affect the cancer treatment.[8, 9] Competition for the limited factors necessary for microbial life, such as space and food, has led to natural selection.[10, 11] Nevertheless, competition does not lead to biodiversity loss, as the co-benefits obtained through cooperation also promote long-term coexistence.[12]

In particular, bacterial infections caused by harmful strains of bacteria are one of the conditions in which microorganisms coexist on or in the human body and have been a major cause of disease throughout human history. It was expected that the introduction of antibiotics would solve this problem. However, the non-targeted bactericidal effect of antibiotics on bacterial cells can also kill beneficial and neutral bacteria. In addition, the misuse and abuse of antibiotics have led to the survival of bacteria that have evolved and mutated to have antibiotic genes. This has led to a significant reduction in the effectiveness of antibiotics, which has caused a global crisis. In addition, antimicrobial resistance also causes deaths; for example, in 2019, antimicrobial resistance caused 4.95 million deaths, more than the number of deaths from HIV/AIDS or malaria.[13, 14] Therefore, understanding the relationship between coexisting bacterial strains might help us reveal antibiotic effects to the bacterial coexistence system and determine the right dose of antibiotic to use, which is critical to our health.[15]

1.2 State of the Art

To better understand the complex microbial communities, it is especially important to address the question of what factors influence microbial coexistence.[16, 17] To answer the question, it is necessary to create a model that can: monitor each member of the community over time, precisely tune and control the microenvironment, and offer informative parameters (such as growth rate, duration of the lag phase, and final population) for analysis.[18]

1 Introduction

Cellular and microbial co-culture systems have been put forward for a long time.[19-21] Bacterial coexistence is usually investigated in solid or well-mixed liquid environments.[22] In solid cultures, bacteria occupy and grow in different areas, making it easier to extract and count colonies of co-cultured strains; however, direct interaction between bacteria is limited.[23-26] For example, in the study by Fenn *et al.* slow-growing colonies and faster-growing bacteria were co-cultured on agar plates to investigate the dependence between two adjacent strains.[27] By observing the colonies formed on the agar, the different strains could be easily identified. However, this method still makes it difficult to monitor the growth dynamics of individual strains. In a well-mixed liquid co-culture environment, bacterial strains coexist in homogeneous media conditions. Besides, liquid environments, such as Fluidic fluidic systems may better reflect the natural environment in which bacteria coexist in the body, such as the digestive system.[28, 29] However, co-culturing microbiota in a liquid environment poses challenges to differentiating and monitoring the kinetics of two or more strains simultaneously and high throughput quantitative analysis.[30] Thus, to facilitate monitoring of the individual growth dynamics of coexisting strains, membranes and barriers are often required to physically separate bacterial strains. For example, Moutinho *et al*. designed culture wells with vertical membranes (separate different strains) and transparent bottoms that allow monitoring bacterial growth by detecting the optical density at 600 nm wavelength.[31] Furthermore, in Osmekhina's group, they tried to co-culture bacterial strains in a microfluidic structure in which the bacteria strains are separated by a nanofabricated cellulose filter in different trapping chambers. In these cases, instead of directly mixing the bacteria in a co-culture environment, the membranes or filters are introduced to separate the bacterial strains and only the conditioned media are exchanged.[32] Co-culture of bacterial strains by diffusion of metabolites is a clever approach, but the direct interactions of neighboring bacteria in a coexisting environment remain uninvestigated.

An effective differentiation method is to genetically modify bacterial strains with an inherited fluorescent reporter and efficiently monitor the kinetics of different strains co-cultured in a liquid environment by fluorescence microscopy or fluorescence flow cytometry.[33-35] Guo[36] and Terekhov[37], for example, used fluorescent microscopy to successfully monitor the division of two co-culture bacterial strains by detecting unique fluorescent proteins expressed within each strain. However, data collection and analysis require a considerable amount of work. In addition, the low resolution of frequency data introduces analytical errors. In contrast, millifluidic methods can be more effective in

tracking bacterial interactions in near real-time. It can be used in practical applications to simulate a more realistic environment, such as predicting bacterial response to antibiotics; however, it has been used primarily for single bacterial strain monitoring so far.[38-40] For example, Cottinet *et al.* designed a drop-based millifluidic system to detect heritable phenotypic changes in evolving bacterial populations.[38] Baraban *et al.* proposed a novel millifluidic droplet analyzer for precisely monitoring the dynamics of microbial populations in an antibiotic environment.[39] Moreover, Illing *et al.* demonstrated a droplets-based millifluidic tool for isolating and longtime monitoring of single bacterial cells in water-in-oil emulsion droplets.[40]

1.3 Structure of this Thesis

The main aim of this work focuses on studying bacterial growth behavior in a complex environment. It includes two main challenges: first, high-throughput and parallel monitoring of the growth kinetics of bacterial strains' coexistence; second, revealing the bacterial interaction between coexistent strains influenced by antibiotics. To achieve these goals, a millifluidic droplets reactor system is first designed and assembled to monitor the growth of different bacterial strains (expressing different colors of fluorescent protein) by tracking their fluorescence signals, which combines the theoretical basis of microfluidic techniques and optical sensors. It achieves automatic monitoring of two fluorescence signals in near real-time and long-term (up to several days). The thesis consists of seven chapters which address the following:

The first chapter serves as an introduction.

In the 2nd Chapter, the concept of microfluidics and millifluidics are introduced and the differences between them laid out. Then, the theoretical background for this work, including bacterial coexistence and bacterial antibiotic resistance, is discussed.

The 3rd Chapter overviews the bacterial strains, materials and chemicals used in this work. Moreover, the experimental protocols and methods are introduced.

The 4th Chapter covers the millifluidic device setup. Four systems of the device are assembled in a black box, including a fluidic system, electricity system, optical sensors system and software control system. The stability of the device is also discussed in this chapter.

The 5th chapter demonstrates the results of the coexistence of two bacterial strains in millifluidic droplet-based reactors. The coexistence of two *Escherichia coli* strains was

monitored by reading their fluorescence signal in two parallel detector channels. These two strains were co-cultured in various inoculum ratios R_0 (ranging from 10^{-3} up to 10^3). By adjusting R_0, the doubling time, lag phase duration, competition coefficients, and final biomass ratio was detected and analyzed. Besides, the experimental results were further compared to the predicted modeling results.

The 6th chapter covers the research of co-culture antibiotic-sensitive and -resistant bacteria to reveal their interaction. In this part, the millifluidic droplet reactor was used to track the survival status of co-cultured sensitive and resistant strains in an antibiotic environment. *E. coli* YFP strain was chosen as an antibiotic-sensitive group, which produces yellow fluorescent protein during growing. Simultaneously, *E. coli* BFP strain produces the blue fluorescent protein and is resistant to antibiotics. Two strains of bacterial growth status were tracked by detecting the change of fluorescence intensity. Moreover, to reveal the role of cross-protection, the initial population ratio of two bacterial strains was set as a constant 1000:1000. By tuning the antibiotic dosage, the cell state such as cell density, viable rates, filamentary cell, cell-free media fluorescence, cell shape and β-lactamase activity of coexistence bacteria and monoculture bacteria were researched and compared in detail.

The 7th Chapter summarizes the main results and accomplishments of the thesis. The conclusions and outlook of this work are also discussed in this chapter.

2 Fundamentals

The fundamental background and the methodology mentioned and used in this study are presented in this chapter. At the beginning, the concept of millifluidics is explained and compared to the microfluidic approach. Next, the study of bacterial growth based on the millifluidic approach is discussed. This strategy is further described in the bacterial co-culture study, and it is compared to the other methods used to study microbial coexistence environments. Next, a more complex bacterial coexistence environment with antibiotics is described. Different types of antibiotics are classified and briefly introduced, followed by a brief statement and definition of antibiotic resistance. Besides, different mechanisms of microbial antibiotic resistance are also listed, especially the β-lactam resistant bacteria. Finally, the detection methods of microbial resistance by measuring the minimum inhibitory concentrations (MICs) and β-lactamase activity are briefly introduced.

2.1 Microfluidics and Millifluidics

2.1.1 Concept

Microfluidic technology is a system for manipulating and processing small amounts of fluids (10^{-9}-10^{-18} L) in order to regulate chemical, biological, and physical processes that are important in sensing.[41-46] This approach has made far-reaching progress for the last two decades, allowing integration with electronic and optical elements necessary for the production of an operational sensor using lithographic techniques.[47-49]

Compared to microfluidics, millifluidics have a larger volume of fluid (approximately 100 nL) but contain most of the advantages of microfluidics.[50] In particular, instead of fabricating the channels and chambers with complex lithographic strategies, the millifluidic system uses tubings or 3D printed structures to store and transfer fluidics.[51, 52] It makes the manufacture much easier, as well as having a lower cost.[53] Moreover, Due to the larger fluidic volumes (~ 100 nL), millifluidics can comprehensively track the microbial growth dynamic, which is tough for microfluidics. Furthermore, problems related to clogging due to sediment formation in microfluidics are greatly alleviated in millifluidics.[52] The comparison of these two strategies is summarized in **Table 1**. It shows the advantages of using millifluidics in monitoring microbial growth.

Table 1: Comparison of microfluidics and millifluidics.

Strategy	Microfluidics	Millifluidics

Fluidics volume	100 pL ~ 1 nL	~ 100 nL
Fluidics transfer and store	lithographic channels	tubings (easy handle)
Microbes culture	low growth dynamic	inoculum can be adjusted
Sediment clog	typical problem	greatly mitigated
Cost	expensive	inexpensive

2.1.2 Droplet-Based Millifluidics

Due to the small fluidic size, microfluidics and millifluidics may have different surface tension, energy dissipation and fluid resistance than macroscopic fluidics.[54, 55] In this case, turbulence hardly occurs due to the very low Reynolds number.[56, 57] The laminar-dominated flow makes it impossible for the two added fluids to mix easily by turbulence and thus form droplets.[58]

To generate the droplets in the millifluidic system, a dispersed phase solution and a continuous phase liquid are injected into a Cross-junction, T-junction or Y-junction (shown in **Figure 1**).[59-61] The varieties of droplets include oil-in-water droplets, water-in-oil droplets, and droplets-within-droplets, depending on the two phases of immiscible solutions and the surface features of the channel or tubings.[62, 63]

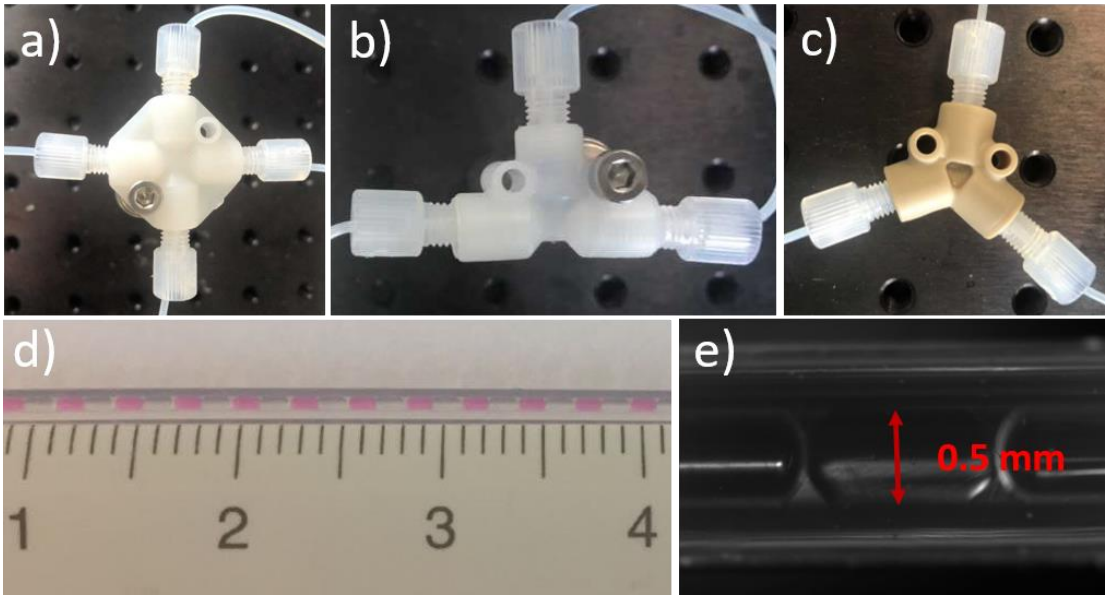

Figure 1: Junctions and generated droplets: **a)** Cross-junction, **b)** T-junction, **c)** Y-junction, **d)** droplets in tubing observed by camera and, **e)** droplets in tubing observed by microscope (tubing with inner diameter of 0.5 mm).

2.1.3 Bacterial Culture in Droplet Reactor

Traditional methods to study the microbial growth dynamic contain solid media cultivation and liquid media acculturation.[64] The bacterial culture on an agar plate is one of the most common culture ways; it allows isolating cells that form colonies under selected media such as biocide agents; however, the inhomogeneous limits its applications.[65-67] Liquid media cultivation plays an important role in microbial cultures because of its homogeneous culture conditions and inexpensive setup.[68] It is used for amplifying the microbial population from a single-cell level to a larger size but can only monitor the mean parameters of microbial growth behavior.[69] Later, the cultivation miniaturization, for example, micro-wells, becomes more and more popular because of its high throughput, efficiency, and automatization.[70-72] However, its limitations are also obvious, for example, the evaporation on the media surface. As one of the microbial diversity study instruments, a flow cytometer allows detecting bacteria at a single-cell level but is limited by kinetic monitoring.[73]

Millifluidics has been considered a combination of micro-well and flow cytometer technologies, especially in applications in the field of microbiology.[50] Droplet-based millifluidic can serve as droplet bioreactors, allowing analysis and sorting phenotypic diversity among microbes.[74] Compared to microfluidics, the excellent reproducible growth conditions on the droplets sequence provided by millifluidic droplet bioreactors allow high-throughput and sensitive readout of colonies over time.[75] Besides, thanks to the excellent analytical and processing capabilities of millifluidic droplet technology, it has been successfully used in several research fields, such as monitoring chemical reactions, synthesizing polymer or metallic particles and analyzing and classifying microorganisms.[39, 40, 76-78]

2.2 Bacterial Coexistence

Many microbial functions are carried out within communities of interacting species.[79] For instance, microbial interacting functions can affect ecosystems through matter's cycling and influence human health by helping to digest food or by causing infections.[80] The study of microbial coexistence is essentially the study of their interactions. In order to study bacterial interactions, it is crucial to understand the bacterial growth behavior of interacting strains in monocultures and co-cultures. As shown in **Figure 2**, monoculture means incubating and monitoring one strain of bacteria growth (cell number N changes with culture time T), and co-culture indicates culturing at least two different bacterial strains in the same environment and monitor their growth separately.

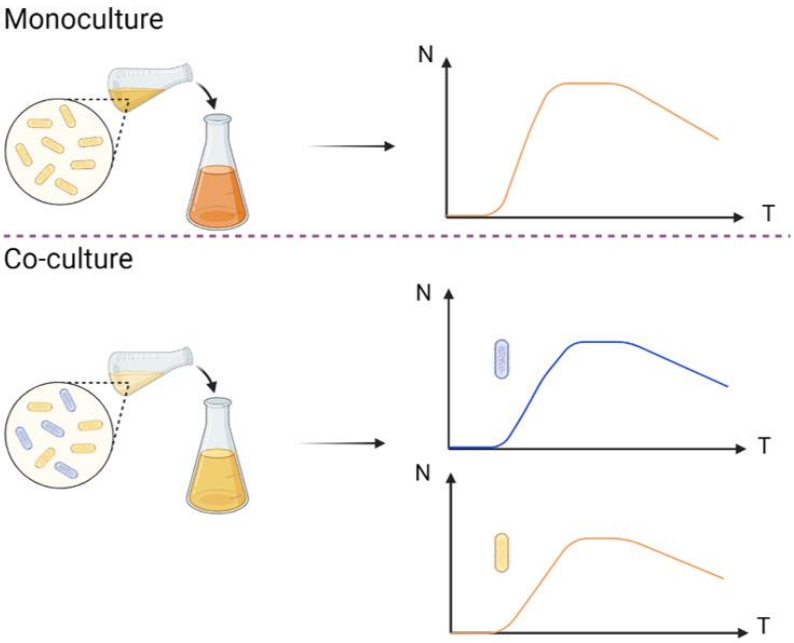

Figure 2: Monoculture and co-culture of bacteria.

2.2.1 Ideal Microbial Growth Model

According to the bacterial growth model investigated by J. Monod, the classical bacterial growth curve contains four phases: lag phase, exponential phase, stationary phase and death phase.[81] Each phase represents a different state of bacterial growth, as shown in **Figure 3**.

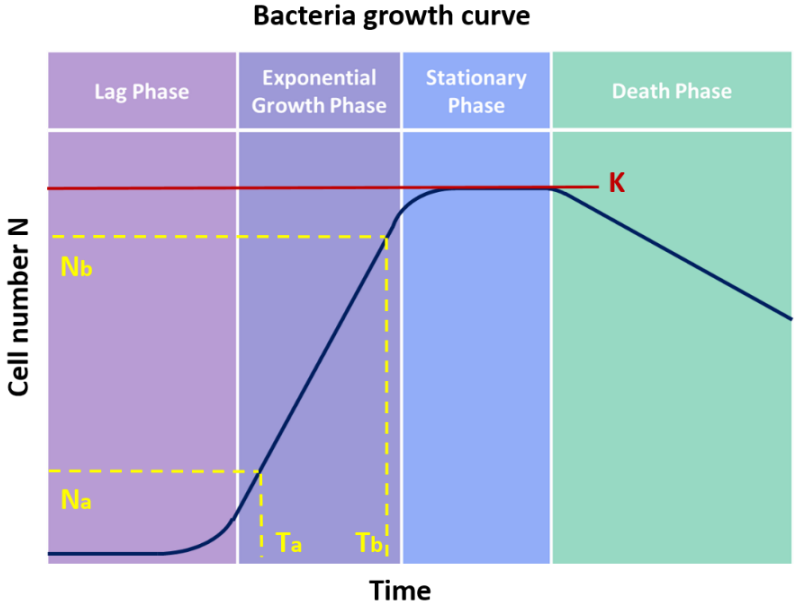

Figure 3: The growth model of bacteria cultures described by J. Monod.

In the lag phase, bacteria need time to adapt to the new environment, and therefore their cell numbers do not change.[82] Afterwards, bacteria start to divide and proliferate in the exponential phase, and their growth rate reaches the maximum, which follows **Equation**

1.[83] In the following stationary phase, the division rate equals the death rate, and the cell number stays at the same level *K*. Later, as the resources in the environment are almost used up, the bacteria growth reaches the death phase.[84]

$$Growth\ rate = \frac{log_2 N_b - log_2 N_a}{T_b - T_a} \quad (1)$$

Where *N* is the cell number, *T* is the time point, and *a* and *b* present the points on the log scale cell number-time growth curve.

2.2.2 Microbial Growth Model for Monoculture and Co-culture in Real Conditions

Due to the limited resources and space in bacterial cultures, the growth rate of microbes during the exponential phase also declines in real cases. Therefore, the ideal model of Monod's growth needs a correction factor. The monoculture model of Baranyi-Robert model[85] (shown in **Equation 2** and **Equation 3**) contains parameter *γ,* which describes the transition rate from fast growth to slow growth.[86] It is widely used for predicting bacterial growth.

$$\frac{dN}{dt} = rN\left(1 - \left(\frac{N}{K}\right)^{\gamma}\right) \quad (2)$$

$$N(t) = \frac{K}{\left(1 - \left(1 - \frac{K}{N_0})^{\gamma}\right) e^{-r\gamma t}\right)^{1/\gamma}} \quad (3)$$

Where *N(t)* is the cell number at time point *t*, N_0 is the initial cell number, *K* is the maximum cell number, *r* is the initial per capita growth rate, and *γ* is a deceleration parameter, which describes the transition rate from fast growth to slow growth.

Bacteria are mostly coexistent with other strains in microbial communities, so the co-culture is the most common case in real conditions. Compared to the monoculture, in the co-culture model, competition factors are considered in the system as shown in 2-strain Lotka–Volterra competition models[87] (shown as **Equation 4-6**).

$$\frac{dN_1}{dt} = r_1 N_1\left(1 - \frac{{N_1}^{\gamma_1}}{{K_1}^{\gamma_1}} - c_2 \cdot \frac{{N_2}^{\gamma_2}}{{K_1}^{\gamma_1}}\right) \quad (4)$$

$$\frac{dN_2}{dt} = r_2 N_2\left(1 - c_1 \cdot \frac{{N_1}^{\gamma_1}}{{K_2}^{\gamma_2}} - \frac{{N_2}^{\gamma_2}}{{K_2}^{\gamma_2}}\right) \quad (5)$$

$$N = N_1 + N_2 \quad (6)$$

Where c_1 and c_2 are the competition factors that can be calculated based on the above equations and experimental data.

2.3 Bacterial Antibiotic Resistance

Since the bacterial communities can impact food digestion or cause bacterial infections of its host, control the balance of the interaction between microbial species will directly influence human health.[79] Using antibiotics can efficiently reduce bacterial infection and influence the balance between microbial interactions and host.[88] In the last several decades, antibiotics have been used in clinical treatment and achieved modern medical procedures, such as cancer treatment and organ transplants.[89, 90] However, abuse of antibiotics has also become a global issue.[91] The rapid rise of antimicrobial resistance means that some infections cannot be effectively treated nowadays.[92, 93] Understanding the effect of antibiotics and antibiotic-resistant pathways could help solve and avoid misuse of antibiotics.

2.3.1 Antibiotics

Antibiotics were first found and obtained from antibiotic-producing microbes and broadly used to treat open wounds in ancient times.[92, 94] Microbes that produce antibiotics aim to kill competitors and predators or inhibit their growth and are nowadays used to extract and purify antibiotics. According to the different ways that affect the bacterial cell, antibiotics are classified into four groups (as shown in **Appendix Figure S1**): i) inhibit RNA synthesis, ii) disrupt cell wall synthesis, iii) inhibit protein synthesis, and iv) inhibit DNA replication.[95, 96] Moreover, according to the chemical structures, antibiotics can also be classified into seven major groups, including β-lactams (cell wall synthesis), aminoglycosides (protein synthesis), macrolides (protein synthesis), tetracyclines (protein synthesis), daptomycin (cell membrane function), platensimycin (fatty acid biosynthesis), glycopeptides (cell wall synthesis).[97, 98]

Antibiotics have transformed medicine and saved millions of lives. However, the rapid emergence of antibiotic-resistant bacteria is a world crisis threatening the efficacy of antibiotics worldwide. Antibiotic resistance occurs mainly due to the misuse of antibiotics. It drives the evolution of resistance, antibiotic-resistant genes can spontaneously occur through mutation and can be transferred to relatives or even among different species.[99]

Among different types of antibiotics, penicillin which belongs to β-lactam was the first discovered antibiotic to cure diseases by killing or injuring bacteria. β-lactam antibiotic

agents contain a β-lactam ring in their molecular structure (as shown in **Appendix Figure S2**)[100], which works by inhibiting cell wall biosynthesis in the bacterial organism, thus inhibiting bacteria survival or growth.[101]

2.3.2 Antibiotic Resistance

Targeting the mechanisms of antibiotics, antibiotic resistance also concludes four groups (as shown in **Appendix Figure S3**): efflux pumps to pump antibiotics outside the cell wall, target gene-product modifications, produce enzymatic to inactivate the antibiotic compound and natural resistance due to an impermeable membrane or lack of a target.[15] Many of the processes are shared by different pathogen species and spread through lateral gene transfer.[102, 103] Notably, cross-protection has also recently been proven to be one of the antibiotic resistance mechanisms. In this mechanism, different bacteria share that the same environment, protect each other to survive in the presence of antibiotics; therefore, the antibiotic-resistant microbes help antibiotic-sensitive species survive to keep the species diversity.[104]

For example, β-lactamase is an important enzyme produced by bacteria, which plays a crucial role in the resistance of β-lactam antibiotics by breaking down the β-lactam ring structure.[105-107] Testing the β-lactamase activity in bacterial culture can reveal the kinetics of enzymatic activity released by bacteria.[108] For instance, nitrocefin assay is the most common method to detect the β-lactamase activity. It serves as a chromogenic β-lactamase substrate that undergoes distinctive color change (from yellow to red) as the amide bond in the β-lactam ring is hydrolyzed by β-lactamase.[109, 110]

Although different antibiotics inhibit bacterial cell growth in different ways, effective methods for confirming resistance that diagnostic laboratories use are primarily based on testing for MICs.[111] MIC is the lowest concentration at which an antimicrobial agent (*e.g.* antifungal, antibiotic, or bacteriostatic) suppresses the observable growth of a microbe after overnight incubation.[112]

3. Materials and Methods

This chapter dedicates the techniques and protocols for bacterial storage, cultivation, detection, and analysis. Firstly, the detailed information of bacterial strains used in this work is listed, followed by an overview of the chemicals. After showing the materials used in experiments and for assembling the millifluidic device, bacteria storage and cultivation protocols with and without adding antibiotics are introduced separately. The various bacterial detection methods such as Biophotometer OD_{600}, fluorescence microscopy (Axiovert 200M, Carl Zeiss), plate reader (Cytation 5, Biotek), fluorescence flow cytometry (Attune NxT, Thermo Fisher), and millifluidic droplet-based reactors are explained. Finally, the methods and protocols for detecting the pH of bacterial media, MIC of antibiotics, the fluorescence intensity in cell-free media, viable cell rates and β-lactamase activity are presented.

3.1 General

3.1.1 Bacterial Strains

Table 2: Bacterial strains used in this work and their gene sequences.

Type	Strain	Gene
antibiotic -sensitive	*E. coli* BFP	MG1655 galK::mTagBFP2-FRT
	E. coli YFP	MG1655 galK::SYFP2-FRT
antibiotic -resistant	*E. coli* BFP 1	MG1655 GALK FLP BFP TEM1
	E. coli BFP 2	MG1655 GALK FLP BFP TEM1 M182T
	E. coli BFP 3	MG1655 GALK FLP BFP TEM1 E104K
	E. coli BFP 4	MG1655 GALK FLP BFP TEM1 G238S
	E. coli BFP 5	MG1655 GALK FLP BFP TEM1 E104K M182
	E. coli BFP 6	MG1655 GALK FLP BFP TEM1 E104K G238S
	E. coli BFP 7	MG1655 GALK FLP BFP TEM1 M182T G238S
	E. coli BFP 8	MG1655 GALK FLP BFP TEM1 E104K M182T G238S

Table 2 shows all the *E. coli* strains used in this work. All these *E. coli* strains are provided by Department of Genetics of Wageningen University in the Netherlands). For the antibiotic-sensitive strains, the *E. coli* YFP and *E. coli* BFP strains were constructed by inserting the fluorescent expression cassette, *cat-J23101-SYFP2* (GenBank accession number: KM018300) or *cat-J23101-mTagBFP2* (GenBank accession number: KM018299), into *galK of E. coli MG1655* using the λ red recombineering system as

described in Datsenko et al.[113] They were modified to possess a chromosomal SYFP2 gene or chromosomal mTagBFP2 gene but not through plasmid to avoid the possibility of gene transfer between different bacterial strains. The chloramphenicol (cat) marker was removed after chromosomal integration using FLP (flippase) recombinase. Both fluorescent proteins are expressed from the constitutive promoter, *J23101*.[114]

For the antibiotic-resistant strains, MG1655[115] represents the strain chosen of a wild-type laboratory strain of *E. coli K-12*, which has little genetic manipulation. Galactokinase (GalK) catalyzes the first step in the Leloir pathway of galactose metabolism FLP protein, much like Cre, is a tyrosine family site-specific recombinase, which causes the recombination of two separate strands of DNA.[116] BFP is the Blue fluorescent protein. TEM1 is the β-lactamase, which results in a β-lactam antibiotic breakdown, including the penicillins and the cephalosporins.[117, 118] M182T, E104K, and G238S are mutants of TEM1 β-lactamase.[119]

3.1.2 Chemicals and Materials

Table 3: Chemicals used in this work and the supplied company.

Chemicals	Company
M9 minimal salt, 5× D-(+) Glucose Magnesium sulfate ($MgSO_4 \cdot 7H_2O$) Casein hydrolysate Phosphate buffered saline (PBS) tablet LB broth Agar Glycerol Cefotaxime sodium salt (CTX) IPTG (Isopropyl β-D-thiogalactoside) Ampicillin Mineral oil Nitrocefin Dimethyl sulfoxide (DMSO) Phosphate buffer (100 mM, pH 7)	Sigma-Aldrich
HFE oil (Hydrofluoroether oil, $C_9H_5F_{15}O$)	Ionic Liquids Technologies
Surface-active agent (2% PicoSurf 1^{TM})	Dolomite
Ethonal (CH_3CH_2OH)	VWR International GmbH

Table 4: Materials used in this work and the supplied company.

Materials		Company
Light path	Slip Ring, M4 Tap	Thorlabs
	SM1 Lens Tube Without External Threads	
	Post-Mountable Ø3.2 mm Ferrule Clamp	
	1x2 Multimode Fiber Optic Coupler	
	Cyan light, LED 505 nm	
	UV light, LED 385 nm	
	BFP Excitation Filter, 390 nm (18 nm)	
	YFP Excitation Filter, 497 nm (16 nm)	
	BFP Emission Filter, 460 nm (60 nm)	
	YFP Emission Filter, 535 nm (22 nm)	
	Objective lens 20×	
	Motorized Filter Flip Mount	
Black box	Board and construction rails	
Sensors	Spectrometer	
	Photomultiplier tube (PMT)	HAMAMASTU
Readout	NI DAQ USB 6002	National Instrument
Control	Relay card	Robotshop
Heater	Heater and thermometer	RS
Fluidic	Tubing (PTFE), 1.6 mm × 0.8 mm × 10 m	Dolomite
	T-junction	
	X-junction	
	2-way in-line valve	
	Female to Female Luer Lock	
Syringes	SGE glass syringe, 2.5 mL and 5 mL	Sigma-Aldrich
Stirring	Magnetic stirring bars, 5 mm × 2 mm	VWR
Filter	Sterile syringe filter with 0.2 μm cellulose acetate membrane	
Needle	Blunt needle	
Syringes	Plastic syringe, 10 mL	
Plates	Sterile plate	
	96 well plate flat bottom (black/transparent)	

3.2 Bacteria Culture

The preparation of the medium followed the same protocols among all the experiments in this work. All antibiotics are prepared with the same protocols as well.[111] The storage methods for different bacterial strains are the same. Liquid mediums used to culture and

detect *E. coli* include the M9 medium, LB (Luria-Bertani broth) medium, and PBS medium. Solid agar medium and semi-solid medium are LB agar. All bacterial sample preparation, medium preparation, and antibiotic preparation were operated on an airflow bench. All the tubes, tips, flasks, and pipettes were autoclaved at 121 °C for 15 min before use. Sterile products such as 0.2 μm filters, Petri dish plates, 96 well plates, needles, and plastic syringes are used directly. Items that cannot be autoclaved (*eg.*, the syringes, T-junctions, Cross-junctions, and valves) were sterile by sinking in 70% ethanol and DI water alternately 3 times (each time 3 min) and using ultrasound Tubings were sterilized by rinsing 70% (v/v %) ethanol with a flow rate of 15 mL/min and keeping the ethanol inside for 1 hour then using the HFE oil to flush the ethanol out. All the wastes produced during the bacterial preparation were autoclaved first before throw away.

3.2.1 Medium and Antibiotics Preparation

In this work, the M9 medium was chosen for bacterial cultivation and detection to avoid fluorescent signal interference from the medium. For preparing the M9 compound medium, 56.4 g M9 minimal salt was first dissolved in 1L of distilled water and autoclaved at 121 °C for 15 min to get the 5× concentrate medium. The 1× M9 minimal salts were obtained by further diluted the 5× concentrate medium as needed. Before each experiment, 8 mg/mL glucose, 1 mg/mL $MgSO_4 \cdot 7H_2O$, and 0.5 mg/mL casein hydrolysate were filtered with a sterile syringe filter and added to the M9 medium. LB medium was prepared by dissolved 25 g LB broth in 1 L of distilled water and then autoclaved at 121 °C for 15 minutes, followed by cooling down at room temperature and kept in the fridge at 4 °C. Due to the fluorescence interference from LB broth, the bacterial growth which is quantified by fluorescence change is cultured in M9 media. LB broth was used for detecting bacterial growth state that was not needed to be quantified by fluorescence, such as pH changing, colony counting on LB agar plate. PBS media is used as a control group in the experiment of pH changing during bacterial growth and for checking the cell size and shape in the flow cytometer. For preparing the medium of PBS, one tablet was first dissolved in 200 ml of deionized water, yields 0.01 M phosphate buffer, and was sterile filtered before use. The LB agar solid media was prepared by dissolving 20 g/L LB Broth and 15 g/L Agar in 500 mL distilled water and autoclaved under 121 °C for 15 min. Then it was kept at room temperature (until cool down to 46 °C), followed by pour 25 mL medium into sterile plates with a diameter of 85 mm. Afterward, pop the bubbles with a sterile tip and cover the plate with a cap. After the LB agar medium solidifies to gel form, wrap the plates with laboratory paraffin sealing film and store it

inverted at 4 °C. The soft agar medium used in this work contains 7.5 g/L agar and 20 g/L LB broth powder. It was prepared and autoclaved before experiments.

Two types of antibiotics are used in this work: Ampicillin and Cefotaxime sodium salt (CTX). Firstly, antibiotic stock solutions are prepared by using **Equation 7**:

$$\frac{1000}{P} \times V \times C = W \tag{7}$$

Where P is the potency given by the supplier (μg/mg), V is the volume (mL), C is the final concentration of the solution (μg/mL), and W is the weight of antibiotic (μg) to be dissolved in volume V (mL).

For example, in this work, the potency of the CTX is 916-964 μg/mg, the average potency is taken as 940 μg/mg. The solvent used here is the M9 compound medium to avoid the concentration of the nutrients decreasing in the prepared culture medium. Finally, the 10 mg/mL CTX solution was prepared by dissolving 10 mg CTX into a 1 mL M9 compound medium. Then, the CTX solution was further diluted to various gradients concentrations and transferred 300 μL in each 500 μL tube. The label, correlated concentration, and dilute method are shown in **Table 5**. All the prepared antibiotic stock solutions were kept in the freezer at -20 °C. The same protocol was used to prepare the ampicillin and IPTG stock solutions. IPTG was used to induce protein expression where the gene is under the control of the lac operator.[120]

Table 5: The label, correlated concentration, and dilute method of antibiotic CTX stocks.

Label	Concentration (μg/mL)	Dilute from CTX (μg/mL)	Dilute method CTX/M9 (vol/vol)
1000	1000	10000	100/900
100	100	1000	100/900
10	10	100	100/900
2048	2048	10000	204.8/795.2
1024	1024	10000	102.4/897.6
512	512	10000	51.2/948.8
256	256	1000	256/744
128	128	1000	128/872
64	64	1000	64/936
32	32	1000	32/968
16	16	1000	16/984
8	8	100	80/920

4	4	100	40/960
2	2	100	20/980
1	1	10	100/900
0.5	0.5	10	50/950
0.25	0.25	10	25/975
0.125	0.125	10	12.5/987.5

3.2.2 Bacteria Storage

All *E. coli* used in this work were kept in three storage ways for different purposes: super-cooled freezer (-80 °C), liquid medium (4 °C), and agar plate (4 °C). Depends on the storage temperature, viable bacteria can be kept in the short term and long term. For the regularly used bacterial cultures, bacteria can be streaked onto agar plates and stored at 4°C for days or weeks. The stock bacterial strains were kept in 70% glycerol at -80 °C in the freezer for long-term storage and unfroze before the culture.

3.2.3 Liquid Medium Cultivation

All *E. coli* cultured with batch culture method was prepared by adding 50 mL M9 compound medium with 1 mL pre-cultured bacterial medium in a 100 mL flask. The medium containing bacteria was incubated at 37°C and cultured overnight by shaking at 170 rpm for approximately 24 hours.

3.2.4 Solid Agar Petri Dishes Cultivation

Culturing bacteria on a solid agar plate allows us to observe and identify colonies and provides a way to count viable bacterial rates.[121] To culture bacteria on agar plates, a sterile stick was first used to dip bacteria from an active bacteria culture medium. It was then scribed on the agar surface and incubated at 37°C for 12 hours with being stored upside down. Then the agar Petri dishes with colonies were stored at 4 °C. For counting the viable bacteria rate in bacteria during incubation time, 0.5 mL samples were taken from bacterial media at the incubation time point of 9 h, 24 h, and 36 h. Then, the samples were diluted to 20-50 cells/mL with PBS solution. 1 mL diluted sample was added to a petri dish (85 mm in diameter) and well-mixed with the 46 °C LB agar medium, followed by kept in an incubator at 37 °C for 36 hours.

3.2.5 Semi-Solid Agar Petri Dishes Cultivation

A soft agar plate can be used to check bacterial motility.[122] Compared to the solid agar, the soft agar, also called semi-solid, contains agar at 0.5 % (w/w%) concentration, which allows the bacteria with flagella or other machinery for propulsion in random directions to move in agar plate during incubation.[123, 124] For the motility experiments, 5 mL of the soft agar medium with 46 °C was poured into Petri dishes with 35 mm diameter. Then, a sterile wire was dipped into an active bacteria culture medium first and then gently stabbed to the agar surface. The semi-solid medium with bacteria was then incubated at 37 °C for 36 hours.

3.3 Bacteria Detection Methods

This work focuses on the study of bacteria coexistence using a millifluidic device. To validate the results and compare the advantages and disadvantages of different bacterial detection methods, classical strategies and devices such as Biophotometer, microplate reader, microscope, and fluorescence flow cytometer were utilized. Moreover, this work examined antibiotic MIC, cell viability, pH in cell-free medium, the fluorescence intensity in cell-free medium, the fluorescence intensity of re-suspended pelleted cells in M9 medium, and β-lactamase activity. A sketch up of the methods used in this work is presented in **Figure 4**.

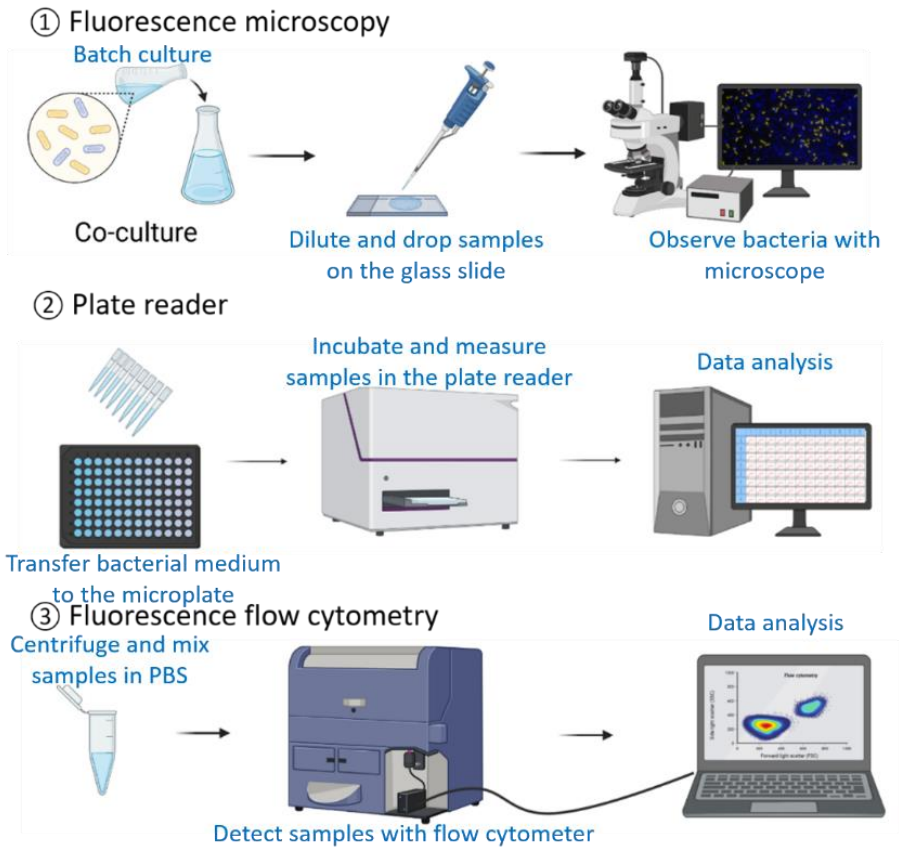

Figure 4: Different methods used for detecting bacteria: fluorescence microscopy, plate reader, and fluorescence flow cytometry.

3.3.1 Biophotometer OD_{600}

In the batch culture method, the Biophotometer is widely used to detect the optical absorption of the bacterial medium at a wavelength of 600 nm (abbreviated as OD_{600}). It is a common and fast way to monitor bacteria and cell biomass in a liquid.[125] In this work, the cell density of *E. coli* was measured by Biophotometer (Eppendorf) and calculated with the following **Equation 8** (M9 compound medium). Before measuring the cell density, the bacterial media was first diluted into the measuring range of $0 \leq OD_{600} \leq 1$. Then, the result was obtained by multiplying the dilution factor. The calibration of the OD_{600} with *E. coli* was already done in a master's thesis by Ye Dan (Detecting microorganism growth with microfluidic resonance detector. Master's thesis, TU Dresden, 2012).[126]

$$Cell\ density\ (\frac{cells}{mL}) = 5.1 \times 10^8 \times OD_{600}\ (0 \leq OD_{600}\ \leq 1) \qquad (8)$$

3.3.2 Fluorescence Microscopy

Fluorescence microscopy has become one of the main devices in the study of biology. It aims to observe the objects of interest among the whole sample.[127] In this work, fluorescence microscopy from Zeiss (Axiovert 200M, Carl Zeiss) was utilized to observe and distinguish the *E. coli* BFP and *E. coli* YFP separately for measuring the cell size and shape and the biomass ratios between two strains. Filter Set BFP with excitation wavelength 380 nm and emission wavelength 439 nm was used to observe *E. coli* BFP. Filter Set GFP with excitation wavelength 489 nm and emission wavelength 509 nm was used to observe *E. coli* YFP.

After incubating for different hours, the bacterial medium was diluted with PBS solution based on the needs. Glass slides were first cleaned with ethanol and acetone and dried with a gas gun before dropped the samples on them. For each experiment, 5 µL sample was dropped on a clean glass slide (22 mm × 40 mm) by a 0.1-10 µL pipette, later a cover glass slide (22 mm × 22 mm) was covered on the top of the sample. After few minutes, until all the bacteria stop flowing between two glass slides, images of the bacteria were taken under bright field, BFP filter set and GFP filter set with different magnifications.

3.3.3 Plate Reader

Plate readers, also known as microplate readers, are foundational instruments in experimental biology to detect biological events of samples. It enables measurements of

absorbance and fluorescence intensity.[128] In this work, plate readers (Tecan and Cytation 5) were employed to measure the excitation and emission wavelength of *E. coli BFP* and *E. coli YFP* and detect the two strains' fluorescence signal and OD_{600} during incubation. According to the experimental design, the bacteria were first pre-cultured for 4 hours and diluted to various initial cell densities for all the experiments. The bacterial samples with a volume of 200 µL were transferred to each well of the 96 well plates. Every 30 min, the plate reader was shaken 5 s and measured. Samples were incubated and measured for 20 hours at 37 °C. **Figure 5** presents the steps for sample preparation and measurement.

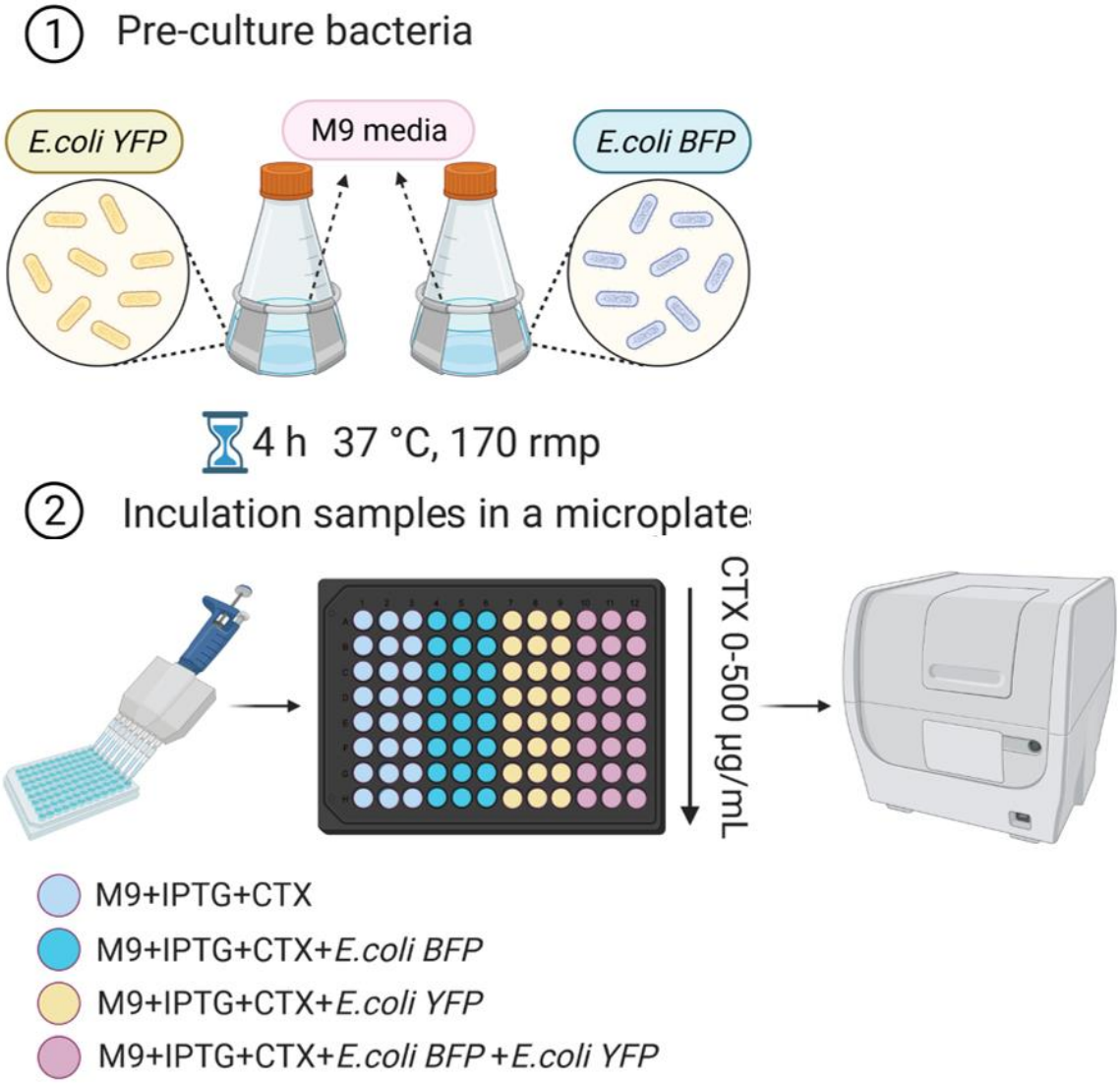

Figure 5: Sample preparation and measurement in a plate reader.

For measuring the BFP, the excitation wavelength was set as 400 nm ± 20 nm, and the emission wavelength was set as 460 nm ± 20 nm. For measuring YFP, the excitation wavelength was set as 490 nm ± 20 nm, and the emission wavelength was set as 530 nm ± 20 nm. After setting the excitation and emission wavelength for measuring BFP and YFP, the fluorescence intensity-bacterial concentration calibration curves were first

obtained by detecting the bacterial fluorescence signal with different cell concentrations. In order to make sure the fluorescence signal can truly reflect the viable cell concentrations, the bacteria were first cultured 8 hours before diluting to various concentrations with gradients. Here, the cell concentrations were measured by Biophotometer and calculated by **Equation 8**.

3.3.4 Fluorescence Flow Cytometry

Fluorescence flow cytometry is utilized to detect the particles, cells, and bacteria with a size range from 0.2 to 150 μm. It gives the information of events' size, shape, granularity, and fluorescence.[129, 130] In this study, a fluorescence flow cytometry (Attune Nxt) was employed to distinguish the *E. coli* BFP and *E. coli* YFP (according to their different fluorescent spectrum) and measure two bacterial strains' cell size, shape, and granularity. The filter set mode VL1 (440/50 nm) and BL1 (530/30 nm) were chosen for BFP and YFP detection, respectively. Before measuring the samples, pre-cultured (batch culture 3 hours in M9 media) *E.coli* BFP, *E.coli* YFP, and wild strain *E. coli* K12 (without fluorescent protein) were tested to decide the BFP and YFP measurement spectrum. In order to control the number of events below 10000 for each measurement, the bacterial medium was first diluted with PBS medium or M9 medium. It then flowed to the detector with a flow rate of 12.5 μL/min for 8 mins. Besides, the cell shapes of different strains of *E. coli* with and without treatment of CTX were also measured with fluorescence flow cytometry. On the two axes, FSC means forward scatter and correlates with cell size, and SSC is side scatter and proportional to the granularity of the cells. Therefore, the shifted dots in the graph indicates the bacterial size or shape changes as well.

3.3.5 Millifluidic Droplet-based Reactor

For preparing the initial bacterial samples for detecting in the millifluidic droplet-based reactors, bacteria were firstly batch cultured in fresh M9 media (1 mL bacteria media diluted in 50 mL M9 fresh media) within a 100 mL flask to pre-grew for 3 hours to reach the early exponential growth phase (37 °C, 170 rpm). Then, the bacteria were diluted by a fresh M9 compound medium (store at 4 °C) in a 1.5 mL tube. Next, they were refilled into a 5 mL syringe and further encapsulated in droplets with a volume of 200 nL (see details in the Chapter 4.6 Device Stability). In order to avoid clumping of bacteria and keep the concentration of each bacteria strain fixed during injection, autoclaved magnetic stirring bars (diameter = 2 mm and length = 5 mm) were placed into the syringes (5 mL, diameter = 10.301 mm,

length = 60 mm) near a magnetic stirrer with the speed of 500 rpm during the droplet generation. The syringes were kept in a horizontal position. M9 compound medium was kept in the fridge at 4 °C before diluting the fresh pre-grown bacterial media. It prolongs the microbes' acclimatization time and ensures no bacteria doubling during the formation of droplets as much as possible. A droplet sequence with approximately 450 droplets was transferred forward and backward in front of the detectors at 37 °C for 20 h.

3.3.6 Bacteria Medium pH Measurement

In order to verify pH value changed during the different incubation times, the bacterial liquid medium samples from batch culture and millifluidic device were collected from different culture time points and measured with a pH meter (pH 1100 L, VWR). In the batch culture method, 3 mL media was taken from each sample and centrifuged (D-78532 Tuttlingen, Hettich) for 5 min with 3370 rpm (revolutions per minute) at 25 °C. The supernatant was collected and its pH was measured with the pH meter. After incubated the bacteria for 0, 9, 24, and 36 hours in droplet reactors, the droplets were flushed out and collected. Then the liquid media with bacteria was centrifuged (D-78532 Tuttlingen, Hettich) for 5 min with a speed of 3370 rpm at 25 °C. Only the supernatant was collected and measured with the pH meter.

3.3.7 Antibiotic MIC Test

Before monoculture and co-culture *E. coli* strains with antibiotics, the antibiotic MIC test for each strain was done. Since the antibiotic-resistant strains can produce different amount of enzymes to deactivate the CTX, 96 well plate with different start CTX concentrations was designed. Start from the maximum concentration in A1 well, the gradient concentrations were generated to both vertical and horizontal directions by dilute factor 2. An example of the gradients generated in 96 well-plate for MIC testing is presented in **Figure 6.** The protocol is followed by the work of 'Determination of minimum inhibitory concentrations' by Andrews, J. M..[111]

From Column 2nd to Column 12th, the wells were first filled with 100 μL M9 compound medium. In Column 1st, from A1 to H1, the wells were filled with 200 μL CTX unfreeze solution with the label from 2048 to 16. With the multiple tip pipettes, 100 μL solution from each well of Column 1st was transferred to Column 2nd and repeated the same step from Column 2nd to Column 12th. Next, 100 μL bacterial medium with 100 μM IPTG was adding to each well. Then a plate reader

was used to detect the OD_{600} of the prepared 96 well plates before incubating and after incubating for 20 hours.

MIC	1	2	3	4	5	6	7	8	9	10	11	12
A	1024	512	256	128	64	32	16	8	4	2	1	0.5
B	512	256	128	64	32	16	8	4	2	1	0.5	0.25
C	256	128	64	32	16	8	4	2	1	0.5	0.25	0.125
D	128	64	32	16	8	4	2	1	0.5	0.25	0.125	0.0625
E	64	32	16	8	4	2	1	0.5	0.25	0.125	0.0625	0.03125
F	32	16	8	4	2	1	0.5	0.25	0.125	0.0625	0.03125	1.56E-02
G	16	8	4	2	1	0.5	0.25	0.125	0.0625	0.03125	1.56E-02	7.81E-03
H	8	4	2	1	0.5	0.25	0.125	0.0625	0.03125	1.56E-02	7.81E-03	3.91E-03

Figure 6: MIC test of *E. coli* BFP 8 with CTX concentration starts from 1024 μg/mL.

3.3.8 Cell-free Medium Fluorescence Intensity Detection

The fluorescence protein release from the lysis cell to the extracellular fluid hypothesis can be confirmed or refuted by testing the fluorescence of cell-free media after 20 hours of incubation. Cell-free media can be obtained by following steps, 1) centrifuging growth culture media to settle down cells and get supernatants; 2) filter sterilizing the supernatants to remove the residual cells; 3) collect the filtrate. The pelleted cells can be resuspended in PBS- or M9-buffer to check their fluorescence. The specific operation is described as follows. First, the bacterial medium was collected after 20 hours of incubation then centrifuged for 5 min with a speed of 3370 rpm. The supernatant was collected and filtered by a 0.2 μm syringe filter and pipetted to a 96 well plate (200 μL per well). The pelleted bacterial cells were resuspended in the M9 medium (with the same volume as previously) and pipetted to a 96 well plate (200 μL per well).

3.3.9 Cell Viability Detection

In this study, solid agar colony counting was used to verify the cell viability at different culture time points. Samples from different incubation time points were collected and measured the OD_{600}. According to the **Equation 8,** the samples were further diluted to 20-50 cells/mL (OD_{600} is from 3.92×10^{-7} to 9.80×10^{-7} A).[131] To prepare the solid LB agar in a petri dish (85 mm in diameter), the autoclaved LB agar solid media (15 mL) was cooled down to 46 °C and then added to the Petri dishes with a 1 mL diluted bacterial sample (obtained from bacterial media at the time point of 0 h, 9 h, 24 h, and 36 h). The LB agar and bacterial media were well-mixed and kept in an incubator at 37 °C for 36 hours. Colonies in LB agar plates were counting and compared to the calculated cell numbers.

3.3.10 β-lactamase Activity Detection

β-lactam antibiotics such as penicillin and cephalosporins have a molecular structure of the β-lactam ring. This molecular structure inhibits the synthesis of the bacterial cell wall, thus inhibiting bacteria survival or growth.[101] β-lactamase, an important bacterial enzyme, plays a crucial role in the resistance of β-lactam antibiotics by breaking down the β-lactam ring structure.[105, 106] Testing the β-lactamase activity in bacterial culture can reveal the kinetics of enzymatic activity released by bacteria.[108] In this work, nitrocefin was chosen as the substrate. It is a chromogenic cephalosporin and generates a colored product when it meets β-lactamase. This color change can be detected at the wavelength of 490 nm and has a proportional relationship to the β-lactamase activity.[132]

Nitrocefin working solution stock (500 μg/mL) was first prepared by dissolving 5 mg nitrocefin in 500 μL dimethyl sulfoxide (DMSO) and followed by adding 9.5 mL phosphate buffer (100 mM, pH 7) to obtain a total volume of 10 mL. The nitrocefin assay was done by testing the β-lactamase activity of the cell-free medium. Centrifuging the bacterial medium (2 mL with initial cell density of 5×10^6 cell/droplet) before incubating and after incubating for 20 hours, then took supernatants and filtered them through a sterile filter. Samples were kept on ice throughout the experiment before testing. Adding 100 μl cell-free medium per well in a 96 well plate, then 100 μl of 10 μg/mL nitrocefin (diluted by fresh M9 compound media from 500 μg/mL working solution stock). Red absorption (OD_{490}) was measured in a plate reader every minute for 1 hour as the nitrocefin was hydrolyzed. The samples with a high absorption signal were diluted to ensure the results are in the nitrocefin assay range. The β-lactamase activity is quantified by the red absorption (OD_{490}) change per minute.[133] The slope of OD_{490}-Time is used for describing the β-lactamase activity among the samples.

3. Materials and Methods

4. Millifluidic Device Setup

The homemade millifluidic device utilized in this work was designed and assembled includes four main systems: fluidic system, electricity circuit system, optical sensors system, and software control system. The fluidic system, electricity circuit system, and optical sensors system were fixed in a black box that protects the whole system in a dark environment to avoid room lights and natural sunshine. It can also keep the heat inside the box. All three systems were combined and controlled by the software control system (LabView program) to detect the samples automatically. The whole system is updated based on a previous version and has better stability, as shown in **Figure 7**. The previous version of the device setup is described in a doctoral thesis 'Rico Iling, Development of a Fluorescent Droplet Analyser for microbiological studies, 2018'.[134]

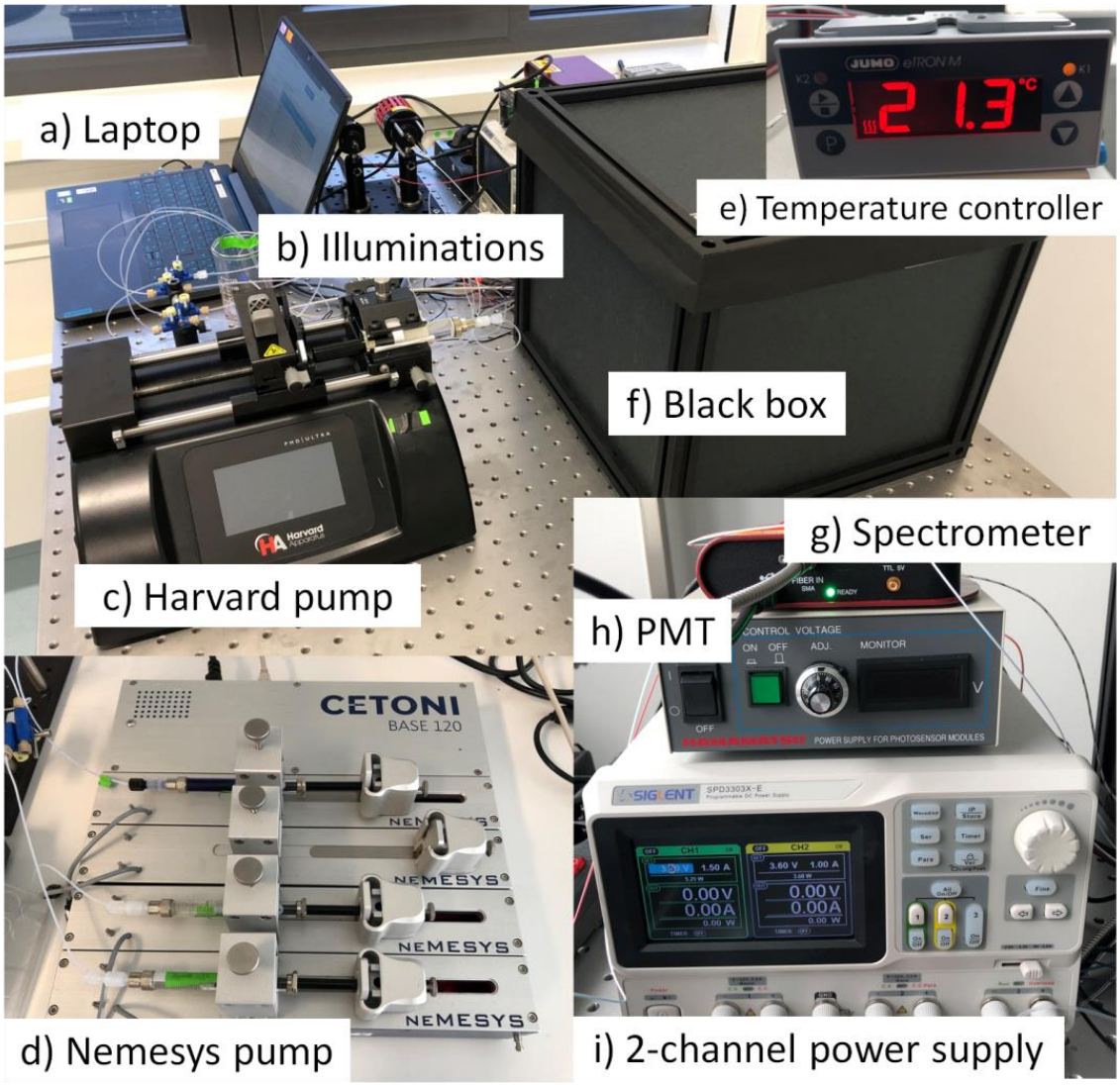

Figure 7: A full picture of the millifluidic device and accessories: **a)** laptop; **b)** illuminations; **c)** Harvard pump; **d)** Nemesys pump; **e)** temperature controller; **f)** black box; **g)** spectrometer; **h)** photomultiplier tube (PMT) power supply and monitor and **i)** 2-channel power supply.

4.1 Fluidic System

In the fluidic system, fluorinated ethylene propylene (FEP) tubings, tubing holders printed by a 3D printer, T-junction and cross-junction, connectors, and 2-channel valves were assembled and fixed into a black box for droplets transferring and storage. To generate droplets, syringes, Nemesys pump (Cetonic) and Harvard pump (PHD Ultra) were used to co-inject the water phase (with microbes) and oily phases into cross-junction. Aqueous droplets were generated by shear force. The HFE oil with 1% PicoSurf surfactant served as a continuous phase to maintain the stability of the aqueous droplets in the oil emulsion. The droplet sequence (containing up to 500 droplets) was transferred to a storage coil and then to the detectors. The sketch of the fluidic system is presented in **Figure 8**.

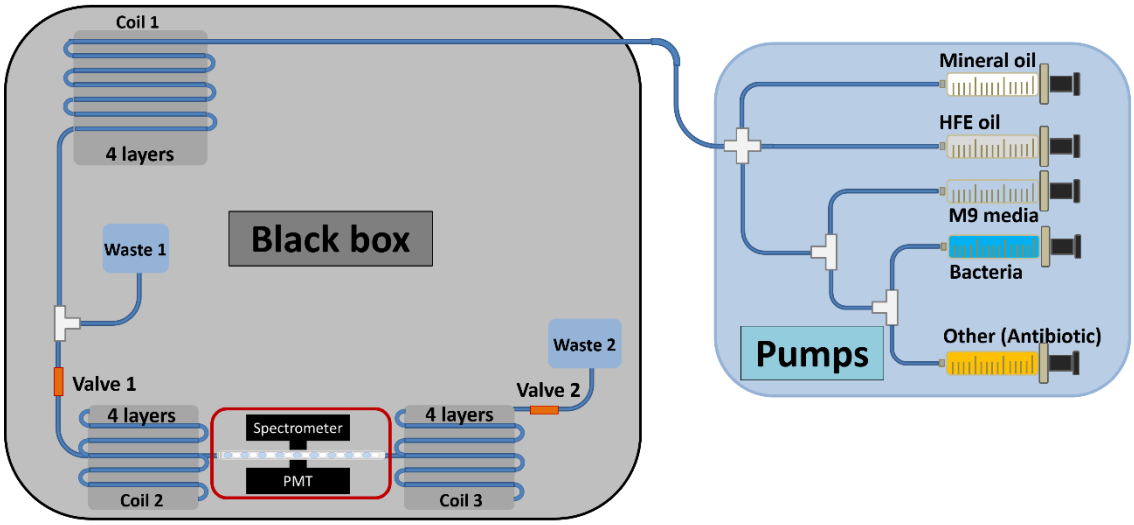

Figure 8: The sketch of the fluidic system (blue lines are FEP tubings) in the black box and connected pumps.

4.1.1 PEF Tubing

In this study, the FEP tubing was used to transfer and store droplets due to its good chemical resistance, optical clarity, and smooth internal surfaces. The parameters of the tubing are shown in **Table 6**.

Table 6: FEP tubing parameters.

Material	Outer diameter	Inner diameter	Thickness	Refraction index
fluorinated ethylene propylene	1.5875 mm	0.5 mm	0.54375 mm	1.338

It is known that diffraction occurs and becomes stronger when the width of the obstacle (slit or pipe) keeps approaching the wavelength of light (<1 μm). We chose a tubing with an inner diameter of 0.5 mm in this work so that diffraction may occur in this case. To solve the problem posed by diffraction, we used a lens to focus the light source on the droplets in the tube. In addition, when detecting fluorescence, only a small portion of the fluorescence is captured, while most of the fluorescence is scattered due to the tubing walls. Compared to refraction and scattering, the effect of diffraction is therefore negligible. Thus, the good optical transparency of the tube makes it possible to observe the droplets generated and stored inside the tube, as shown in **Figure 9**.

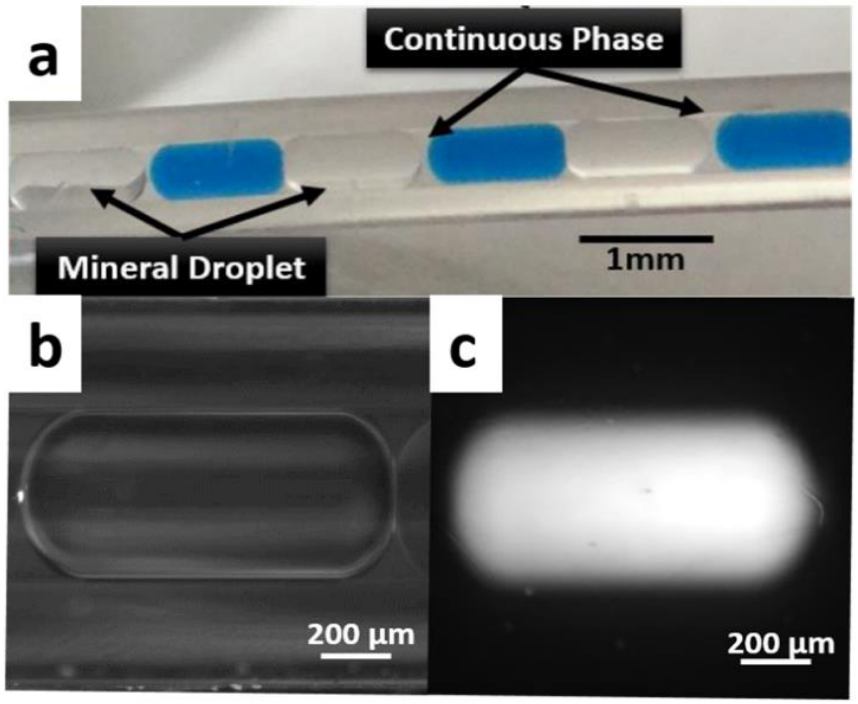

Figure 9: The shape and size of droplets photographed by camera and microscopy. **a)** Droplet sequence generated by water-phase droplets (with blue dye), mineral oil spacer (transparent droplets), and continuous phase (HFE oil) with a flow rate ratio of 5:5:1 mL/h in the FEP tubing and photographed by a camera. Water-phase droplet (with Rhodamine dye) observed with microscopy under **b)** bright field and **c)** blue light.

4.1.2 Droplet Sequence Capacity

A high throughput readout of experimental data is our aim to design a millifluidic device. This can be easily achieved by increasing the number of droplets in each experiment. However, a higher number of droplets also means a longer preparation time, as the time to generate droplet sequence and transfer it to the detector is proportional to the droplet number, as shown in **Figure 10 a**.

Moreover, droplet number is also correlated to the scanning time for each measurement cycle, as shown in **Figure 10 b**. Taking into account all the mentioned factors, we chose

to generate 450-500 droplets as the number of droplets for each droplet sequence to keep the optimal time between consecutive measurements for each cycle.

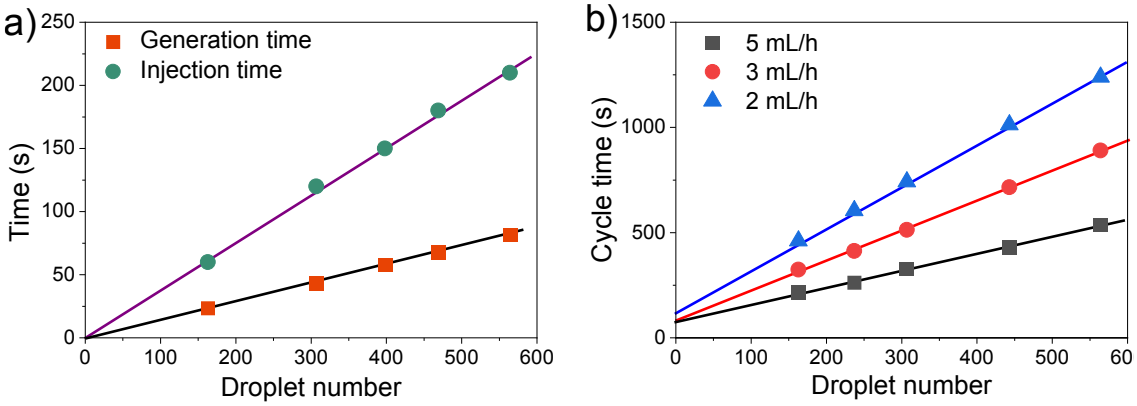

Figure 10: Relationship between droplet number with **a)** generation and injection time, and **b)** cycle time with different moving speeds.

4.1.3 Tubing Holder

Since each droplet has a length of around 1.1 mm (as shown in **Figure 9**), in order to store around 500 droplets and spacers (mineral oil droplets) in the fluidic system, we need tubing with a length of at least 1.1 m. To better fix and store these tubings, we designed tubing holder structures (work as a storage coils or holder to collect the tubing) with the online software ThinkerCAD and printed them with a 3D printer (Formlab 3.0), as shown in **Figure 11**.

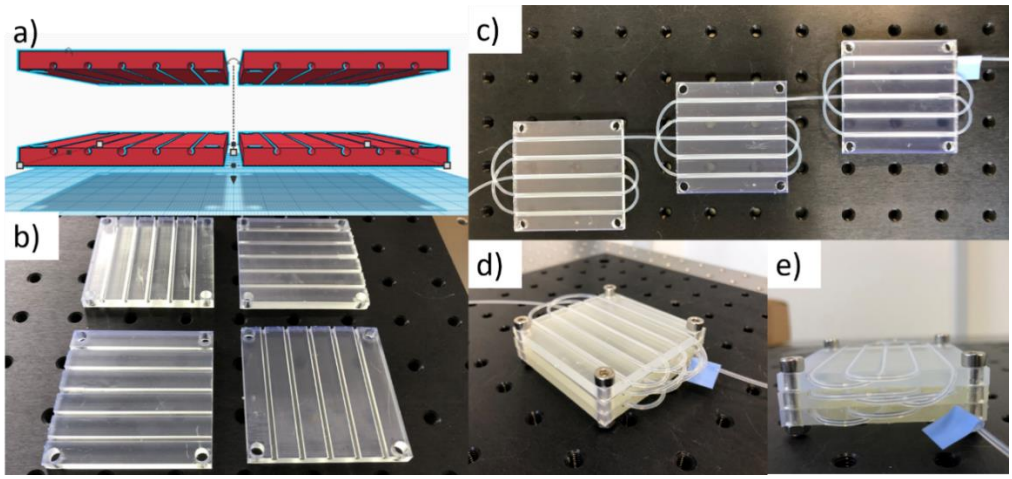

Figure 11: Structure of Coil 1 fabricated by 3D printer. Structure **a)** designed with online software ThinkCAD; **b)** printed out four layers; **c)** 3 layers with insert tubing; **d)** and **e)** 3 layers fixed with screws.

The tubing holder structures have a resolution of 25 µm with the material of clear resin. Coil 1 was designed with four separate layers (60 mm × 60 mm) with four holes at each corner. These layers with holes can be combined with screws and fixed in the black box.

In each layer, there are five channels with a diameter of 1.9 mm. Tubings can be inserted into the channels (diameter 1.6 mm), as shown in **Figure 11 b** and **c**. The total thickness of the 4-layer fixed tubing holder Coil 1 is 2 cm (each layer is 5 mm). This thickness can efficiently reduce the dislocation of droplets caused by inertia and gravity while being transferring.

Coil 2 and Coil 3 have a similar structure with five layers (5 tubing channels in each layer with 50 mm in length), as shown in **Figure 12**. The two coils were placed face to face with the optical sensor area set in the middle. The upper layers of the middle channels were connected by the tubing, which passes through the two detectors. The protruding part of the channel is used to fix the tubing at a certain location to reduce the tubing deformation caused by heating.

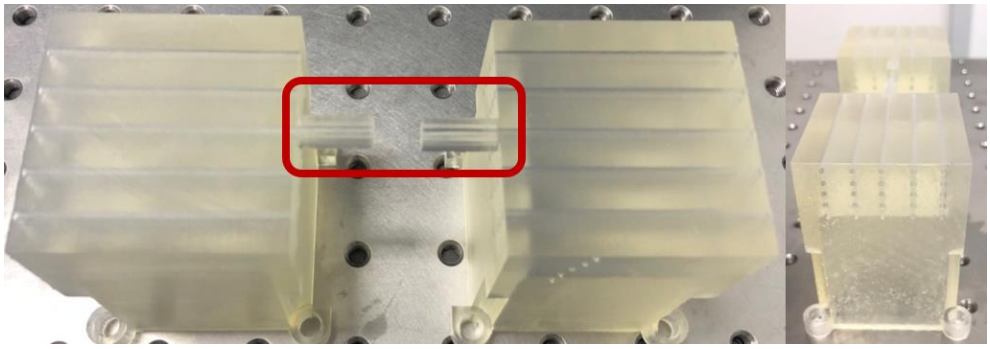

Figure 12: Structure of Coil 2 and Coil 3 and their protruding part marked in a red circle.

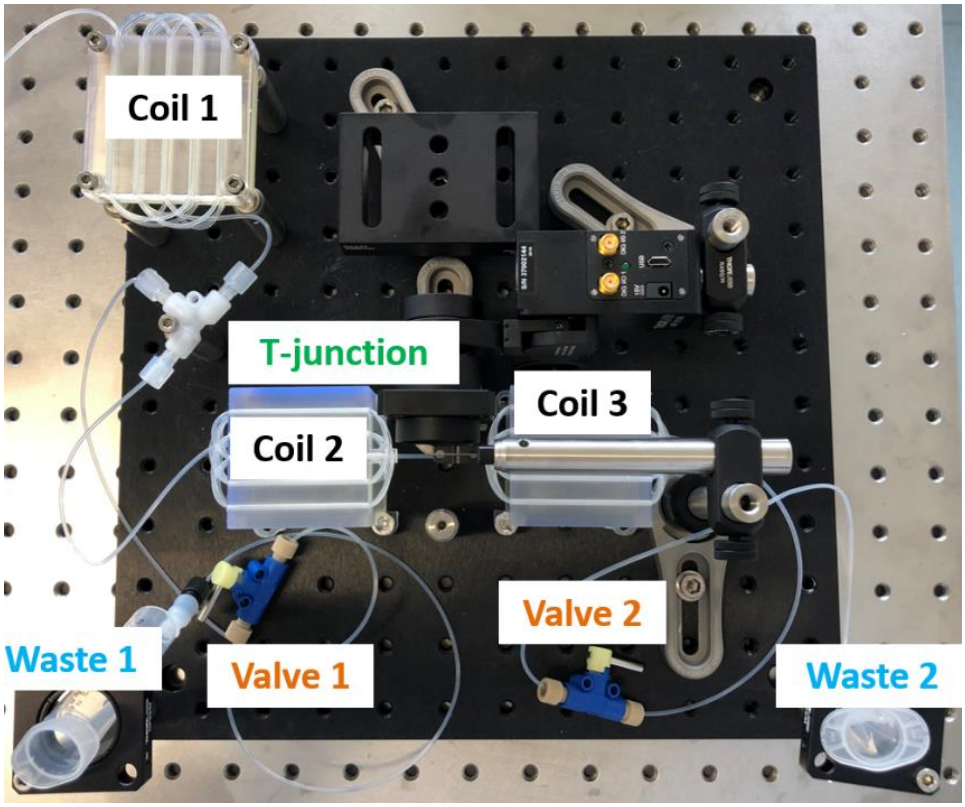

Figure 13: The fluidic system fixed on a black aluminum board.

After combining the coils and tubing with T-junction, cross-junction, connectors and valves, the whole fluidic system was completed, as displayed in **Figure 13**. To generate the droplets, we also need the Nemesys pump and Harvard pump to inject the different liquid phases into the fluidic circuit.

4.2 Electricity Circuit System

The electricity circuit system contains a 4-channel relay card controlled filter switcher, illuminations (LEDs), Harvard pump, and separately controlled heater (DBK Enclosures, FGC1031.2), spectrometer, PMT, and Nemesys pump. The 4-channel relay card serves with LabView software to automatically control the lights switch on and off and change filter switcher and Harvard pump operation mode. The temperature in the black box is controlled by a heater connected with a thermometer, fan, and thermal controller. The connect method and operate voltage for different devices are displayed and marked in **Figure 14**. Except for the motorized flip filter switcher, light sources, and fan, all devices are directly plugged into the lab power jacks.

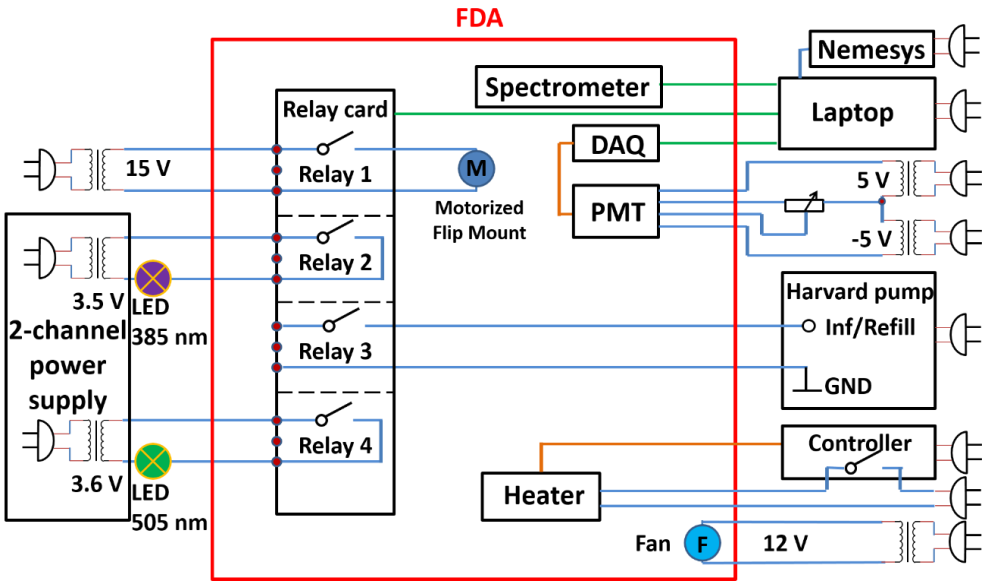

Figure 14: The electricity circuit system of the millifluidic devices.

It takes less than 15 minutes for the heater system to reach 37 °C from room temperature after setting operate temperature and the temperature floating range is 0.5 °C. The features of refill and infuse of Harvard pump were connected to relay card by connecting a 15-pin USB and user I/O connector, as shown in **Figure 15**. By switching on and off the 3rd channel of the relay card, the Harvard pump refills or infuses the syringe fixed on it.

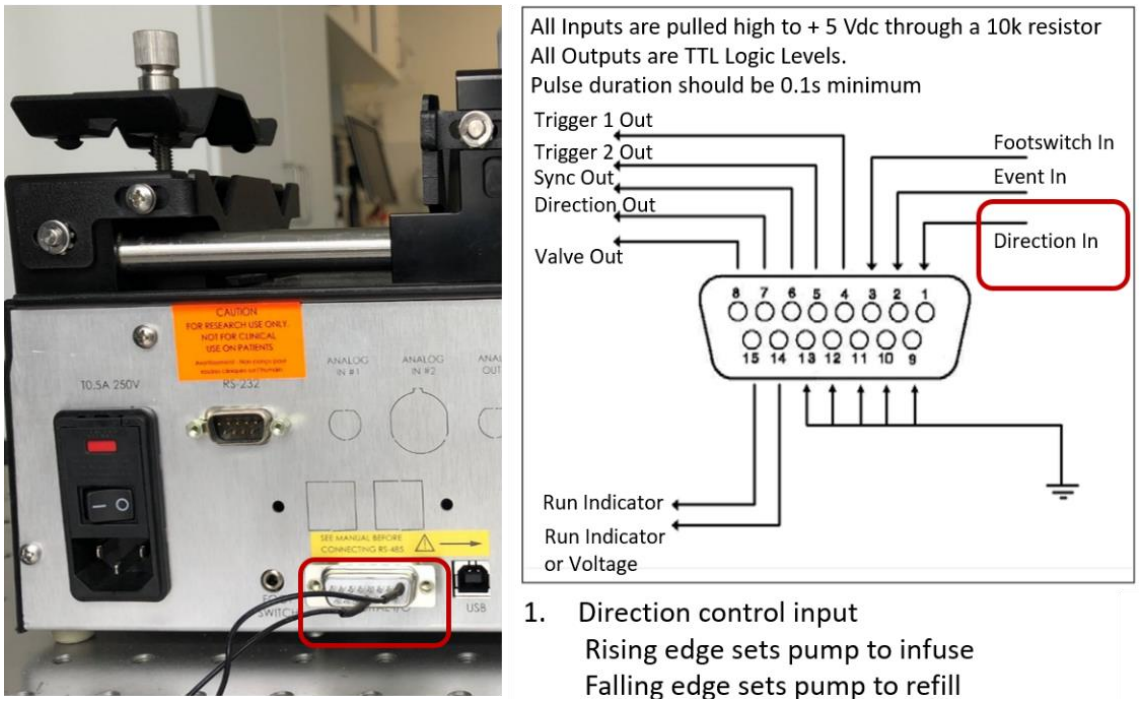

Figure 15: Harvard pump user I/O connector connected with a 15-pin USB.

4.3 Optical Sensors

4.3.1 Optical Detectors

The optical sensors system includes two sensors: a spectrometer (CCS 100, Thorlabs) and a photomultiplier tube (PMT, H10722-20, Hamamatsu). The spectrometer coupled with fiber was used with a wavelength range from 350 nm to 700 nm. Due to the different refractive index numbers between the aqueous droplet and mineral oil, the two types of droplets show different intensities when passing by the detection area. The spectrometer signal vibration peaks tell the location of the droplet sequence. A susceptible PMT was used to detect the fluorescence signal emitted from *E. coli* with a spectral range from 230 nm to 920 nm. An objective lens (20×, Zeiss) was placed between the PMT sensor and tubing to focus the fluorescence light emitted from bacteria. The LED lights and filters were chosen according to the excitation and emission wavelength of BFP and YFP, as shown in **Figure 16**.

The BFP detection mode contains an LED light source (385 nm, Thorlabs) and a BFP filter set (390/18 nm excitation and 460/60 nm emission, Thorlabs) as shown in **Figure 17 a**. The YFP detection mode contains an LED light source (505 nm, Thorlabs) and a YFP filter set (497/16 nm excitation and 535/22 nm emission, Thorlabs), as shown in **Figure 17 b**.

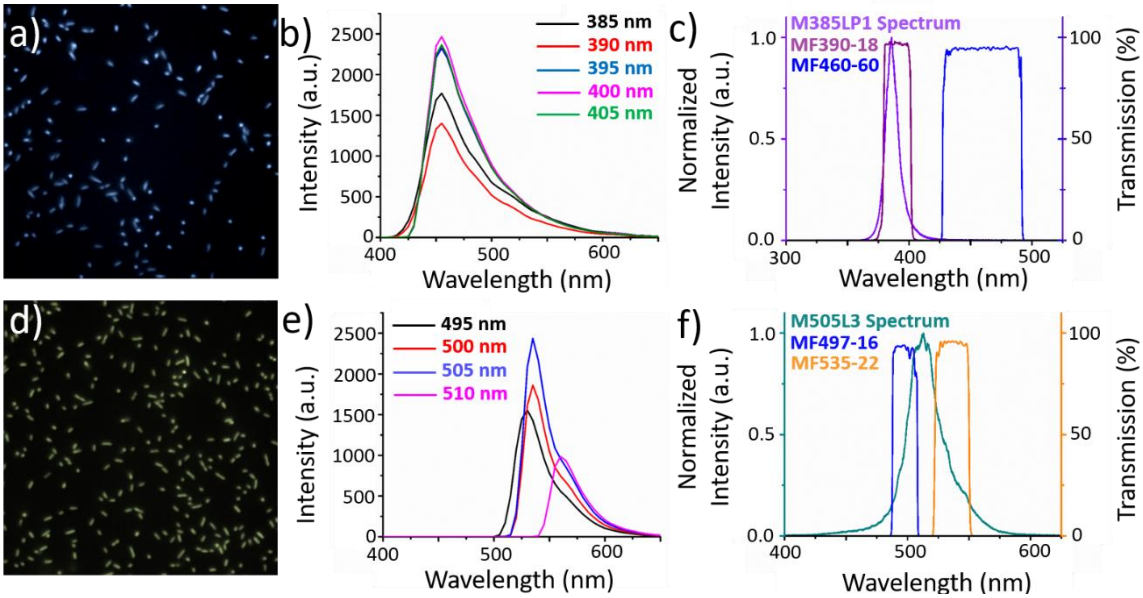

Figure 16: Fluorescence detection of *E. coli* BFP and *E. coli* YFP: **a)** *E. coli* BFP observed with a fluorescence microscope and excited by UV light with a magnification of 100×; **b)** the fluorescence emission spectrum of *E. coli* BFP excited by a different wavelength of the light source; **c)** light source and optical filters spectrum of BFP detection mode; **d)** *E. coli* YFP observed with a fluorescence microscope and excited by blue light with a magnification of 100×; **e)** the fluorescence emission spectrum of *E. coli* YFP excited by a different wavelength of the light source; **f)** light source and optical filters spectrum of YFP detection mode.

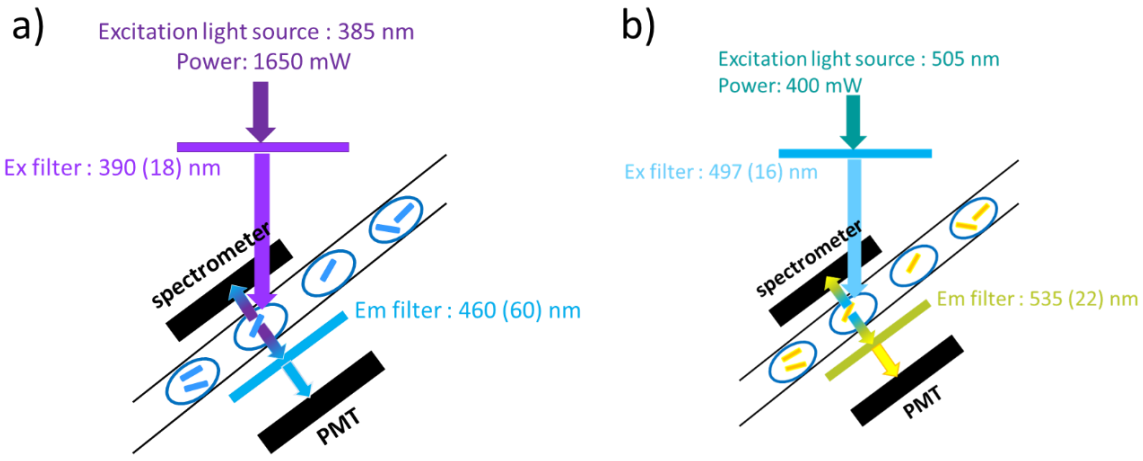

Figure 17 Two detection modes of optical system: **a)** BFP mode and **b)** YFP mode.

4.3.2 Optical Fibers

In this work, a 2-in-1 optical fiber was used to transfer the light from LEDs to the focusing area on tubing (between two detectors), as shown in **Figure 18**.

The optical fiber was fixed by a post mountable ferrule clamp (FCM32, Thorlabs). One side of the signal output port was connected to UV LED (with excitation filter, 390/18 nm), and the other signal output port was connected to Cyan LED (with excitation filter, 497/16 nm). Input port was fixed by ferrule clamp between optical sensors and tubing.

Compared to the previous way to glue the optical fibers on a holder, fixing a fiber with a clamp is much more stable. Besides, coupling two LED light sources in one fiber eliminates the deviation of the two detection modes caused by different fiber positions.

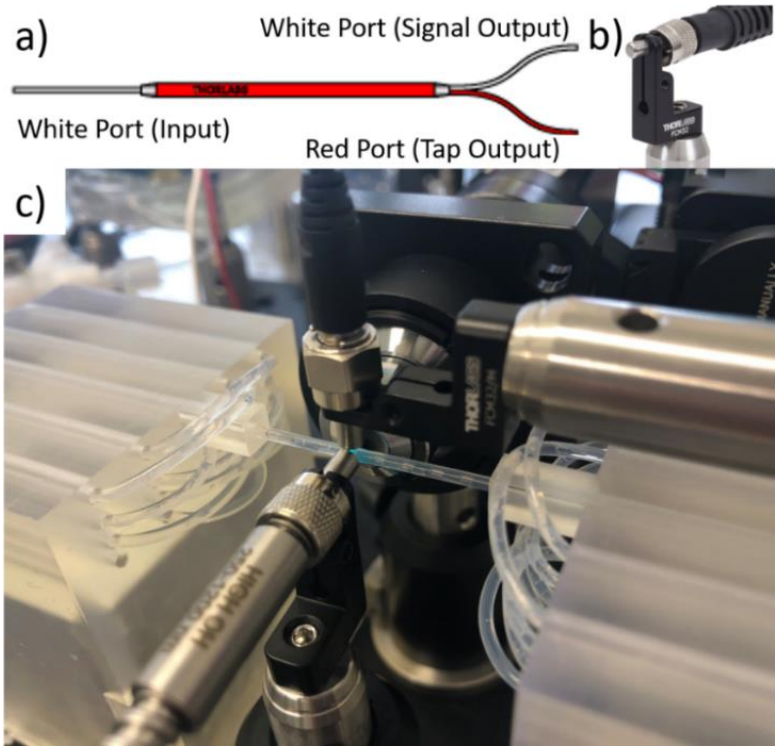

Figure 18: 2-in-1 optical fiber fixed with a post mountable ferrule clamp. **a)** 2-in-1 optical fiber; **b)** post mountable ferrule clamp; **c)** optical fiber fixed between optical sensors and tubing.

4.3.3 LED Operating Voltages

The principle of choosing the operating voltages of light sources for this work is i) allowing light sources to work within the rated voltage while still have sufficient brightness to excite the fluorescent protein; ii) adjusting the light source intensity to avoid damaging fluorescent protein or causing photobleach, and iii) keeping the temperature of the LED chips working in a safe range. According to the product introduction from the supplier, the information on two LED lights is presented in **Table 7**.

Table 7: Information of UV and Cyan LED lights offered by the supplier.

LED	Item	Minimum Power	Maximum Current	Forward Voltage
UV	M385LP1	1650 mW	1700 mA	3.9 V
Cyan	M505L3	400 mW	1000 mA	3.3 V

Based on these requirements, we measured the light source power and temperature with

different operating voltages and decided the operating voltages for two LED lights. **Figure 19** shows the measurement results of light power and temperature of two LED lights with various operating voltages. Both LED chips were soldered out of their previous mount and reconnect to a copper mount. From **Figure 19 b-d**, increasing the voltage, the temperature, power, and current of both lights increased. Notably, the UV LED chip is much more sensitive to voltage change. From 3.0 V to 3.8 V, both LED chips worked in the safe current range. Still, the UV LED chip temperature was above 45 °C with an operating voltage of 3.6 V. After considering the safety and light intensity, the operating voltages were set as 3.5 V for UV LED (385 nm), and 3.6 V for Cyan LED (505 nm).

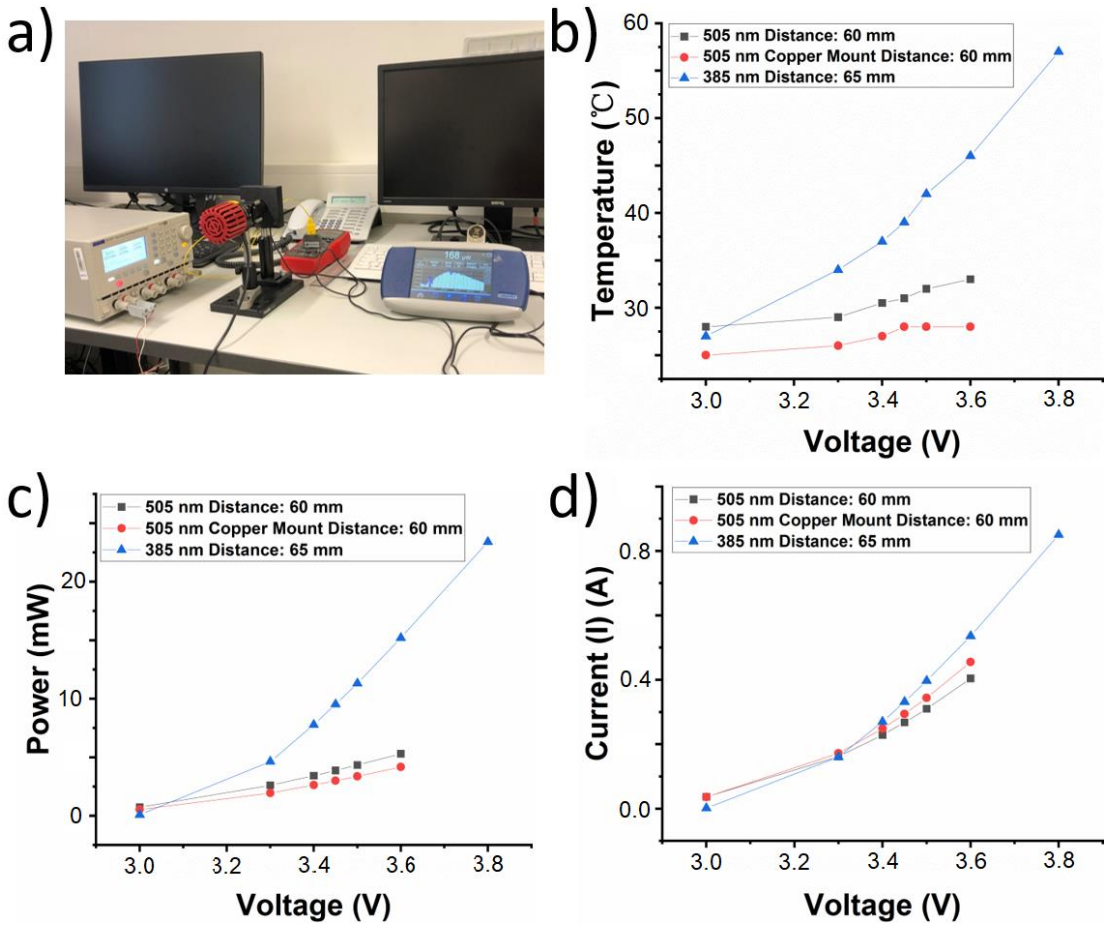

Figure 19: a) UV LED light power checked by an optical power meter, **b)** the temperature of the LED lights with different operating voltages, **c)** the power of the LED lights with different operating voltages, and **d)** the current of the LED lights with different operating voltages.

The final light intensity (with excitation lens) from optical fiber, which focuses on the tubing, was measured and compared to the light intensity of other fluorescence detection devices, as shown in **Table 8**. In principle, within a certain range, higher illumination intensities can excite substrates to emit stronger fluorescent signals. However, high-intensity light also increases the potential for damage to bacterial cells and fluorescent

proteins, especially for UV light. Since it takes 150 ms for droplet flow past the light source in a millifluidic device, the light intensity is set to be around 0.4 mW in order to avoid light damage to bacteria and proteins. It also ensures that the instrument can receive the fluorescence signal.

Table 8: Comparison of the light intensity and exposure time in different detection devices.

Device	Millifluidic device		Plate reader		Flow cytometry	
light intensity	BFP	YFP	BFP	YFP	BFP	YFP
	0.41 mW	0.35 mW	value not given (light power 5W)		50 mW	50 mW
exposure time	150 ms		25 ms		depends on the flow rate	

4.4 Software Control System

In order to control the measurement and read out the results of the millifluidic device, a program for controlling the whole system was designed by LabView software and connected with the 4-channel relay card. It automatically measures the variation of the two fluorescence signals (BFP and YFP) with high precision during tens of hours.

4.4.1 Single Signal Detection

In single fluorescence signal measurement, the main task is to constantly pump the droplet sequence to pass through the detectors. It was achieved by switching the 'infuse' and 'refill' mode of the Harvard pump to push and pull the droplet train in the tubing; thereby, the droplets flew forward and backward alternately through detectors. **Figure 20** shows the relay card controlled system and the programmed code in the front panel and operation panel (block diagram) in LabView. LED lights, Harvard pump (HP), and filter switcher can be controlled by clicking the corresponding buttons in the front panel.

4.4.2 Multiple Signals Detection

In multiple fluorescence signals measurements, except for the Harvard pump, the UV and Cyan LED light needs to be automatically switched on and off alternately; in the meantime, optical emission filters also need to be exchanged.

To get this feature, the system needs six steps to complete one loop measurement, and they are programmed to switch in order automatically. 1) droplets pass through detectors and move forward, motorized flip mount stays at BFP mode, UV light on; 2) 150 droplets pass detectors; 3) the last droplet of the droplet sequence passes by the detectors for 10 s,

pump switches from ‘infuse’ mode to ‘refill’ mode, UV LED light off, motorized flip mount exchanges to YFP mode, Cyan LED light on; 4) droplets pass through detectors and move backward, Cyan light keeps on, motorized flip mount keeps at YFP mode; 5) 150 droplets pass detectors; 6) the last droplet of the droplet sequence passes by the detectors for 10 s, pump switches from ‘refill’ mode to ‘infuse’ mode, Cyan LED light off, motorized flip mount exchanges to BFP mode, UV LED light on.

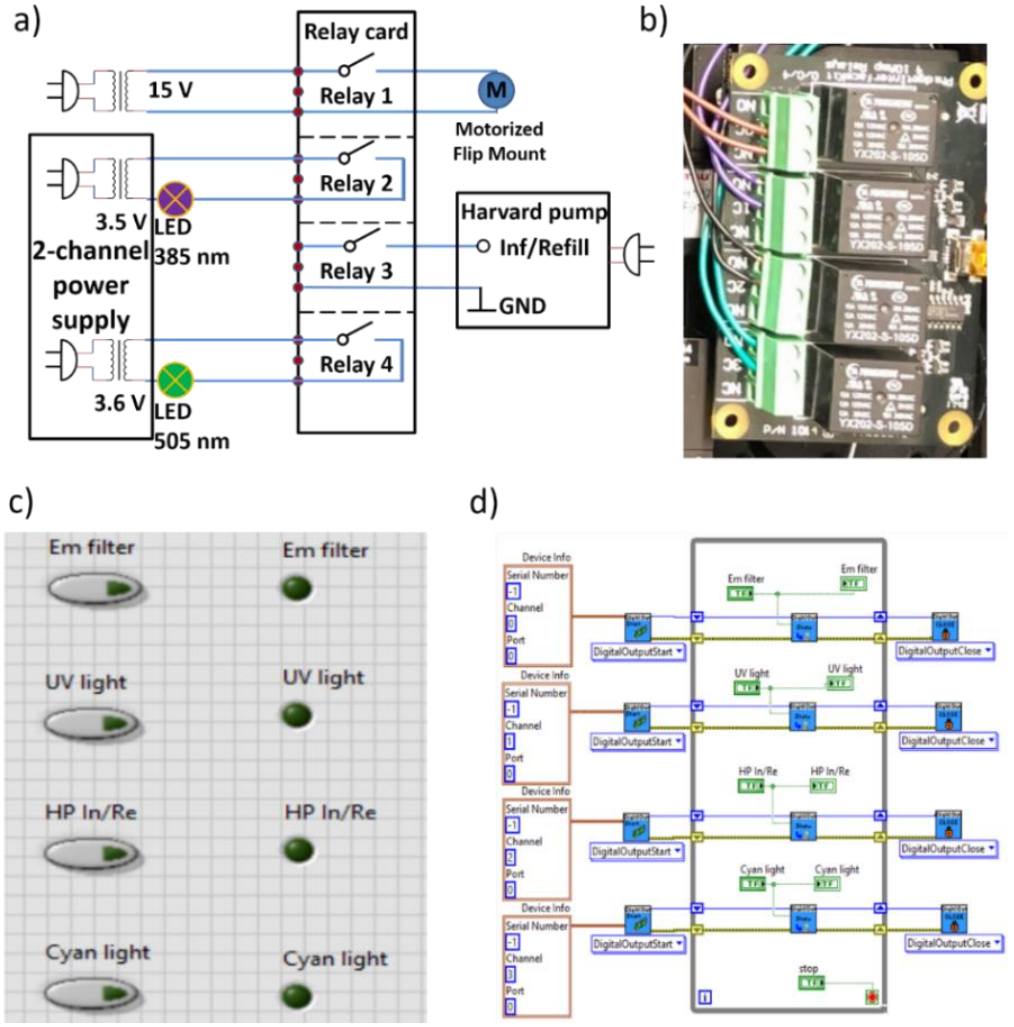

Figure 20: Relay card connection way and programmed code in LabView. **a)** relay card controlled electricity circuit system, **b)** relay card connected with electricity wires, and the programmed code in **c)** the front panel and **d)** operation panel (block diagram) in LabView.

4.4.3 Merged System

After merging all systems, the millifluidic device is divided into droplet generation area and detection area. **Figure 21** depicts a schematic diagram of the millifluidic system.

In the droplet formation module, syringes and pumps were utilized to co-inject the water and oily phases into cross-junction to form aqueous droplets. The HFE oil with 1% PicoSurf surfactant served as a continuous phase to maintain the stability of aqueous

droplets in the oil emulsion. Mineral oil worked as spacers to separate adjacent droplets. The droplet sequence (containing up to 500 droplets) was transferred to a storage coil and then to the detection area. In the detection area, the double fluorescent detector elements were used to measure the abundance of two *E. coli* strains.

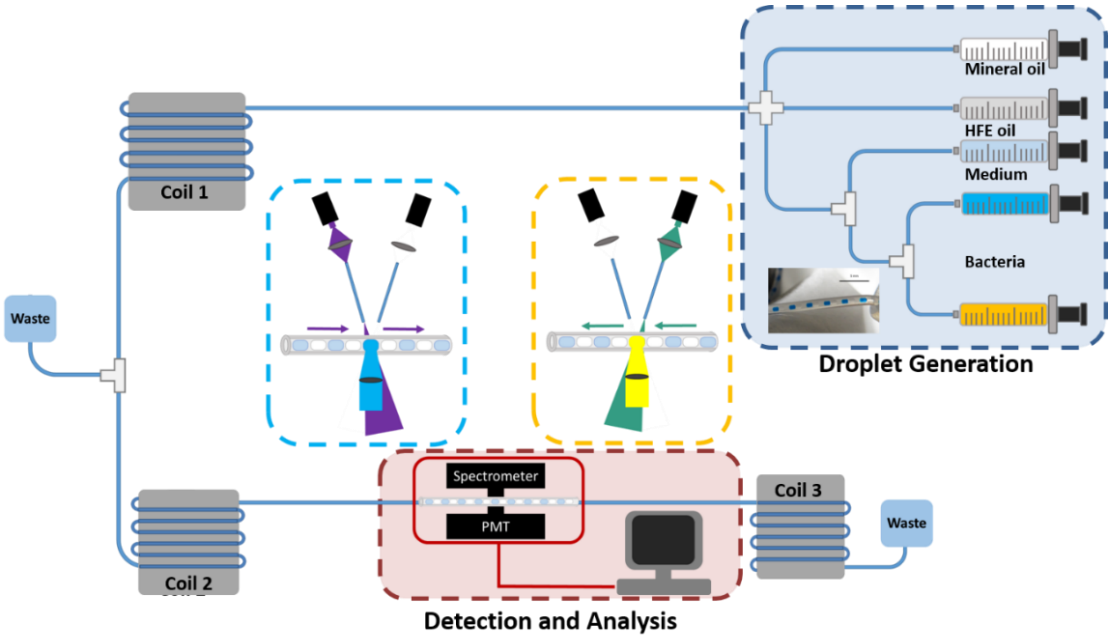

Figure 21: Millifluidic device with droplet generation area and detection area.

Since the fluorescence proteins expressed by two strains have distinct fluorescence excitation and emission spectra, the specifically selected light sources and filters for two detection modules were used here. The LED lights and filter were switched with flow direction changing, separately. Two detectors of the spectrometer and PMT (connected with DAQ) recorded and collected the data by Labview, as shown in **Figure 22** and **Figure 23**.

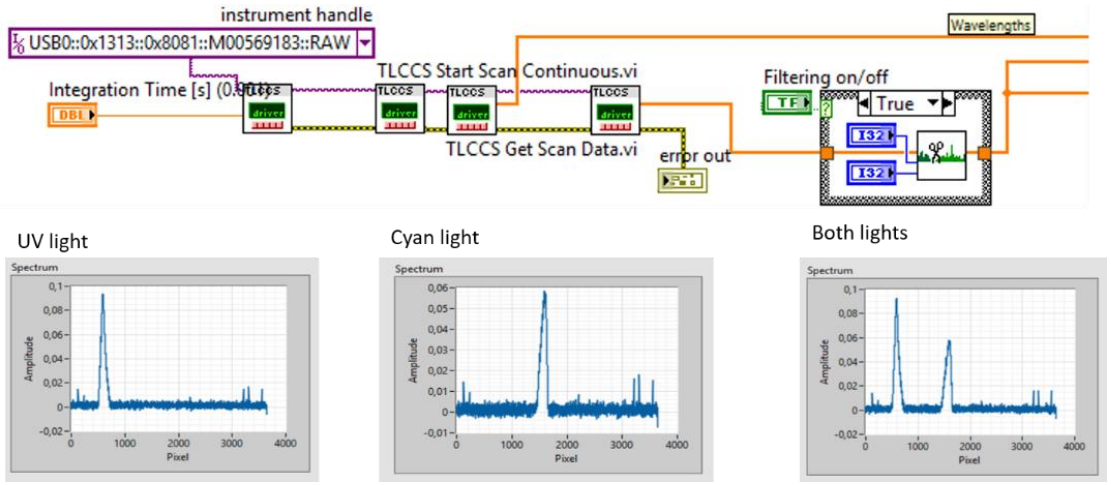

Figure 22: LabView code (control pattern) for collecting data from the spectrometer: UV light (385 nm) spectrum detected by a spectrometer and shown in LabView Front pattern (lower left);

Cyan light (505 nm) spectrum detected by a spectrometer and shown in LabView Front pattern (lower middle); Both light spectrum detected by a spectrometer and show in LabView Front pattern (lower right).

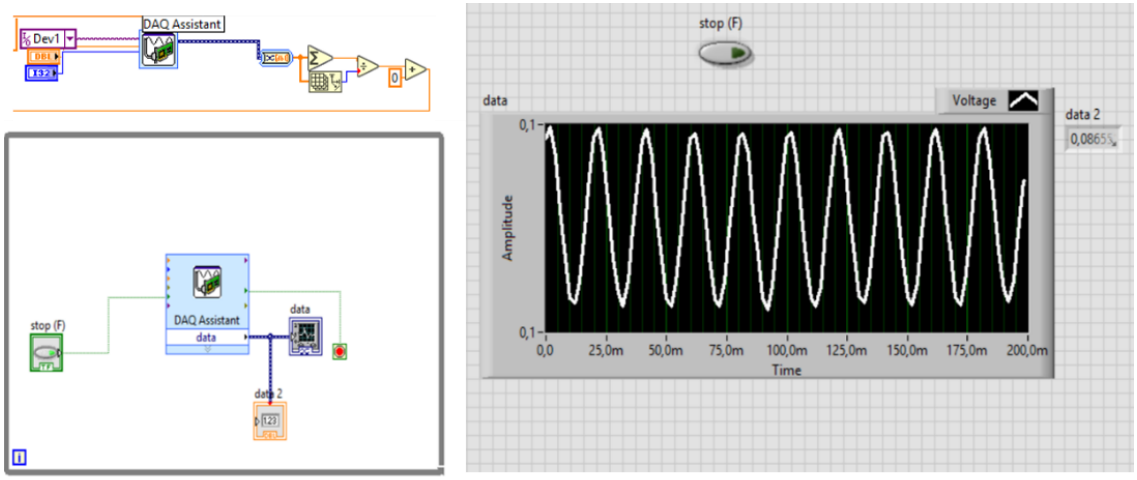

Figure 23: LabView code for collecting data from the PMT: Control pattern (left) and Front pattern (right).

4.5 Black Box

In order to operate the millifluidic device at 37 °C and record the fluorescence intensity from samples, a black box was designed and assembled to keep the heat and protect all optics in a dark environment. In this work, the materials used to assemble the black box are listed in **Table 9**.

Table 9: Items for assembling the black box.

Item	Type	Amount	Company
Construction Rails	300 mm	12	Thorlabs
Construction Rails	225 mm	4	
Counterbored Construction Cubes	25 mm	12	
Breadboard Lifting Handles	Reinforced Polymer	1	
Hinge for Enclosures	25 mm	2	
Lid Stop for Enclosures	25 mm	2	
Black Hardboard	610 mm×610 mm	3	
Aluminum Breadboard	300 mm×300 mm	1	

The size of the box is 300 mm in both length and width and 225 mm in height. The box

base is an aluminum breadboard that has M6 screw holes to fix the optics on it. Aluminum rails were used as a skeleton to support the box and its cover. The remaining five surfaces of the box were cut out of black cardboard. Rails and cardboards were assembled with twelve counterbored construction cubes and screws. The inside and outside views of the black box are shown in **Figure 24**.

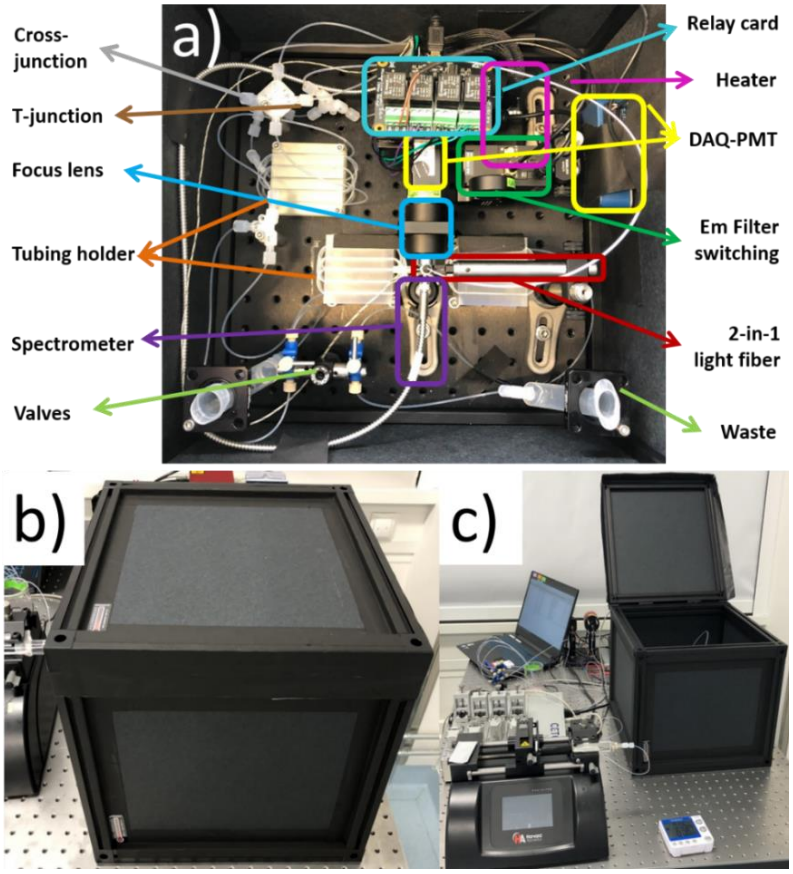

Figure 24: Overview of the black box: **a)** Inside view of the black box and all parts identification. Outside view of the black box with **b)** cover close and **c)** cover open.

4.6 Device Stability

The stability of the millifluidic device is presented in terms of the droplet size formed, the distribution of bacteria in each droplet, and system-related instability. The generated droplets with spacers (mineral oil) and HFP oil are shown in **Figure 9 a** (in paragraph *4.1.1 PEF Tubing*). The droplet is approximated to a cylindrical shape according to the shape of the droplet shown in **Figure 9 b and c**. Thus, the volume of the droplet can be calculated with the following **Equation 9**:

$$V = {}^{\pi}/_{4} \times D^2 \times L \tag{9}$$

Where V is the volume of a droplet; D is the diameter of a droplet; L is the length of a droplet. Thus, the final volume of the droplet is calculated to be approximately 200 nL

(in **Figure 9**).

The size and shape of droplet formation are stable. By measuring the length of the 100 droplets, the variation of droplet length is less than 2%. Similar variation was observed between the parallel tests, as the same flow parameters were used. Furthermore, as the same protocol was used to prepare the bacterial samples and the same steps were followed to encapsulate them in droplets, the inoculum size variation was also similar.

The droplet sequences with 1 or 2 cells in each droplet were generated and measured in the millifluidic device. Cell numbers were counted based on their bacterial growth curves in each droplet. The distributions of both *E.coli* BFP and *E.coli* YFP in each droplet are similar to the theoretical values of the Poisson distribution, as shown in **Figure 25**. The one/two cells placed to the droplets were done by first measuring the OD600 of pre-grew bacteria and diluting the cell density to 0.0000098 A or 0.0000196 A, then using syringes and pumps to inject the bacterial media into droplets. The distributions of *E.coli* with one/two cells per droplet were investigated in around 450 droplets for each droplet sequence.

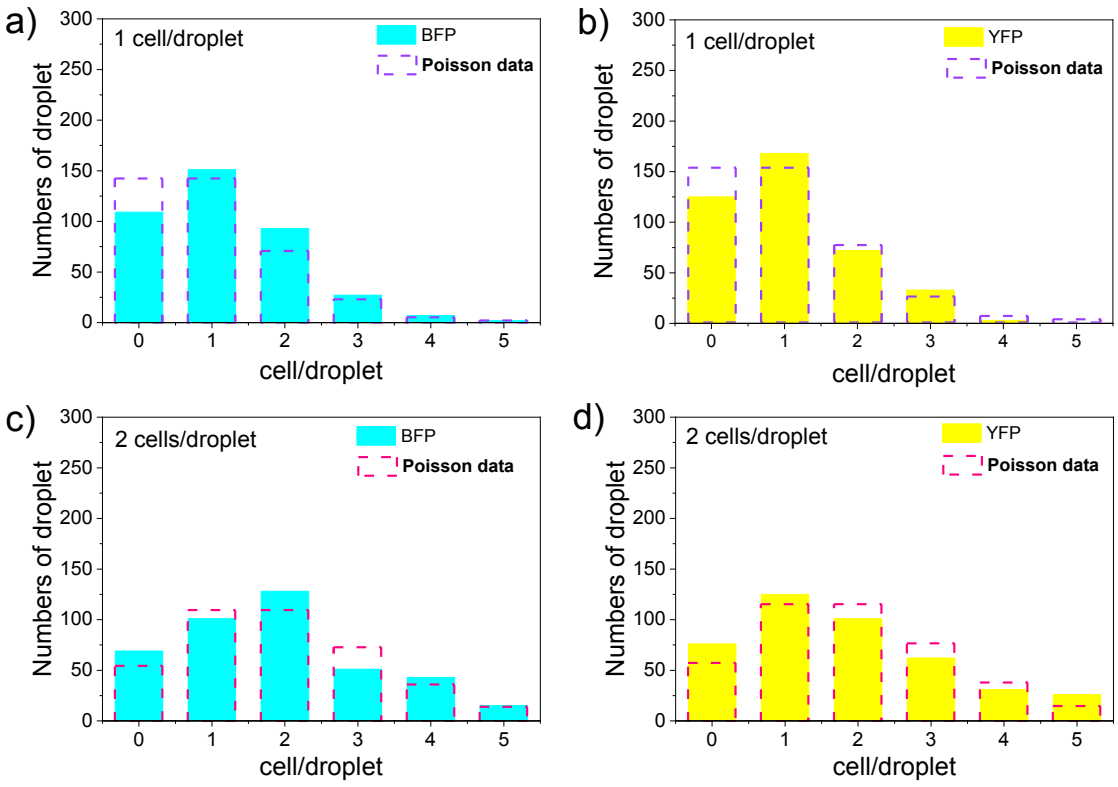

Figure 25: Cell distribution of *E. coli* BFP and *E. coli* YFP with 1 or 2 cells in each droplet compared with the theoretical values of the Poisson distribution (dash line). *E. coli* BFP with cell concentration of **a)** 1 cell/droplet and **c)** 2 cells/droplet. *E. coli* YFP with cell concentration of **b)** 1 cell/droplet and **d)** 2 cells/droplet.

The system-related instabilities also include pipetting precision error which may lead to

the variation of the encapsulation rate (inter-tests); inhomogeneity of the microbial distribution in the syringe during injection (intra-test; supported by magnet stirrer); time-dependent inhomogeneities of the pumping operation (intra-test; Cetoni system helps to minimize the flow rate variations).

4. Millifluidic Device Setup

5. Coexistence of Two Bacterial Strains in Millifluidic Droplet Reactors

5.1 Overview

Understanding the competition and cooperation within microbiota are of high fundamental and clinical importance, helping to comprehend species' evolution and biodiversity. In this chapter, two isogenic *E. coli* strains, which express blue (BFP) and yellow (YFP) fluorescent proteins, were co-encapsulated and cultured in numerous emulsion droplets. Their growth was quantified by employing fluorescence intensity measurements, as shown in **Figure 26**. The work in this chapter has been published in *Lab on a Chip* journal.[135]

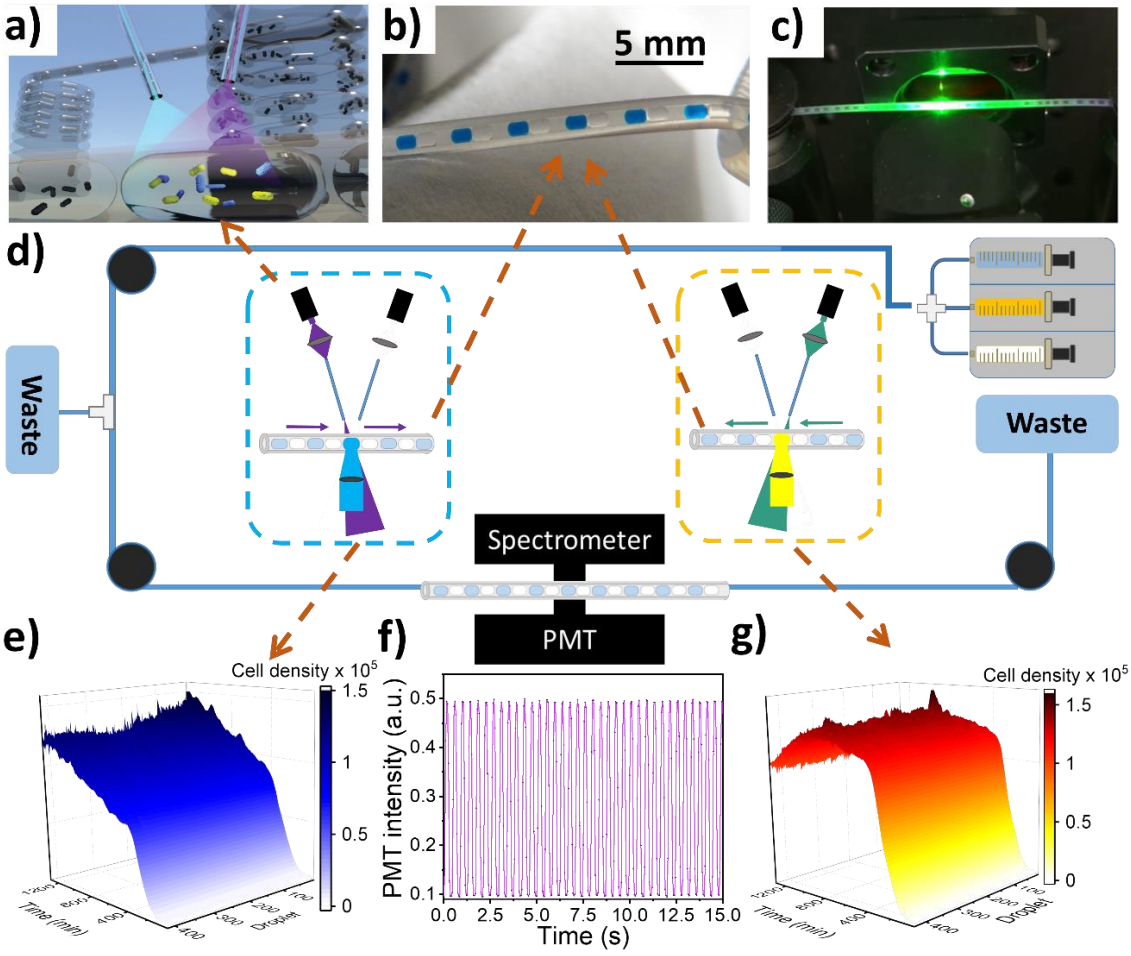

Figure 26: Sketch of setup. **a)** Monitoring *E. coli* growth in the droplets; **b)** A combination with water droplets (blue) and clear mineral oil droplet in the tubing; **c)** The optical fiber from the LED focus on tubing in the detection area; **d)** Sketch of setup with two detection modes; **e)** 3D growth curves of *E. coli* BFP detected under UV light when droplet sequence moving forward; **f)** The fluorescent signal caught up by PMT when droplet contains bacteria passing by the detector; **g)** *E. coli* YFP detected under Cyan LED light while droplet sequence moving backward.

We compared the experimental observations with predictions from a simple growth model to characterize and compare the bacterial growth kinetics and behavior in mono and co-culture. In addition, we varied the initial ratio (R_0) of both cell types injected and observed a broad landscape from competition to cooperation between both strains in their confined microenvironments depending on start frequency: from a nearly symmetric situation at $R_0 = 1$, up to the domination of one subpopulation when $R_0 >> 1$ (or $R_0 << 1$). Due to competition between the strains, their doubling times and final biomass ratios (R_1) continuously deviate from the monoculture behavior. The correlation map of the two strains' doubling times reveals that the R_0 is one of the critical parameters affecting the competitive interaction between isogenic bacterial strains. The droplet-based millifluidic allows monitoring different species of bacteria simultaneously in real-time. Furthermore, it has advantages of high statistical output, unaffected bacteria growth, and long-time measurements in a well-mixed environment. This strategy is expected to be utilized for practical clinical applications, such as bacterial antibiotic resistance and enzyme reaction kinetics studies.

5.2 Cell Culture in Droplets Analyzer

5.2.1 Cell Density Calculation by Biophotometer (OD_{600})

The growth curves and calculated doubling time of both strains measured by Biophotometer OD_{600} are displayed in **Figure 27**.

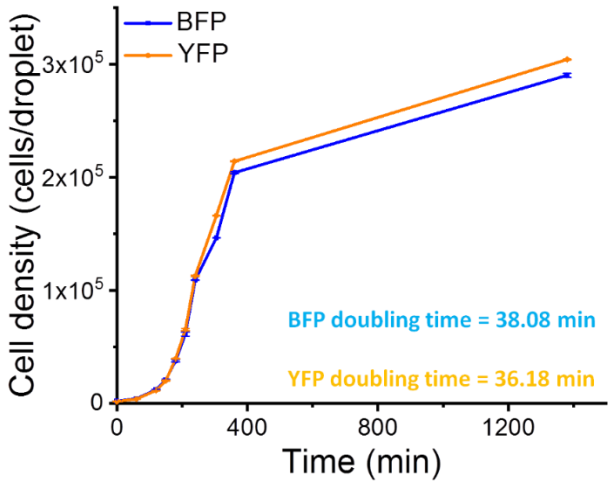

Figure 27: Growth curves of *E. coli* BFP (blue line) and *E. coli* YFP (yellow line) obtained by batch culture method and measured with OD_{600}. The doubling time of the two strains is marked.

The optical density of bacterial strains was measured every 60 min for both strains. From the 2nd h to the 4th h, the measurement was taken every 30 min. The final cell density of *E. coli* YFP reaches a high point around 1.5×10^9 cells/mL, slightly higher than *E. coli*

BFP 1.4×10^9 cells/mL. However, the doubling time of *E. coli* BFP is calculated to be 38.08 min, which is slower than *E. coli* YFP 36.18 min. Overall, the batch culture method results suggest the growth rate of *E. coli* YFP is greater than *E. coli* BFP. Besides, the final population size (cell density or number) of *E. coli* YFP is also slightly larger than *E. coli* BFP in the same culturing environment. Relative to other cultivation methods, the faster growth rate in the batch culture method is likely due to higher dissolved oxygen levels in flasks.

5.2.2 Cell Density Calculation by Droplet Analyzer

To describe the bacterial growth in the millifluidic device, we first calibrated the relationship between fluorescent signal and cell density for each strain. The calibration curves of cell density (cells/droplet)-fluorescent intensity were obtained by detecting bacterial medium fluorescence intensities with different dilutions with PMT (**Figure 28**). Calibration curves of the two bacterial strains are shown in the following **Equation 10** and **Equation 11**:

$$E.coli\ BFP\ (\frac{cells}{droplet}) = 2.9975\ \times 10^5 \times FDA - 2.7742 \times 10^4 \qquad (10)$$

$$E.coli\ YFP\ (\frac{cells}{droplet}) = 1.1995\ \times 10^6 \times FDA - 7.4108 \times 10^4 \qquad (11)$$

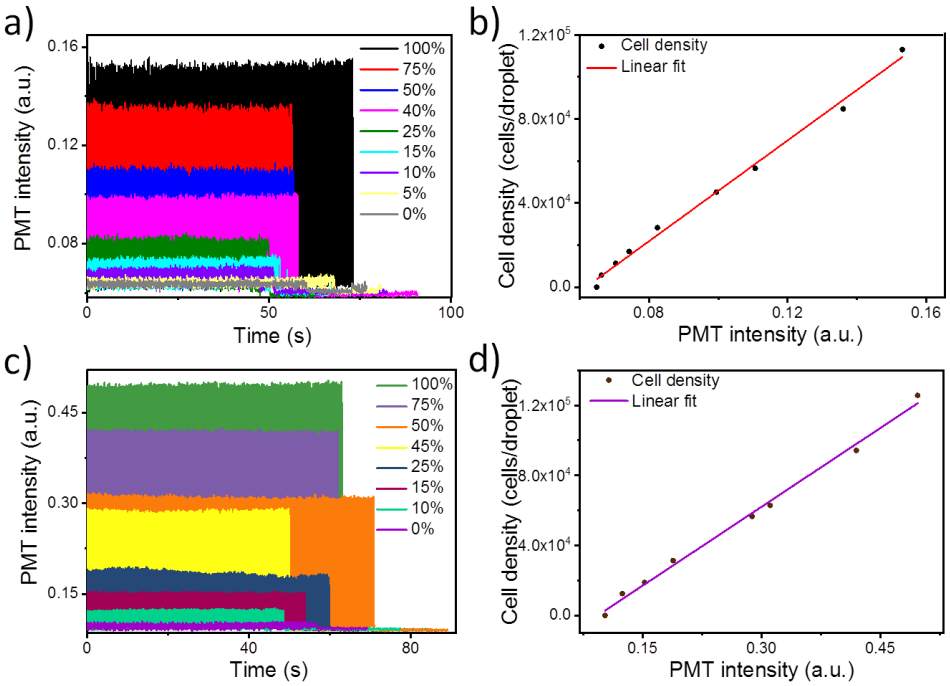

Figure 28: Calibration curves for Multiple Fluorescence Droplet Analyzer (MFDA) of *E. coli* BFP and *E. coli* YFP. *E. coli* BFP: **a)** Signals of several droplet sequences with a known concentration and **b)** the final calibration curve. *E. coli* YFP: **c)** signals of several droplet sequences with a known concentration and **d)** the final calibration curve.

According to the calibration curves, the limits of detection (LODs) of the droplets analyzer were determined as *E. coli* BFP around 5650 cells/droplet, and the LODs of *E. coli* YFP around 6000 cells/droplets.

5.2.3 Signal Cross Check in Droplet Analyzer

In order to prove there is no mixed signal between two strains' detection, the possibility of a signal cross was checked and compared with the single strain signal (**Figure 29)**.

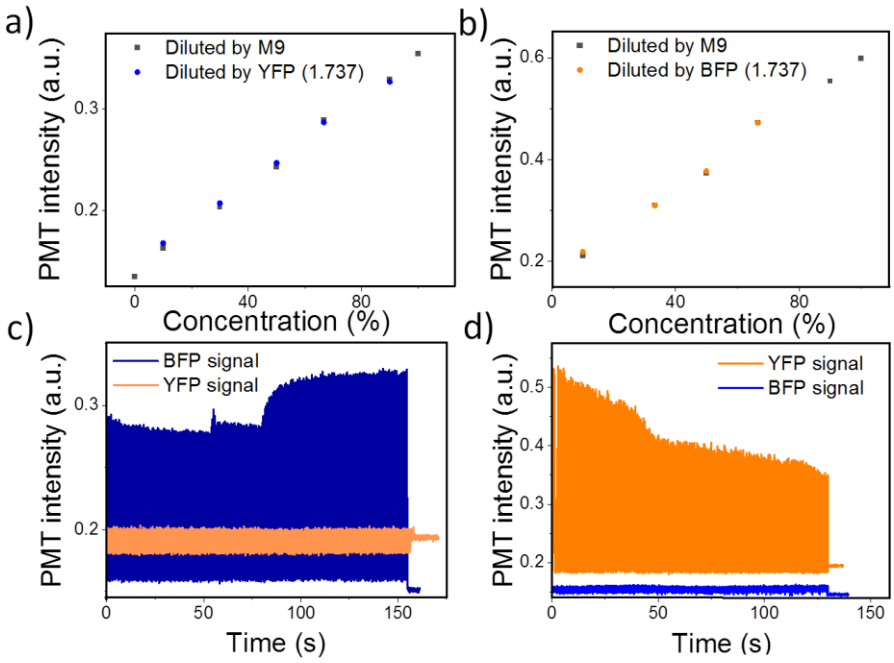

Figure 29: Comparison of single strain and mixed strains signal for FDA of *E. coli* BFP and *E. coli* YFP. **a)** BFP signal (black dots) with different concentrations diluted by M9 as the ratio of 9:1, 2:1, 1:1, 1:2, and 1:9 (the original BFP cell density OD_{600} = 1.737 A), and BFP signal (blue dots) with different concentrations mixed with YFP as the ratio 9:1, 2:1, 1:1, 1:2, and 1:9 (original BFP and YFP cell density are the same, OD600 = 1.737 A). **b)** YFP signal (black dots) with different concentrations diluted by M9 as the ratio of 9:1, 2:1, 1:1, 1:2, and 1:9 (the original YFP cell density OD_{600} = 1.737 A), and YFP signal (orange dots) with different concentrations mixed with BFP as the ratio 9:1, 2:1, 1:1, 1:2, and 1:9 (original BFP and YFP cell density are the same, OD_{600} = 1.737 A). **c)** The real-time signal of the droplet sequence contains *E. coli* BFP and *E. coli* YFP with the cell density ratio tuned from 100:1 to 900:1 and caught by two detection modes (the blue line represents BFP signal, the orange line represents YFP signal). **d)** The real-time signal of the droplet sequence contains *E. coli* BFP and *E. coli* YFP, with the cell density ratio tuned from 1:900 to 1:100 and caught by two detection modes (the blue line represents BFP signal, the orange line represents YFP signal.

The *E. coli* BFP solutions were diluted to the same concentrations by M9 and the original *E. coli* YFP solution, respectively (**Figure 29 a**). The *E. coli* BFP diluted with these two different solutions has the same intensity of the signal at the same dilution factors, indicating that the addition of *E. coli* YFP does not alter the *E. coli* BFP signal. Similarly, **Figure 29 b** demonstrates *E. coli* BFP does not affect the detection of *E. coli* YFP. In **Figure 29 c** and **d**, two bacterial strains' signal interference was examined using the extreme cell density ratio from 1:100 to 1:900. In both

assays, only the larger strains showed the signal changes that matched the calibration curve. In comparison, the smaller strains maintained the baseline level, demonstrating that the two assays' signals of co-cultured strains did not interfere with each other. The cross-tested results eliminate the possibility of signal interference and prove that the fluorescent signal can genuinely reflect the bacteria's growth status.

5.3 Two Bacterial Strains Monocultures Analysis

In this section, the reference growth curves of monoculture with various initial cell densities (from 1000 to 1 cell/ droplet) were first measured. To accurately describe bacteria's growth kinetics, we took the doubling time as an important parameter to describe the bacterial growth rate. It was calculated based on the growth model of J. Monod and the bacterial growth curves obtained from experimental results.[35, 136, 137]

5.3.1 Monoculture Growth Curves of Two Strains

After converting the PMT fluorescent intensity changing during the time to cell density changing during the time, the growth curves of *E. coli* BFP and *E. coli* YFP with different initial cell densities were obtained (the initial cell density means the initial inoculum cell concentration in each droplet), as shown in **Figure 30**.

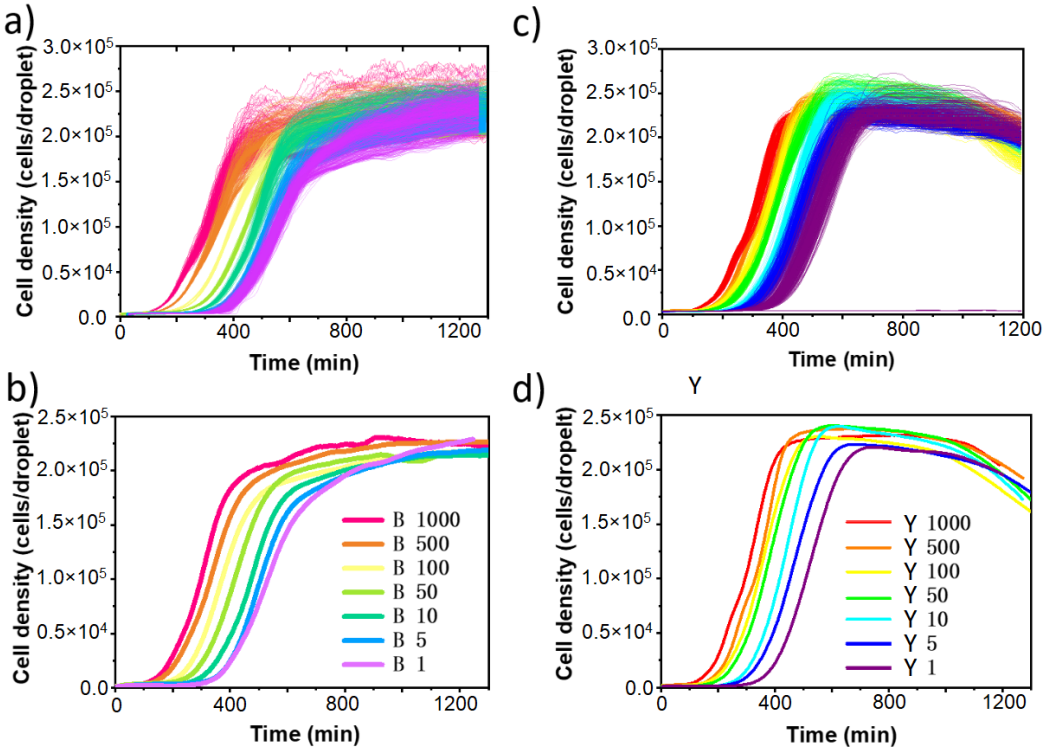

Figure 30: Growth curves and doubling time of *E. coli* BFP and *E. coli* YFP. **a)** The family and **b)** average growth curves of *E. coli* BFP monoculture with an initial cell density of 1000, 500, 100, 50, 10, 5, 1 cell/droplet; **c)** The family and **d)** average growth curves of *E. coli* YFP monoculture with an initial cell density of 1000, 500, 100, 50, 10, 5, 1 cell/droplet.

For both strains of *E. coli*, the growth curves with different initial cell densities have almost the same maximum cell density (Cmax). Interestingly, the Cmax of *E. coli* YFP is larger than *E .coli* BFP, similar to batch culture. The lag phase time shifts due to the LODs. Besides, the monoculture growth curves of *E. coli* BFP and *E. coli* YFP incubated and detected in 96 well plates with different initial cell densities are shown in **Figure 31** as a comparison. Due to the LODs, the lag phase shifting is also observed in the microplate results. Moreover, the bacteria incubated in the microplate grew slower than in the droplet reactor. Both microplate and droplet reactor demonstrates that the final population yield is slightly different for both strains (higher for YFP signal).

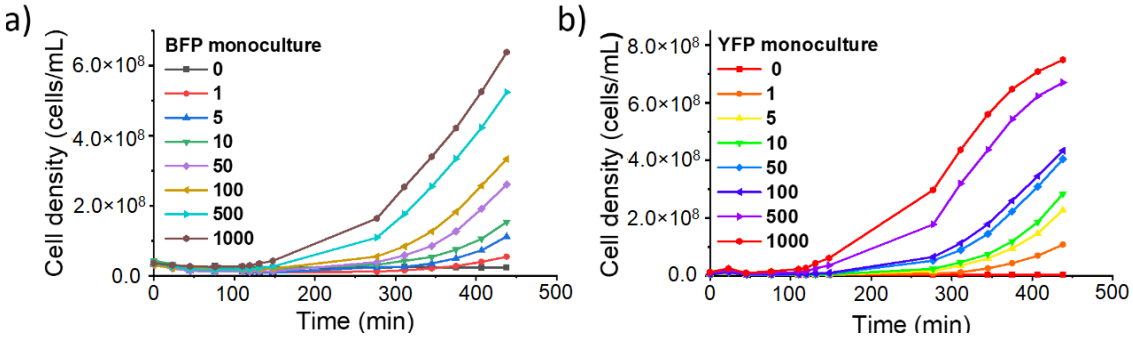

Figure 31: Comparison of the growth curves of two bacterial strains detected by plate reader. The growth curves of **a)** *E. coli* BFP monoculture with initial cell density of 0, 1, 5, 10, 50, 100, 500, and 1000 cells/droplet; **b)** *E. coli* YFP monoculture with initial cell density of 0, 1, 5, 10, 50, 100, 500, and 1000 cells/droplet.

5.3.2 Fluorescence Signal and the Cell Number Relationship Verification

Notable among the *E. coli* YFP monoculture growth curves is the decrease in fluorescence signal after 1000 min, which can be attributed to the photobleaching, and was not observed in the *E. coli* BFP case or the batch culture method.[138] Due to the limitation of nutrients in the medium and a long time shined under a light source, the YFP became unstable or even damaged. Especially when the cells were no longer dividing and replacing their fluorophores, the cells were aged. Their YFP activity decreased over time, leading to the drop of fluorescence intensity; thus, irreversible photobleaching occurred.[139]

The typical growth curve of *E. coli* is S-shaped (cell number vs. incubation time). Either optical density detection[140] or other detection methods such as electrical sensor[141] and our fluorescent millifluidic sensor, the cell number detected is the total number accumulation, but not the net live cell number. During the stationary phase, the number of new cells equals the number of dead cells so that there is no net increase in viable cells. The dead cells and new dividing cells accumulate together, making the growth curve slightly

increase in the stationary phase. This phenomenon was also observed from the obtained growth curves of other methods such as flow cytometry counting, optical density absorption analysis, and plate reader counting (in **Figure 32**). All the growth curves of *E. coli* BFP slightly go up in the stationary phase. In another word, all the methods mentioned here measured the accumulation of the total number of cells (both dead and alive), but not the net increase in viable cells. Except for the *E. coli* YFP growth curves measured by plate reader decline as the same as in millifluidic droplet reactor (both measured the fluorescence intensity), the *E. coli* YFP growth curves measured by other methods in the stationary phase have the same increase trend as *E. coli BFP*.

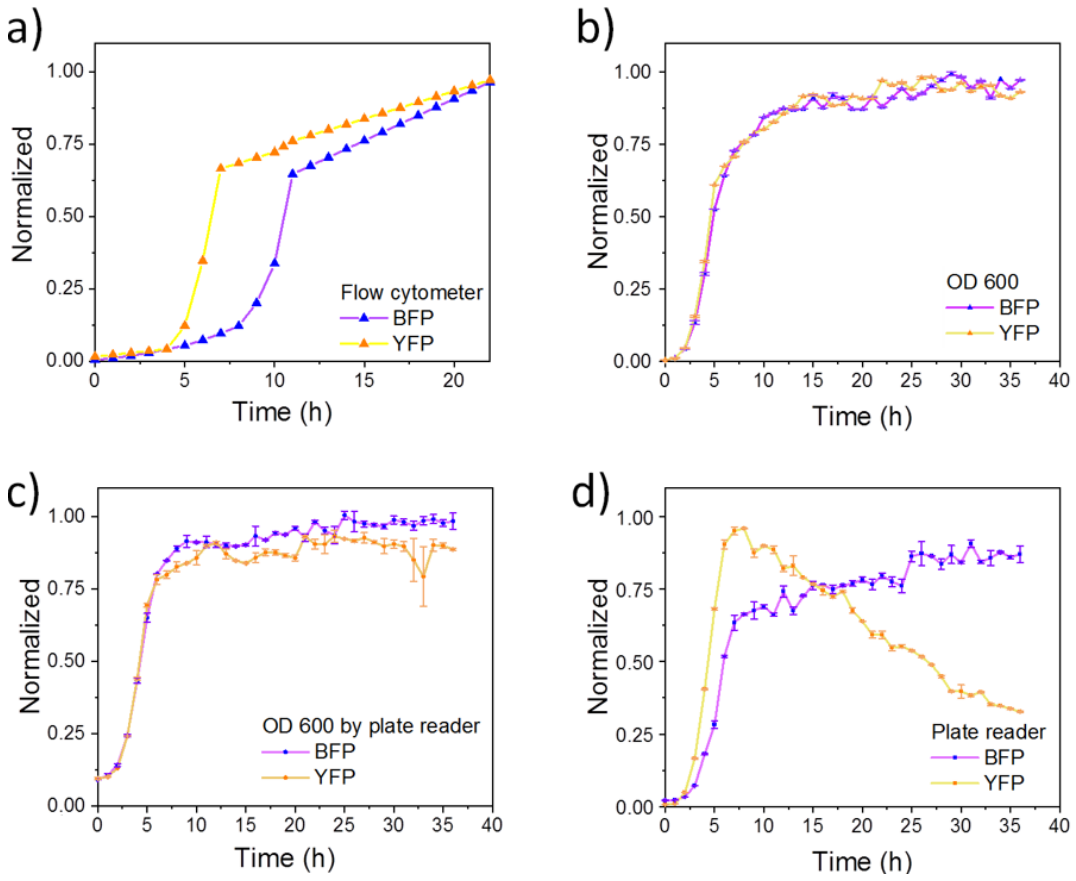

Figure 32: The growth curves of *E. coli* BFP (blue line) and *E. coli* YFP (yellow line) measured by **a)** flow cytometer, **b)** Biophotometer, **c)** plate reader measured optical density and **d)** plate reader measured fluorescence signal.

In **Figure 33**, compared to the Cmax of *E. coli* BFP (blue dotted line), the *E. coli* BFP incubated in PBS (light blue curves) remains unchanged in the stationary phase while going up in M9 media (purple curves). Moreover, compared to the Cmax of *E. coli YFP* (orange dash line), the *E. coli YFP* incubated in PBS (orange curves) slightly decreased but not as obvious as *E. coli YFP* in M9 decreased (yellow curves), might be due to the photobleaching happened stronger to dead cells than to alive cells. The signal difference between *E. coli* incubated in the M9 media and the PBS media is because after washing

and incubating bacteria by PBS media, the environmental effects were eliminated; for example, during the stationary phase, nutrients and oxygen levels were becoming depleted, the pH was changing, and toxic wastes were building up. Here is **Equation 12** to help explain the signal changing in the stationary phase:

$$Total\ cell\ accumulation = Death\ cell + Live\ cell \quad (12)$$

For *E. coli* BFP incubated in M9 media, death rate equals regeneration rate and they both increase in the stationary phase. Even though there was no net increase in viable cells, the total cell number increased, in purple curves. For *E. coli* BFP incubated in PBS media: no regeneration happened. The total cell accumulation did not change whether cells were dead or still alive (as light blue curves). For *E. coli* YFP incubated in M9 media: in the stationary phase, death rate = regeneration rate, the dead cell increased, but there was no net increase in viable cells. However, photobleaching happened from the beginning. In the death phase, the rate of cell death was faster than regeneration since photobleaching happened stronger to dead cells, so the total cell accumulation decreased faster and faster. For *E. coli* YFP incubated in PBS media: there was no regeneration. A slight decrease in the signal was due to the dead cell YFP photobleaching.

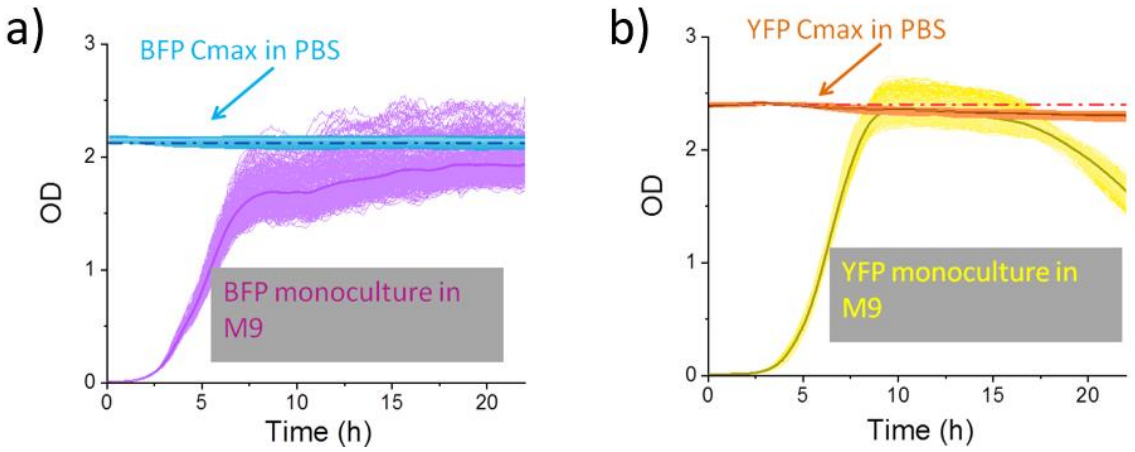

Figure 33: The changes in the fluorescence signals of *E. coli* incubated in different media in millifluidic device: **a)** the growth curves of *E. coli* BFP incubated in M9 media (purple curves) and PBS media (light blue curves, culturing *E. coli* in a flask to reach maximum cell concentration Cmax first and then centrifuging and incubating them into PBS medium with cell concentration of Cmax), and the Cmax of *E. coli* BFP (blue dash line); **b)** The growth curves of *E. coli* YFP incubated in M9 media (yellow curves) and PBS media (orange curves) and the Cmax of *E. coli* YFP (orange dash line).

The relationship between the fluorescence signals and the cell number was further verified in measuring pH value, cell size, and viable cell rate after incubating for 0, 9, 24, and 36 h. The results show that the cell size of both strains did not change during cultivation, while pH value and viable cell rate dropdown. Viable cell rates were checked

by plating dilutions on LB medium and counting colonies (by ImageJ) of live cell numbers and shown in **Figure 34**.

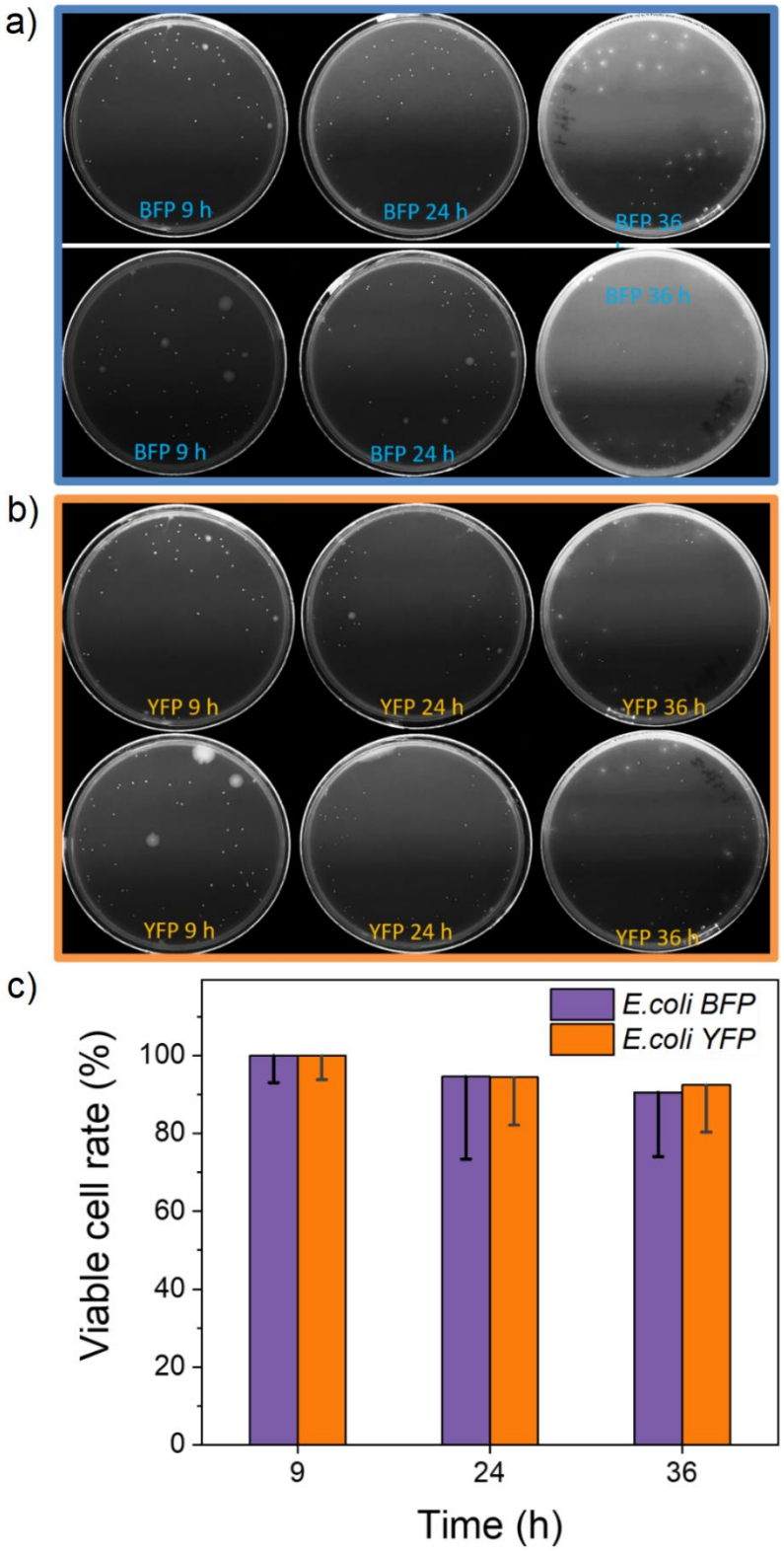

Figure 34: Comparison of viable cell rates of **a)** *E. coli* BFP, **b)** *E. coli* YFP, and **c)** their statistic after incubating bacteria for 0 h, 9 h, 24 h, and 36 h.

Cell size change was verified by observing and statistic bacterial cell length with the microscopy, and the results are presented in **Figure 35**. The results show that the cell

lengths of both strains remain at around 2 µm during the culture time.

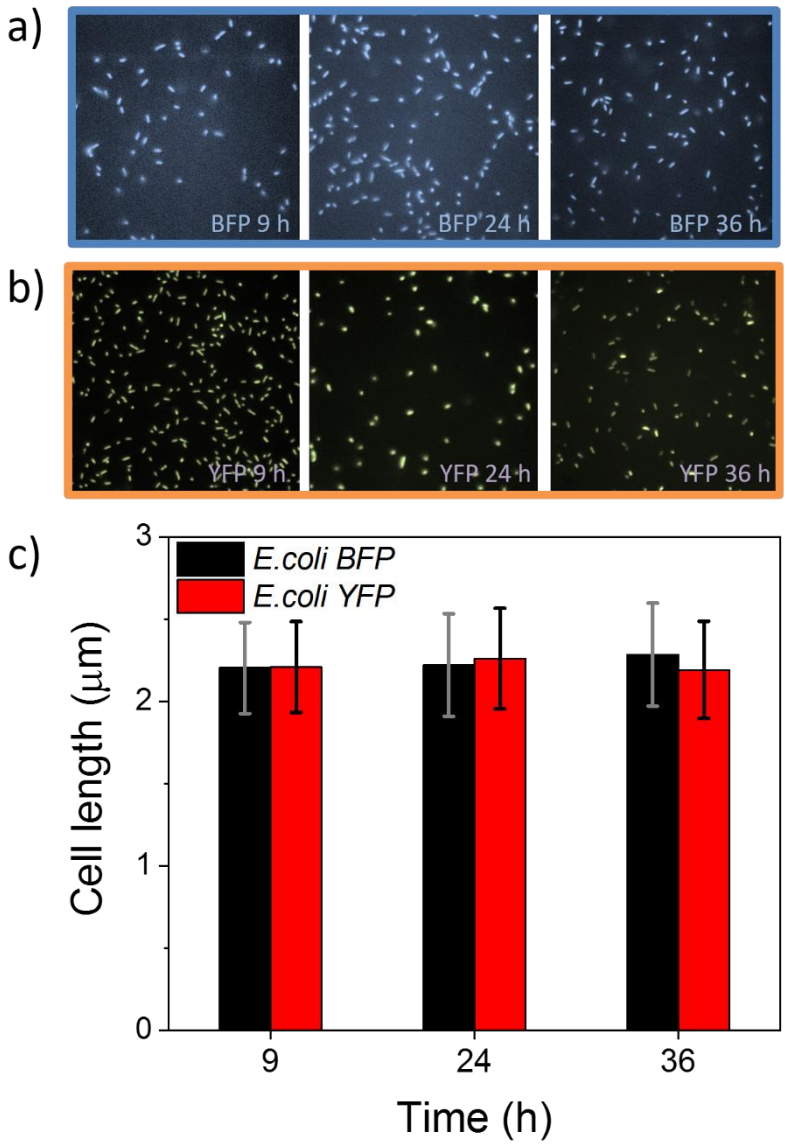

Figure 35: Comparison of cell size of **a)** *E. coli* BFP, **b)** *E. coli* YFP, and **c)** their statistic after incubating bacteria for 0 h, 9 h, 24 h, and 36 h.

However, the pH of the bacterial medium in droplets decreased during the incubation of both strains of *E. coli*, as shown in **Figure 36 a**. It shows the same overall trend as the bacterial medium in the batch culture method. Note that during the first 10 hours of the incubation, the pH drop was not substantial (from 7 to 6 pH), which supports that photobleaching has a negligible effect on the growth curves (taking into account the information that the pH value of the solution strongly influences the bleaching of the fluorophore). Moreover, the pH value and OD_{600} changed during incubating for 5 hours, showing the details of pH dropdown with cell growth. The differences in growth rate are due to subtle differences in metabolic costs involved in the expression of the fluorophores or perhaps differences in the rate at which they produce certain metabolites. This could well affect the pH, as shown in **Figure 36 b**. However, instead of preventing such pH

effects (*e.g.* by buffering the growth medium), the explicit purpose of this work is to allow the pH change or metabolic costs to affect the competitive growth dynamics of both strains differentially.[142, 143] It gives a way to demonstrate the utility of the millifluidic system for monitoring and analyzing competitive microbial dynamics in the context of a general growth model.

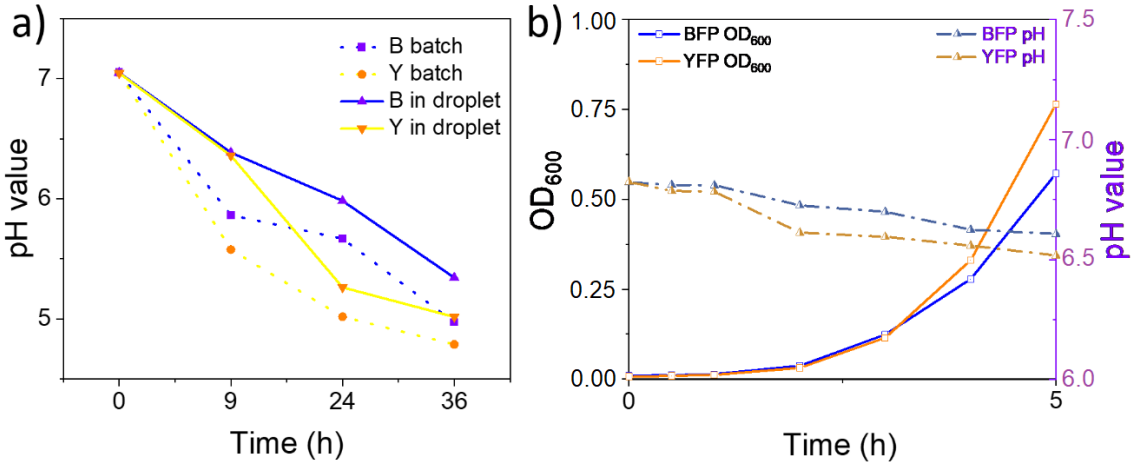

Figure 36: Comparison of **a)** pH value in batch culture and in droplets at the incubation time point of 0, 9, 24, 36 hours; **b)** pH value and OD_{600} in batch culture and in droplets during incubating for 5 hours.

Comparing the results obtained between different methods suggests these differences observed in the late stationary phases of YFP and BFP are associated with the various fluorophore stability and photobleaching rates. For instance, YFP fluorescent signal decrease is related to the degradation of the fluorescent protein, which is affected by the pH value, fluorescent lifetime, and cell state, but not the cell size.[144-147]

5.3.3 Doubling Time of Two Strains in Monoculture

According to the generation rate **Equation 13** in the exponential phase, the steepest slope was taken to calculate the growth rate in all growth curves.[148, 149]

$$Growth\ rate = \frac{log_2 N_b - log_2 N_a}{T_b - T_a} = \frac{log_2\left(\frac{N_b}{N_a}\right)}{T_b - T_a} \qquad (13)$$

Where N is the cell number (cells), T is the time point (min), a and b are present on the log scale cell number-time growth curve points.

Since,

$$N = C \times V = OD_{600} \times 5.1 \times 10^8 \times V = (c \times FDA \pm d) \times V \qquad (14)$$

So,

$$Growth\ rate\ = \frac{log_2\left(\frac{C_b}{C_a}\right)}{T_b - T_a} = \frac{log_2\left(\frac{OD_b}{OD_a}\right)}{T_b - T_a} = \frac{log_2\left(\frac{c \times FDA_b \pm d}{c \times FDA_a \pm d}\right)}{T_b - T_a} \quad (15)$$

C is the cell concentration or cell density. V is the volume of a droplet and calculated to be 200 nL. OD is the optical density of samples measured at a wavelength of 600 nm (A), c is the slope of calibration curves for FAD, and d is the intercept of calibration curves for FAD.

Finally, the doubling time is inversely proportional to the growth rate:

$$Doubling\ time\ (\tau) = Growth\ rate^{-1} \quad (16)$$

Here, the range of bacterial cell density used to calculate the doubling time is within FAD's calibration curve. Besides, the calibration curves were measured, starting from a cell density below the LODs.

Based on **Equation 14-16**, the doubling time of monoculture *E. coli* BFP and *E. coli* YFP with different initial cell densities in different methods were calculated. The results from the millifluidic device are shown in **Figure 37**.

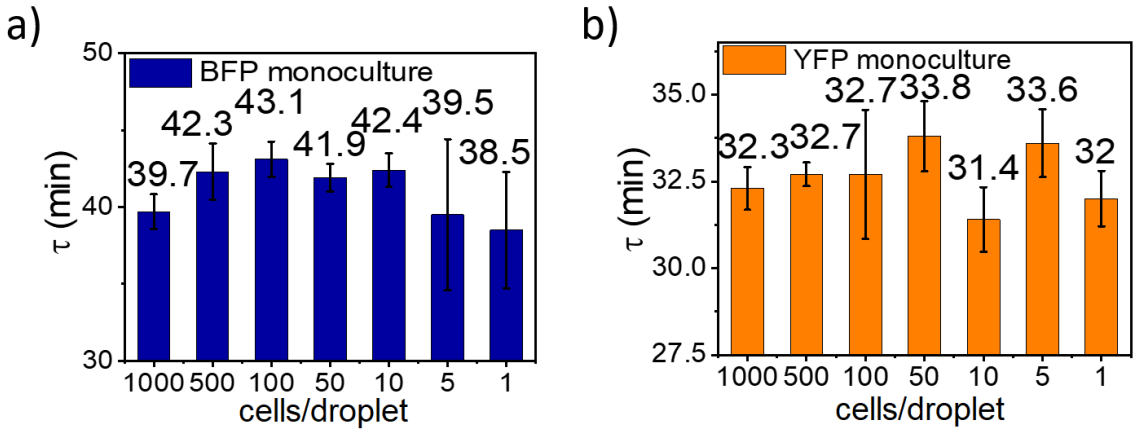

Figure 37: The doubling time of **a)** *E. coli* BFP and **b)** *E. coli* YFP with an initial cell density of 1000, 500, 100, 50, 10, 5, 1 cell/droplet (obtained in the millifluidic device). Error bars show the standard error of the mean.

From the doubling time results of the two strains, there is no significant difference between the doubling time of different initial cell densities. However, the doubling time of *E. coli* BFP is less than *E. coli* YFP, similar to the batch culture results. It indicates that the *E. coli* YFP grows faster than *E. coli* BFP when monocultures in the same environment. The exact cause of YFP growing faster than BFP is still unclear and could be due to an increased metabolic burden of the *mTagBFP2* protein. A previous study also

found that isogenic strains carrying the *mTagBFP2* protein are less fit than those carrying *SYFP2*.[150] Besides, the doubling time calculated from the microplate results also suggests the same trend and is presented in **Figure 38**. However, all the doubling times in 96 wells are slower than in other methods. This phenomenon is ascribed to poor mixing during culturing, which is unfavorable to bacterial growth.[151]

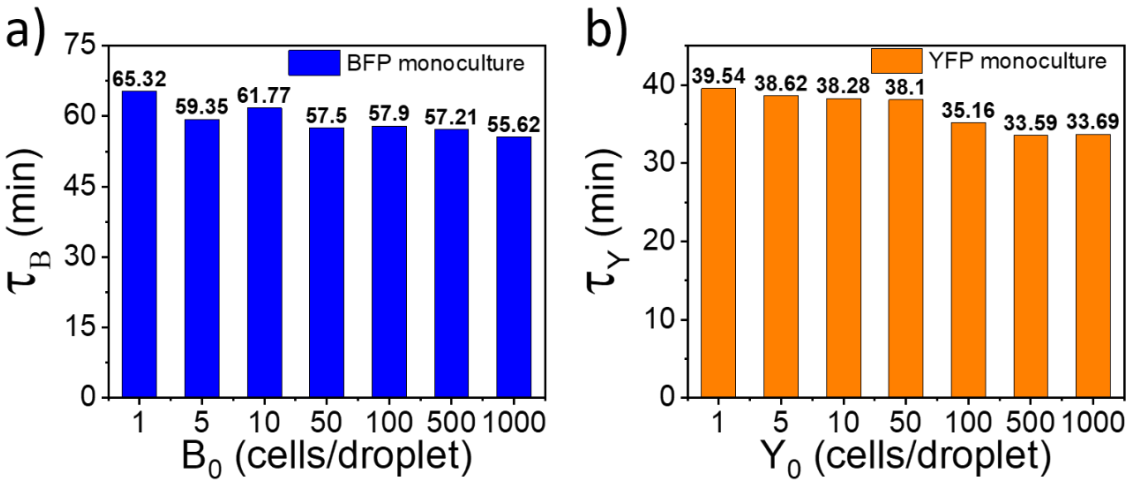

Figure 38: The doubling time of **a)** *E. coli* BFP and **b)** *E. coli* YFP monoculture with an initial cell density of 1, 5, 10, 50, 100, 500, and 1000 cells/droplet in 96 well plates.

5.4 Bacteria Co-culture with Different R_0

Compared to monocultures, a trade-off relationship is found in the co-cultures: (i) negative freq-dependent interactions for final biomass on growth rate and (ii) positive freq-dependent effects on growth rate.

To determine the competitive relationship between two bacterial strains, two *E. coli* strains were encapsulated into the droplets with a specific R_0 (the ratio between initial cell density of *E. coli* BFP B_0 and *E. coli* YFP Y_0). Then, the R_0 was taken as a variable from 10^{-3} to 10^3 for each parallel experiment by droplet-based millifluidic automatic setup, and the growth data was collected, as shown in **Figure 39**.[39, 40] The 'ratio' represents the proportion of *E. coli* BFP to *E. coli* YFP, and the 'fraction' is used to describe the proportion of *E. coli* BFP or *E. coli* YFP to the total co-culture cell density. Ratio $R_0 = 1$ was reached by injecting 1000 cells of each strain in droplets (1000:1000). Other values of R_0 were achieved by the serial decrease of the cell numbers of the other strain, down to the extreme value 1000:1 (and 1:1000) for BFP/YFP, respectively. Subsequently, the bacterial competition dynamics were comprehensively characterized by comparing the average doubling time and their variance, Cmax, R_1 (the ratio between

final cell density of *E. coli* BFP B_1 and *E. coli* YFP Y_1), ratio fold change, and competition coefficients.

Furthermore, by comparing different methods such as flow cytometry, photometer, plate reader, and co-culture curves modeling and prediction, the droplet-based reactor system is shown to precisely and efficiently track bacteria competitive dynamics. To avoid the influences of the photobleaching effects on competition studies, in the following, the growth curves of both strains were analyzed until the time frame when the stationary phase starts. Namely, the ratio R_1 was taken from the start point of the stationary phase (after culturing 10 hours).

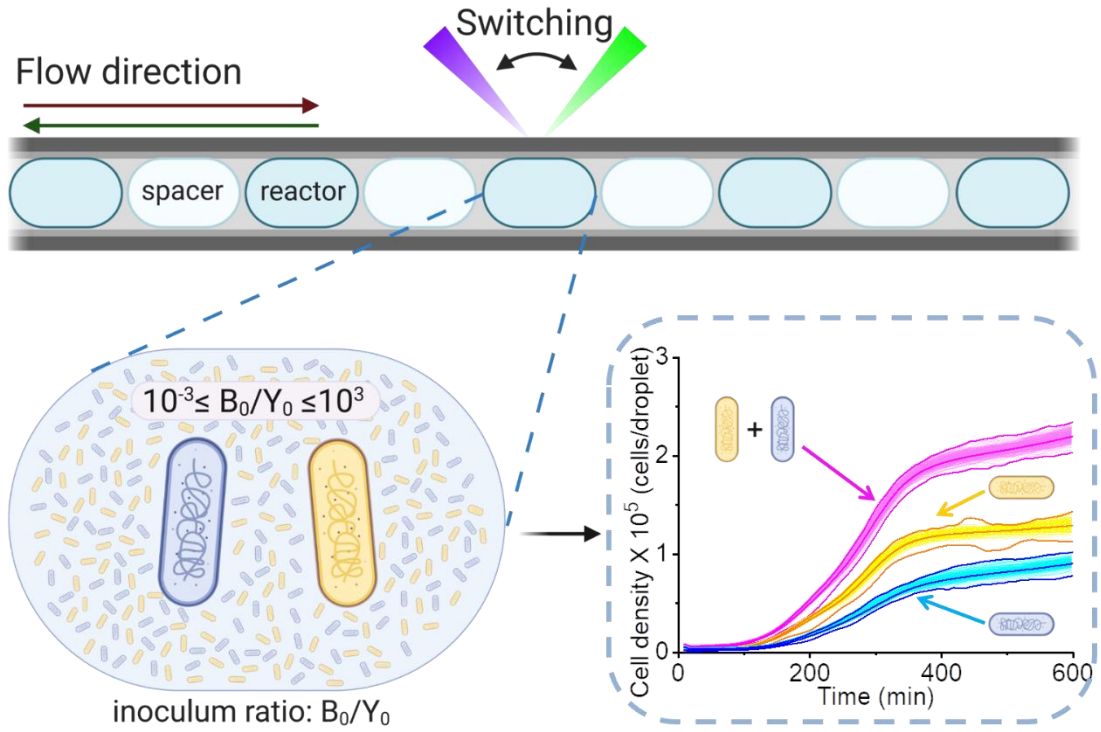

Figure 39: Schematic illustration of the millifluidic droplet-based reactor: monitoring the growth of co-cultured *E. coli* BFP and *E. coli* YFP with initial cell densities R_0 from 10^{-3} to 10^3.

5.4.1 Co-culture Growth Curves of Two Strains

By contrasting the growth curves of two strains and their combination under various R_0, the behavior changes of two strains can be intuitively observed, as presented in **Figure 40**. When $R_0 = 1$, the *E. coli* YFP appeared earlier and grew faster than *E. coli* BFP, as shown in **Figure 40 a**. This advantage was also observed in monoculture by photometer OD_{600}, millidroplet reactor, and plate reader (**Figure 27**, **Figure 30**, and **Figure 31**). However, when $R_0 = B_0/Y_0 > 2$, this advantage gradually disappeared with the further increase of R_0 (**Figure 40 (b-g)** for $R_0 > 1$, and **Figure 40 (h-m)** for the $R_0 < 1$). From the final combination of the growth curves, we observed all groups with different R_0 reached

a similar Cmax of around 2.5×10^5 cells/droplet, indicating that R_0 does not affect total final biomass. Notably, even in extreme ratios such as $R_0 = 10^3$ (**Figure 40 g**) or $R_0 = 10^{-3}$ (**Figure 40 m**), the bacterial strain with lower initial frequency can still survive.

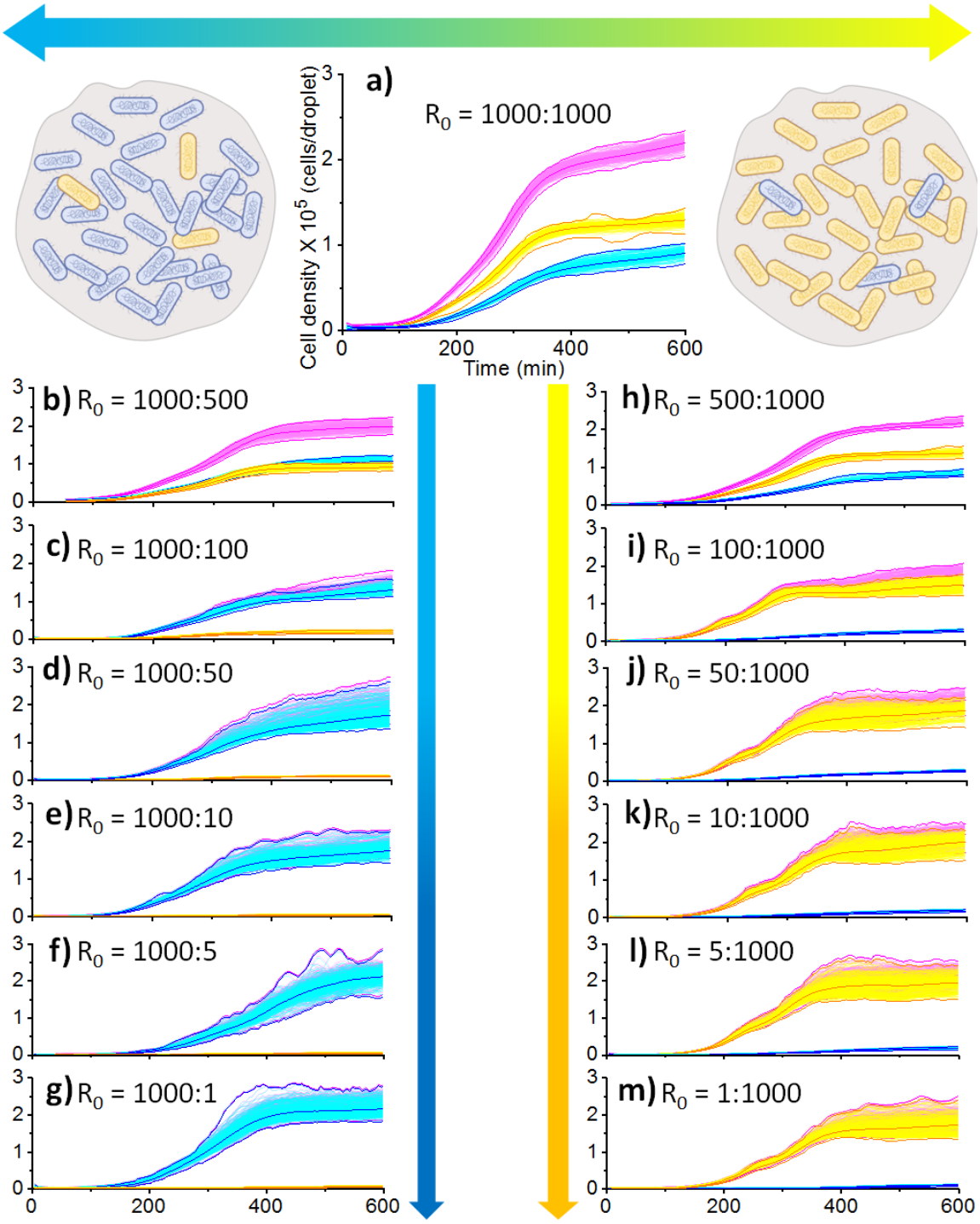

Figure 40: The combination (pink lines) of *E. coli* BFP (blue lines) and *E. coli* YFP (yellow lines) co-culture growth curves. The R_0 of *E. coli* BFP: *E. coli* YFP are **a)** 1000:1000, **b)** 1000:500, **c)** 1000:100, **d)** 1000:50, **e)** 1000:10, **f)** 1000:5, **g)** 1000:1, **h)** 500:1000, **i)** 100:1000, **j)** 50:1000, **k)** 10:1000, **l)** 5:1000, **m)** 1:1000.

The co-culture growth curves were also obtained by incubating *E. coli* BFP and *E. coli* YFP with various initial ratios in 96 well plates, as shown in **Figure 41**. When the initial

cell density of *E. coli* YFP Y_0 is a constant as 1000 cells/droplet, the growth curves of *E. coli* BFP have a significant change by increasing the initial cell density of *E. coli* BFP B_0 (**Figure 41 a**). But when B_0 is a constant as 1000 cells/droplet, the growth curves of *E. coli* BFP have a much smaller change by tuning the Y_0 (**Figure 41 c**). A similar phenomenon can be found by comparing **Figure 41 b** and **Figure 41 d**. In addition, in the same duration, the *E. coli* YFP has greater cell densities than *E. coli* BFP.

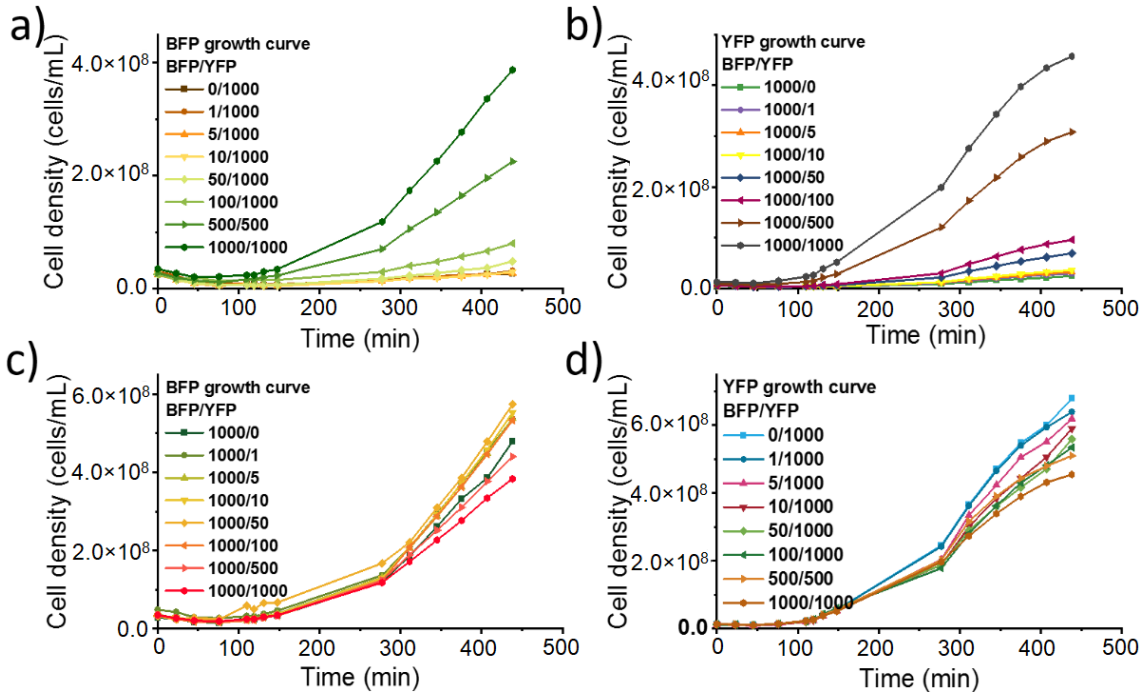

Figure 41: Comparison of the growth curves of two bacterial strains obtained with the plate reader. The growth curves of **a)** *E. coli* BFP with initial cell density of 1, 5, 10, 50, 100, 500, and 1000 cells/droplet co-culture with 1000 cells/droplet of *E. coli* YFP; **b)** *E. coli* YFP with initial cell density of 1, 5, 10, 50, 100, 500, and 1000 cells/droplet co-culture with 1000 cells/droplet of *E. coli* BFP; **c)** 1000 cells/droplet initial cell density of *E. coli* BFP co-culture with 1, 5, 10, 50, 100, 500, and 1000 cells/droplet *E. coli* YFP; **d)** 1000 cells/droplet initial cell density of *E. coli* YFP co-culture with 1, 5, 10, 50, 100, 500, 1000 cells/droplet *E. coli* BFP.

5.4.2 Predict Co-culture Growth Curves by Modeling

Based on the monoculture and co-culture growth curves of two *E. coli* strains, the co-culture growth curves were predicting by modeling and compared to experimental data, as shown in **Figure 42**. The monoculture model (Baranyi-Robert model[85], see **Equation 2-3** in *Paragraph 2.2.2*) was first fitted to monoculture growth experimental data, then the co-culture model (2-strain Lotka–Volterra competition models[87], see **Equation 4-6** in *Paragraph 2.2.2*) to co-culture experimental combination data.

The relative co-culture growth of both strains was predicted by using the estimated growth and competition parameters with the Python code programmed by Y. Ram *et al.*[152] For most of the prediction curves, the Cmax (the final cell density at T = 10 hours) reaches a

similar level as the experimental results. All the estimated growth curves of *E. coli* BFP match relatively well with the experiment results. The *E. coli* YFP has a longer lag time ($R_0 \leqslant 1$) and less Cmax (R_0 from 100 to 10) in prediction results. The similar growth curves of experimental data and modeling results indicate the reliability of the millifluidic droplet reactors in the application of monitoring co-existent bacterial growth.

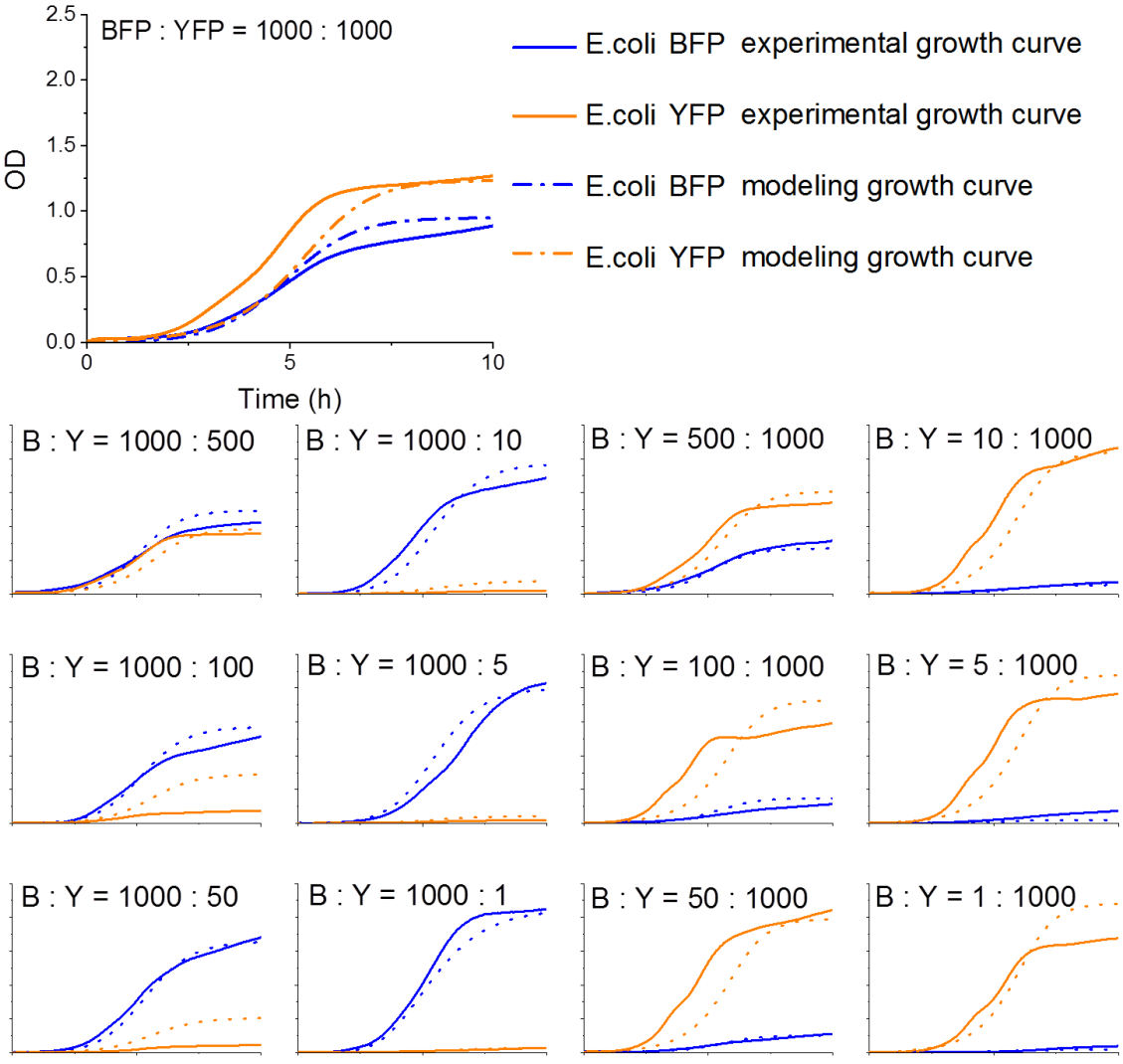

Figure 42: Comparison of experimental growth curves and modeling growth curves of co-culture *E. coli* BFP and *E. coli* YFP.

5.5 Biomass Ratios at the Beginning of the Stationary Phase

The comparison of R_1 (the biomass ratios at the beginning of the stationary phase) with R_0 shows how the composition of two strains changes with different R_0. From the experimental and modeling results (**Figure 43**), the larger R_0 leads to a larger R_1, but $R_1 = R_0$ is the "null expectation" when competitive interactions between both strains do not affect fitness, *i.e.* the ratio of Malthusian parameters = 1.

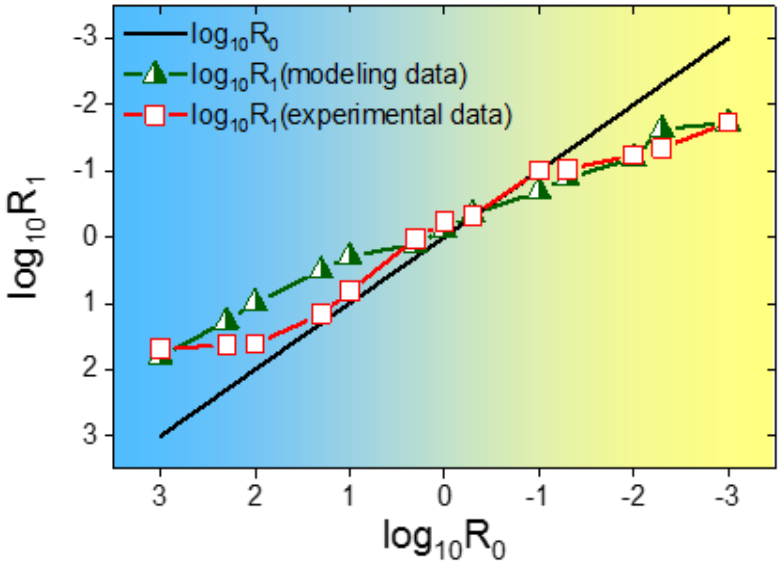

Figure 43: Comparison of biomass R_1 at the beginning of the stationary phase ($R_1 = B_1/Y_1$) between two strains of *E. coli* with different R_0.

This can also be proven by counting the final cell numbers of *E. coli* BFP and *E. coli* YFP with $R_0 = 1$ after co-culturing for 10 hours (**Figure 44**).

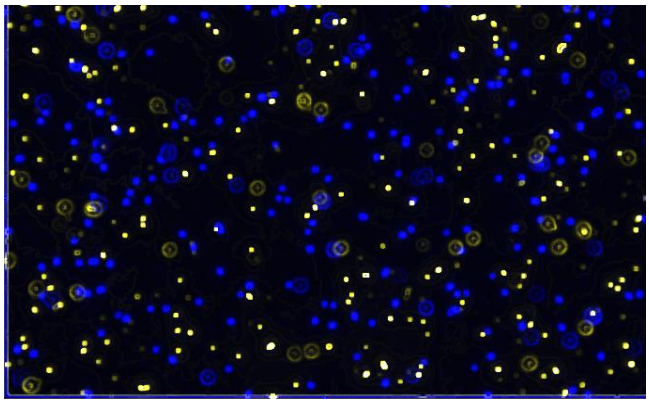

Figure 44: The merged graph of *E. coli* BFP and *E. coli* YFP observed with a fluorescence microscope excited by UV light and blue light separately with a magnification of 100×.

The co-culture group with $R_0 = 1$ was observed with fluorescence microscopy with a magnification of 100×. No clumps of two strains were observed, and the R_1 is calculated to be 0.798.

When R_0 is scaled from 10^3 to 10^{-3} ($\log_{10}R_0$ is from 3 to -3), R_1 constantly reduces and shows a trend to narrow the gap of population size (cell density or number) between the two strains, indicating a negative frequency-dependent effect on yield for both strains (the lower the relative initial frequency, the higher its comparable yield). When $R_0 = 1$ ($\log_{10}R_0 = 0$), $R_1 = 0.579$, suggesting that *E. coli* YFP is more fit than *E. coli* BFP in a co-culture environment. Furthermore, the same trend observed with droplet reactor and modeling

results indicates that the millifluidic droplet strategy has an excellent ability to track bacterial strains and reflect their growth in co-culture separately.

From R_0 = 1 to 10^3 or to 10^{-3}, the initial fraction between *E. coli* BFP and *E. coli* YFP becomes more and more unmatched; a clear asymmetry between the R_1 shows up and constantly amplifies as more clearly described in **Figure 45**. From R_0 = 1 to 10^3 or to 10^{-3}, the ratio fold change reverses from negative to positive, but its absolute value increases all along. In other words, the lower the relative initial frequency, the higher its relative yield. To sum up, the competition hierarchy inversion occurred between two strains and constantly approached the stable coexistence.

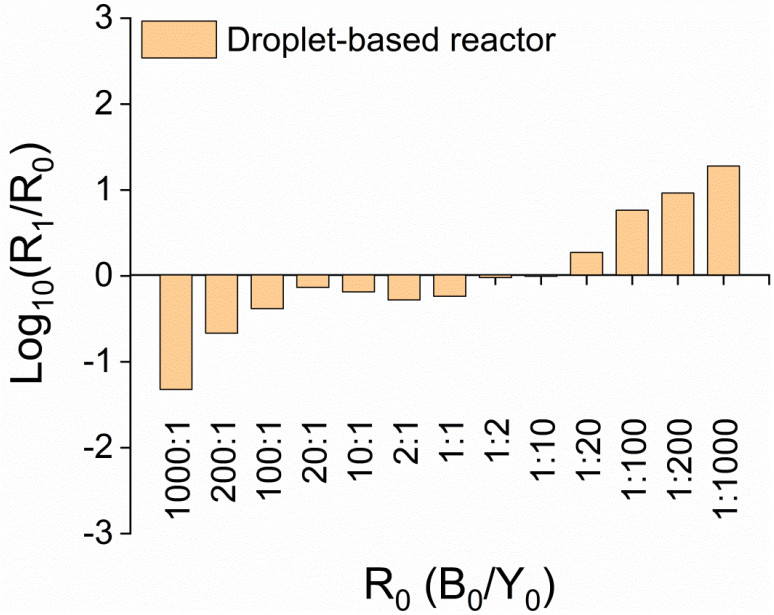

Figure 45: The relationship between ratio fold change $\log_{10}(R_1/R_0)$ and R_0. $R_0 = B_0/Y_0$, the initial biomass ratio between *E. coli* BFP and *E. coli* YFP; $R_1 = B_1/Y_1$, the biomass ratio (at the beginning of stationary phase) between *E. coli* BFP and *E. coli* YFP.

To demonstrate that the negative frequency-dependent effect on yield for both strains was caused by R_0 and not by the droplet-based reactor method, the R_1 was detected with different devices such as fluorescence flow cytometry (**Table 10**) and plate reader (**Table 11**) and compared in **Figure 46**.

Table 10: Cell numbers and R_1 with different R_0 measured by a fluorescence flow cytometry.

R_0	B_1	Y_1	R_1
1000:1	325	11	29.545
1000:5	391	14	27.929
1000:10	331	13	25.462
1000:50	70	7	10.000
1000:100	90	15	6.000

1000:500	81	31	2.613
1000:1000	113	137	0.825
500:1000	22	22	1.000
100:1000	22	61	0.361
50:1000	55	199	0.276
10:1000	14	138	0.101
5:1000	24	161	0.149
1:1000	16	132	0.121

Table 11: Cell densities and R_1 with different R_0 measured by a plate reader.

R_0	B_1 10^8 (cell/mL)	Y_1 10^8 (cell/mL)	R_1
1000:1	5.360	0.299	17.925
1000:5	5.370	0.325	16.502
1000:10	5.530	0.365	15.126
1000:50	5.740	0.696	8.246
1000:100	5.330	0.959	5.555
1000:500	4.400	3.080	1.429
1000:1000	3.870	4.550	0.851
500:1000	2.250	5.110	0.441
100:1000	0.800	5.350	0.150
50:1000	0.484	5.600	0.086
10:1000	0.297	5.900	0.050
5:1000	0.277	6.190	0.045
1:1000	0.312	6.390	0.049

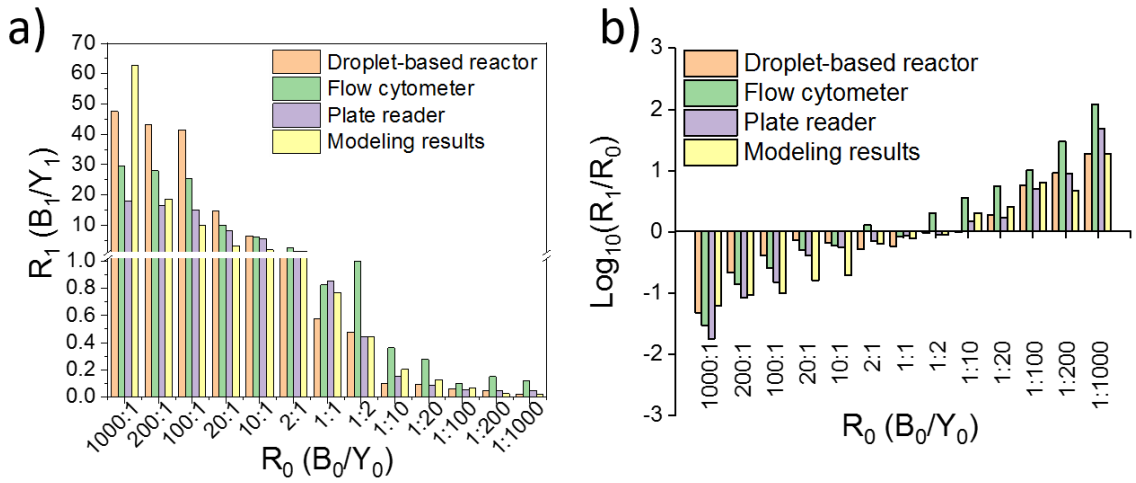

Figure 46: Comparison of R_1 and R_0 between two strains of *E. coli* measured by different methods. **a)** The R_1 changes with various R_0; **b)** The relationship between ratio fold change $\log_{10}(R_1/R_0)$ and R_0.

5.6 Doubling Time of Two Strains in Co-culture

Unlike in the monoculture case, the doubling time of both *E. coli* strains changed in the co-culture case with different R_0 (**Figure 47**), which is similar to final biomass that varies with the change of the R_0.

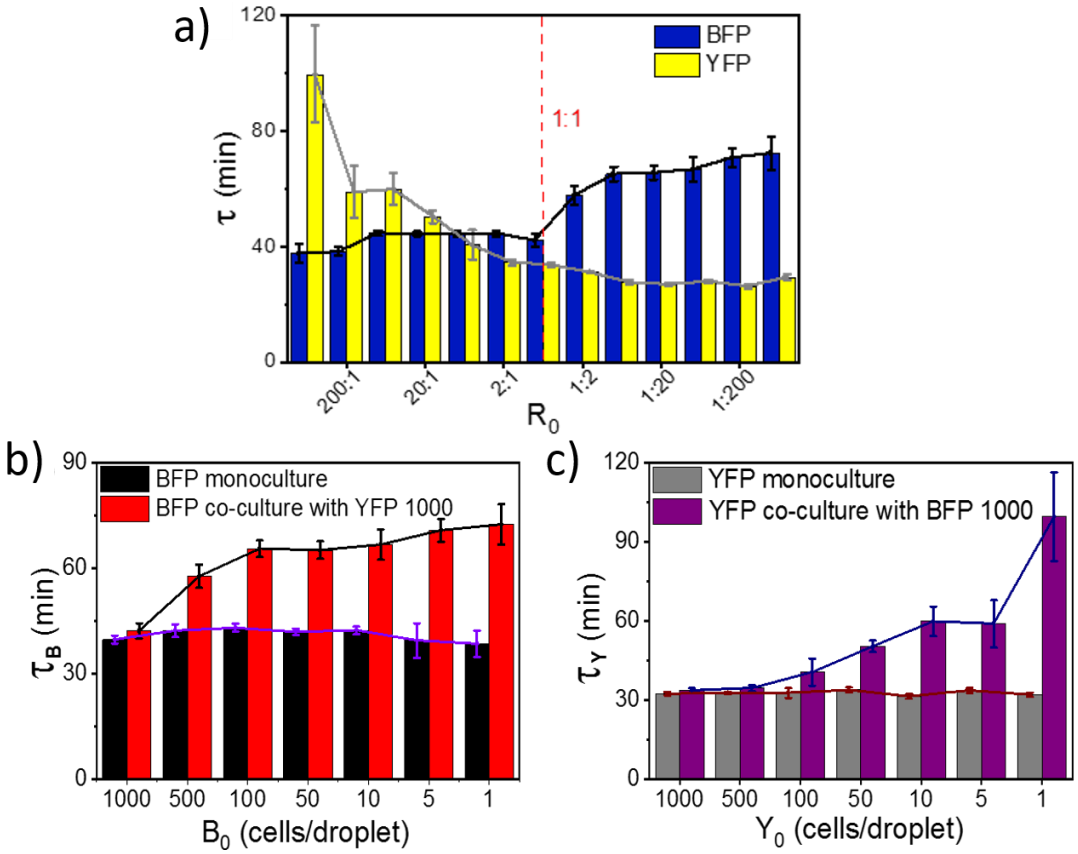

Figure 47: Comparison of doubling time between two strains of *E. coli* with different R_0: **a)** doubling time of each strain in co-culture as a function of R_0; **b)** doubling time of *E. coli* BFP with different initial cell densities in a monoculture environment and co-culture with initial cell density 1000 cells/droplet *E. coli* YFP; **c)** doubling time of *E. coli* YFP with different initial cell densities in a monoculture environment and co-culture with initial cell density 1000 cells/droplet *E. coli* BFP. Error bars show the standard error of the mean.

Relative to the monoculture, adding another bacterial strain in a co-culture environment reduces the growth rates of both strains to varying degrees. The magnitude of this effect depends on the R_0. Remarkably, the doubling time τ of *E. coli* YFP is lower than that of *E. coli* BFP, even when R_0 equals 10. However, once the inoculated cell number of the slower strain *E. coli* BFP is higher than those of YFP ($R_0 > 1$), doubling time τ_B does not change substantially, while τ_Y increases as superlinear (**Figure 48 a**). In the opposite case, once *E. coli* YFP dominates ($R_0 << 1$), τ_Y stays unchanged at a certain value, while τ_B reveals slow quadratic function growth (**Figure 48 b**).

For *E.coli* BFP, the function is close to polynomial function, and *E.coli* YFP is close to power functions:

$$y = -14.447x^3 + 54.192x^2 - 68.67x + 70.365\ (E.coli\ BFP, R^2 = 0.9423) \quad (17)$$

$$y = -27.949x^{-0.17}\ (E.coli\ YFP, R^2 = 0.9748) \quad (18)$$

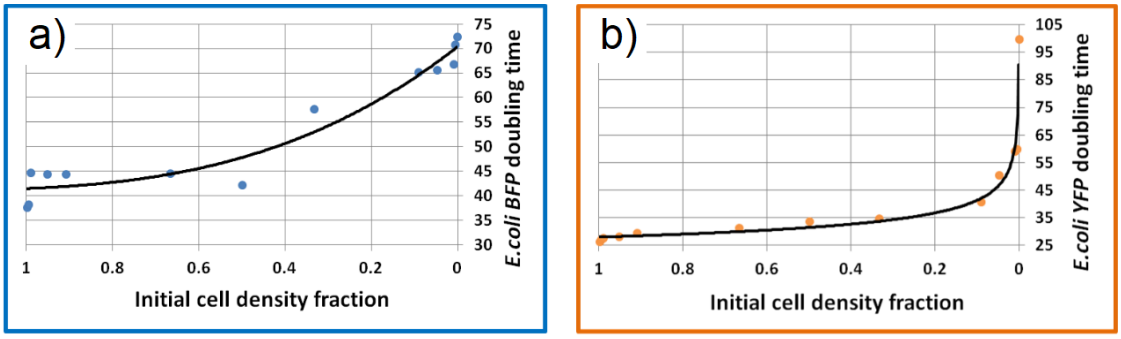

Figure 48: The development of doubling time changing with the decrease of initial cell density fraction: **a)** *E. coli* BFP and **b)** *E. coli* YFP.

It seems that the larger initial fraction bacterial strain becomes dominant with its fraction increasing.[153] Based on these results, it is speculated that the larger initial cell density helps the bacteria get more access to the nutrients for their cell division efficiently. The adding of other strains does not influence its doubling time much. Conversely, the growth of the fewer fraction bacteria is affected more and more when its fraction decreased. The doubling time was further checked by culturing bacteria in 96 wells plates and measuring in the plate reader (**Figure 49 a**), as well as compared to the doubling time obtained from co-culture prediction results (**Figure 49 b**). All results reveal similar patterns as in the droplet analyzer. But all the doubling times in 96 wells are slower than in other cultures and detect methods. This phenomenon is ascribed to poor mixing during culturing, which is unfavorable to bacterial growth.[45]

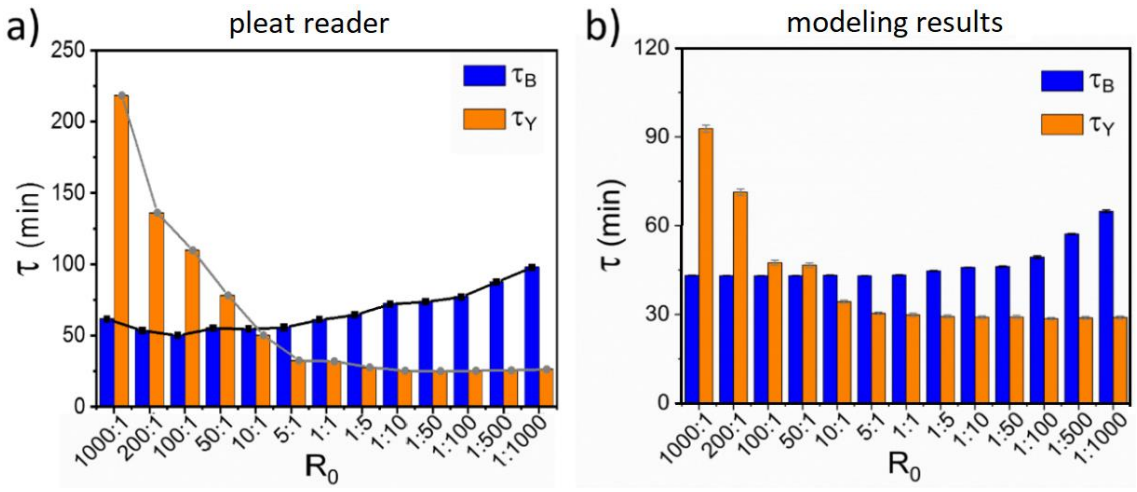

Figure 49: Comparison of doubling time between two strains of *E. coli* with different R_0 from 10^3 to 10^{-3} **a)** measured by a plate reader and **b)** modeling results.

5.7 Competition Coefficient Calculation

The competition coefficient was calculated with the ratio of the Malthusian parameters[154] of the co-culture and monoculture:

$$C_{by}(effect\ of\ E.coli\ YFP\ on\ E.coli\ BFP) = \frac{\ln[(N_{b,co-culture,t=12\ h})/(N_{b,co-culture,t=0\ h})]}{\ln[(N_{b,monoculture,t=12\ h})/(N_{b,monoculture,t=0\ h})]} \quad (19)$$

$$C_{yb}(effect\ of\ E.coli\ BFP\ on\ E.coli\ YFP) = \frac{\ln[(N_{y,co-culture,t=12\ h})/(N_{y,co-culture,t=0\ h})]}{\ln[(N_{y,monoculture,t=12\ h})/(N_{y,monoculture,t=0\ h})]} \quad (20)$$

Where N_b is the cell number of *E. coli* BFP in either monoculture or co-culture case after incubating few hours; N_y is the cell number of *E. coli* YFP in either monoculture or co-culture case after incubating few hours. If C_{by} = 1, means *E. coli* YFP does not affect *E. coli* BFP, and *E. coli* BFP grows similar in monoculture compared to co-culture; C_{by} < 1: *E. coli* BFP is negatively affected by *E. coli* YFP; C_{by} > 1: *E. coli* BFP is positively affected by the presence of *E. coli* YFP. According to the competition coefficient **Equation 19** and **Equation 20**, the competition coefficients (C_{by} and C_{yb}) between two co-culture strains were calculated and compared from experimental data and modeling data (**Figure 50**).

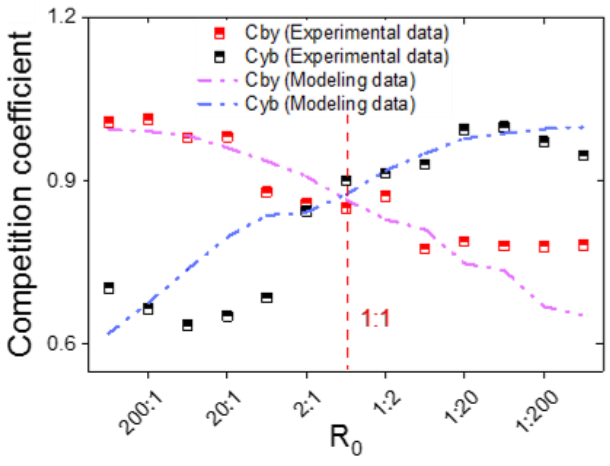

Figure 50: Comparison of the competition coefficients calculated based on experimental data and modeling data.

As R_0 decreased, C_{by} and C_{yb} show diametrically opposite and symmetrical trends. It indicates that the strain with a higher initial frequency suppresses the growth of the other

strain. Remarkably, this unequal effect strengthens with R_0 change from 1 to extreme ratios of 10^3 or 10^{-3}.

5.8 Competition Distribution Map

To more intuitively display how the R_0 affects the relationship between two *E. coli* strains, the doubling time of two strains from each droplet is presented in a two-dimensional (2D) distribution map.[36] Lower doubling times mean a faster growth rate, which leads to a competitive advantage. The 2D distribution map is divided into four regions by the average monoculture doubling time of each strain (blue dotted line and yellow dotted line), as shown in **Figure 51 a**. As a result of the competition for resources, one strain's growth can be affected by the other due to nutrients domination, toxic releasing, or even predation.[11]

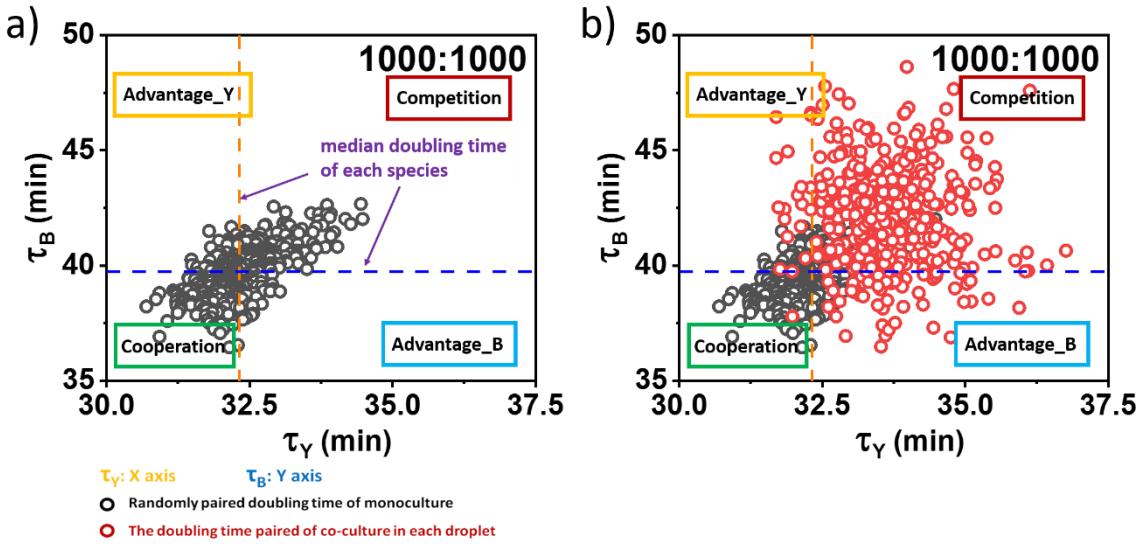

Figure 51: Correlation between doubling time of the two strains of *E. coli*: **a)** monoculture (black dots, randomly paired) and **b)** co-culture in the droplets (red dots) with R_0 of *E. coli* BFP: *E. coli* YFP = 1000:1000.

Table 12: The doubling time of two *E. coli* strains change in four regions of the 2D distribution map.

Region	Doubling time τ	
	τ_Y	τ_B
Cooperation	↓	↓
Advantage_Y	↓	↑
Advantage_B	↑	↓
Competition	↑	↑

The four regions are named Cooperation, Advantage_Y, Advantage_B, and Competition, based on the relative doubling times of both strains. If co-culture results in a shorter doubling time than monoculture for both strains, it is an indication that they are benefiting from each other's cooperation; hence this region is called 'Cooperation'. Vice versa situation named as 'Competition' as summarized in **Table 12**. Compared to the monoculture clouds (black dots, randomly paired of the monoculture doubling time of the two *E. coli* strains, shown in **Figure 51 a**), the co-culture clouds (red dots, doubling time of the two *E. coli* strains from each droplet were paired) shifted to the direction of the competition region, as shown in **Figure 51 b**.

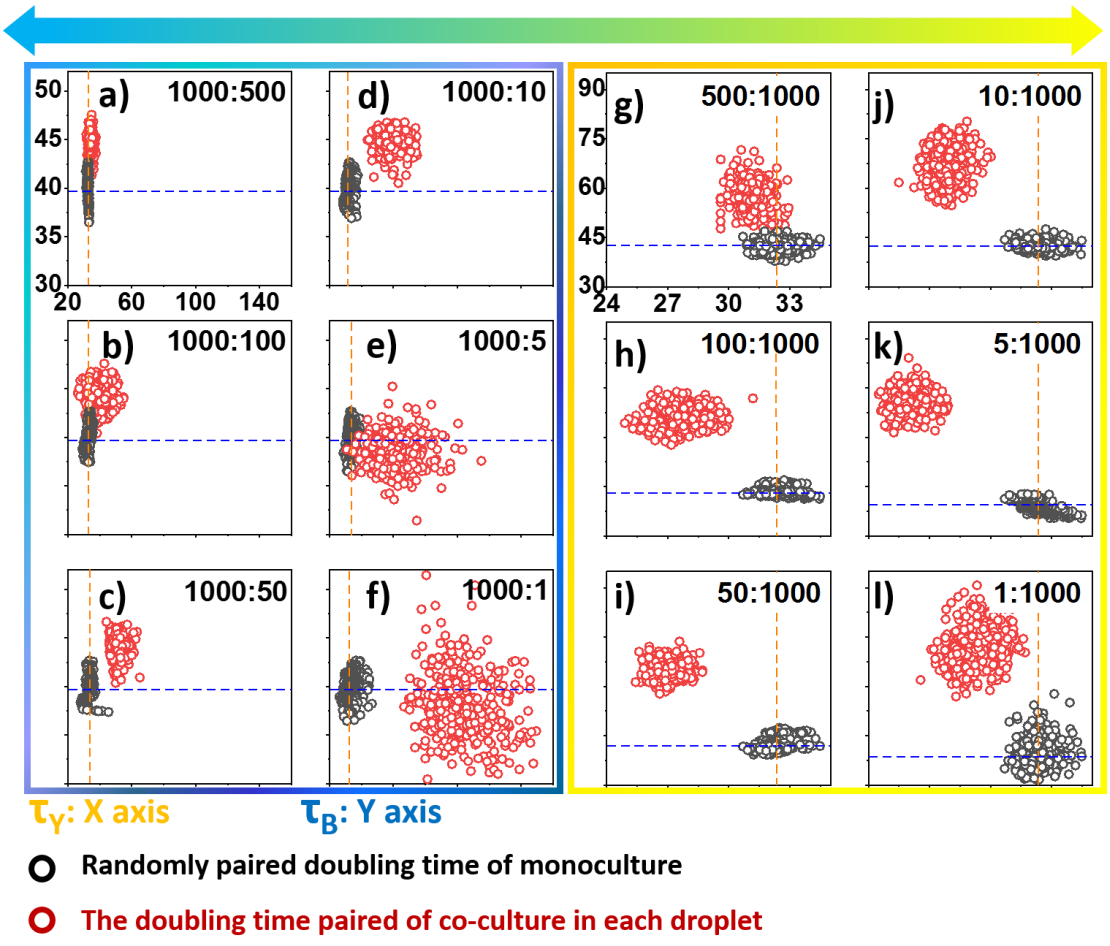

Figure 52: Correlation between doubling time of the two strains of *E. coli*: monoculture (black dots, randomly paired), and co-culture in the droplets (red dots) with R_0 of *E. coli* BFP: *E. coli* YFP. **a)** 1000:500, **b)** 1000:100, **c)** 1000:50, **d)** 1000:10, **e)** 1000:5, **f)** 1000:1, **g)** 500:1000, **h)** 100:1000, **i)** 50:1000, **j)** 10:1000, **k)** 5:1000, and **l)** 1:1000. The blue dotted line and yellow dotted line separately represent the average doubling time of *E. coli* BFP and *E. coli* YFP in monoculture cases.

When $R_0 > 1$ (blue box in **Figure 52 a-f**), the co-culture clouds (red dots) shifted to the competition region first, and then with R_0 increased, they moved to the Advantage_B region. Differently, when $R_0 < 1$ (yellow box in **Figure 52 g-l**), the co-culture clouds (red dots) shifted directly to the Advantage_Y region. Moreover, as R_0 deviates from 1, the

co-culture clouds (red dots) further moved to the Advantage_Y region. In both cases, there is a gradual trend that when the initial cell density fraction of one *E. coli* strain dominates and continuously rises, the co-culture clouds finally move to the Advantage region. We also summarized and compared the distribution of dots, as shown in **Table 13**.

Table 13: Distribution statistics of dots with different R_0 in four regions (in monoculture and co-culture cases).

R_0	Monoculture (%)					Co-culture (%)				
	Mutualism	Domination_Y	Dmination_B	Competition	Total	Mutualism	Domination_Y	Domination_B	Competition	Total
1000:1	32.22	11.37	18.01	18.01	422	0.00	0.00	70.99	29.01	362
1000:5	30.57	14.69	19.91	34.12	422	0.23	0.00	81.25	18.52	432
1000:10	21.90	15.83	23.48	38.79	420	0.00	0.00	0.00	100.00	379
1000:50	34.86	14.66	15.63	35.01	416	0.00	0.00	0.00	100.00	406
1000:100	39.04	10.12	10.84	40.00	415	0.00	10.17	0.00	89.83	423
1000:500	10.19	37.91	36.49	10.19	422	0.00	2.27	0.00	97.73	396
1000:1000	39.34	12.56	11.14	36.97	422	0.24	4.33	12.02	83.41	416
500:1000	27.27	25.17	27.04	20.51	429	0.00	96.46	0.00	2.78	396
100:1000	31.93	20.51	18.18	29.37	429	0.00	100.00	0.00	0.00	432
50:1000	27.51	25.17	12.12	35.20	429	0.00	100.00	0.00	0.00	425
10:1000	27.75	28.25	25.50	23.75	400	0.00	100.00	0.00	0.00	397
5:1000	13.05	39.16	36.60	11.19	429	0.00	100.00	0.00	0.00	422
1:1000	25.76	26.23	21.55	25.76	427	0.00	100.00	0.00	0.00	412

The two different movement pathways also reveal differences in the competitiveness of the two bacterial strains in the co-culture environment, *i.e.* the *E. coli* YFP is stronger than *E. coli* BFP. Furthermore, the co-culture clouds dispersion range becomes more expansive as the R_0 change from 1 to 10^{-3} (more frequent of YFP) or 10^{3} (more frequent of BFP). In other words, the variance of doubling time increases with decreasing inoculum. One possibility is that due to competition for resources, stochastic cell death happens, which affects smaller subpopulations more than larger subpopulations -- hence the lower growth rate for small inocula.[152, 155, 156]

5.9 Conclusion

To summarize this chapter, two strains of bacterial *E. coli* BFP and *E. coli* YFP were individually monoculture with different initial cell densities in the millifluidic droplet reactors. The results show that both strains' growth rate and final cell density of both strains are dependent on the initial cell density. *E. coli* YFP was observed to grow faster than *E. coli* BFP strains. Then, two strains were co-cultured with various initial cell

densities ratios. Comparing the doubling time and biomass ratio, a trade-off between growth rate and biomass yield (a faster growth comes with a lower yield and vice versa) was observed. It may explain the negative frequency-dependence of final biomass in co-culture. So far, the millifluidic device successfully monitored the growth of two strains of *E. coli* in monoculture and co-culture. Compared to the results obtained with other traditional methods, such as microplate, flow cytometer, batch culture and agar plate culture, and the predicted modeling results, this strategy is accurate and reliable. Besides, it can automatically track the growth of bacteria in the near real-time and long term with high throughput. It proves that the millifluidic device has the potential to be used in microbial study applications.

5. Coexistence of Two Bacterial Strains in Millifluidic Droplet Reactors

6. Reveal Bacterial Interaction in Antibiotic Environment by Millifluidic System

6.1 Overview

Microbial communities affect human health not only by assisting food digestion but also by causing infections.[79] In daily life, bacterial infections frequently occur, such as cuts, wounds, bug bites, food and drinks, and even airborne. Antibiotics play an important role in solving infection issues in human history. However, the abuse and misuse of antibiotics also cause a global crisis. Antibiotic-resistant gene mutants from bacteria could transfer to the next generation and even to other strains, leads to the sharp reduction of antibiotic efficacy. Recent research also reveals the cross-protection also causes the antibiotic-sensitive strain to survive in an antibiotic environment. Thus, finding the interaction between a bacterial community in antibiotics is crucial to human health.

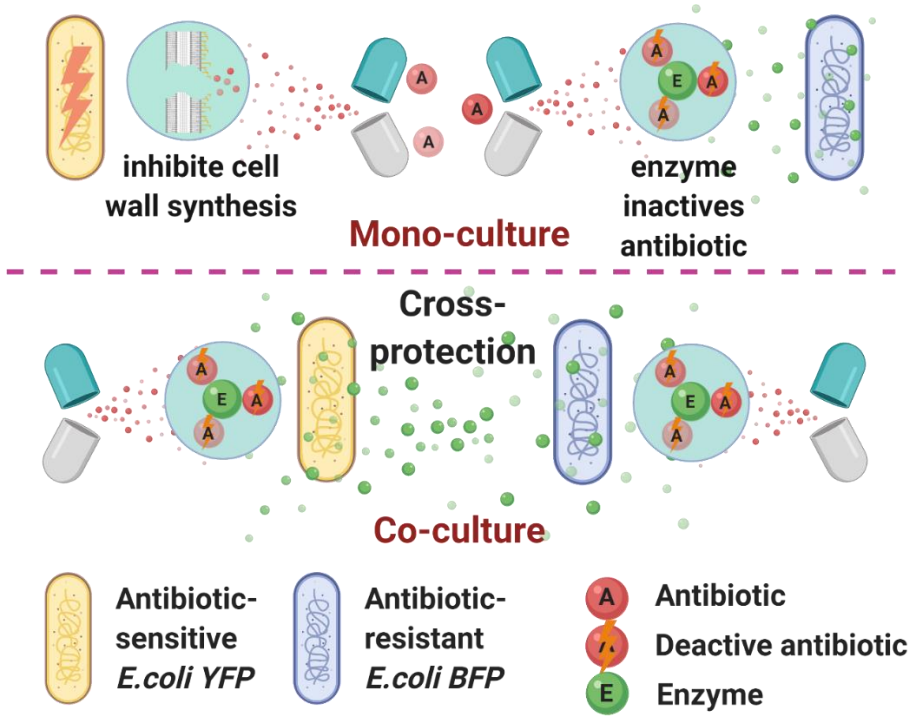

Figure 53: Mechanisms of cross-protection between antibiotic-resistant bacteria (*E. coli* BFP) and antibiotic-sensitive bacteria (*E. coli* BFP) in monoculture (upper part) and co-culture (lower part) environment.

Cross-protection is one of the mechanisms by which different bacteria, sharing the same environment, protect each other to survive in the presence of antibiotics. The antibiotic-resistant microbes help antibiotic-sensitive species survive. For example, β-lactam resistant bacteria deactivate the β-lactam antibiotics by secreting β-lactamase. As shown

in **Figure 53**, β-lactam rings of the β-lactam antibiotics kill the Gram-negative bacteria by inhibiting bacterial cell wall synthesis. However, the β-lactamase released by antibiotic-resistance bacterial strains will hydrolysis β-lactam rings; thus, antibiotic-resistant bacteria can survive in the antibiotic environment. This antibiotic-resistant effect has the potential to protect the nearby sensitive bacteria that are surrounded by β-lactamase released from resistant bacteria.[104, 157]

In this part of the thesis, the millifluidic droplet reactors were used to track the survival status of co-cultured sensitive and resistant strains in an antibiotic environment. The millifluidic reactor system real-time monitored the growth of two bacterial strains by detecting their different emission fluorescent signals. The *E. coli* YFP strain is chosen as an antibiotic-sensitive group, which produces yellow fluorescent protein during growing. Simultaneously, the *E. coli* BFP strain produces the blue fluorescent protein and is resistant to antibiotics. Fluorescence heat maps are used to describe the fluorescence signals change of each bacterial strain during incubation in millifluidic droplet reactors. The initial population ratio of two bacterial strains was set as a constant 1000:1000. Besides, to reveal the role of cross-protection, the antibiotic dosage was tuning, and the cell state such as cell density, viable rates, filamentation, cell-free media fluorescence, and cell fluorescence of coexistence bacteria and monoculture bacteria were researched and compared in detail.

6.2 Reference Growth Curves Obtained with Millifluidic Device

In this paragraph, the eight strains of antibiotic-resistant *E. coli* BFP (named *E. coli* BFP 1-8 according to the TEM-1 β-lactamase and mutants) first were monoculture in millifluidic droplet reactors to get their reference growth curve without external pressure sources such as antibiotics or other bacterial strains. Similarly, the sensitive strain of *E. coli* YFP was also monoculture in the same environment for obtaining the reference growth curve. Doubling times of all the strains were calculated and presented. All the strains were cultured with an initial cell density of 1000 cells/droplet for all the experiments.

6.2.1 Reference Monoculture Growth Curves of antibiotic-resistant E. coli BFP

From the growth curves obtained by the droplet-based reactor in **Figure 54**, no significant difference between each strain is observed. By comparing the average growth curves and doubling time of eight strains of antibiotic-resistant *E. coli* BFP (in **Figure 55**), we further proved there is no significant difference of doubling time (around 30 min) or Cmax

(around 2.0×10^5 cells/droplet) between eight strains. It indicates that the resistance ability did not affect the monoculture results of bacteria in an antibiotic-free environment with sufficient nutrients.

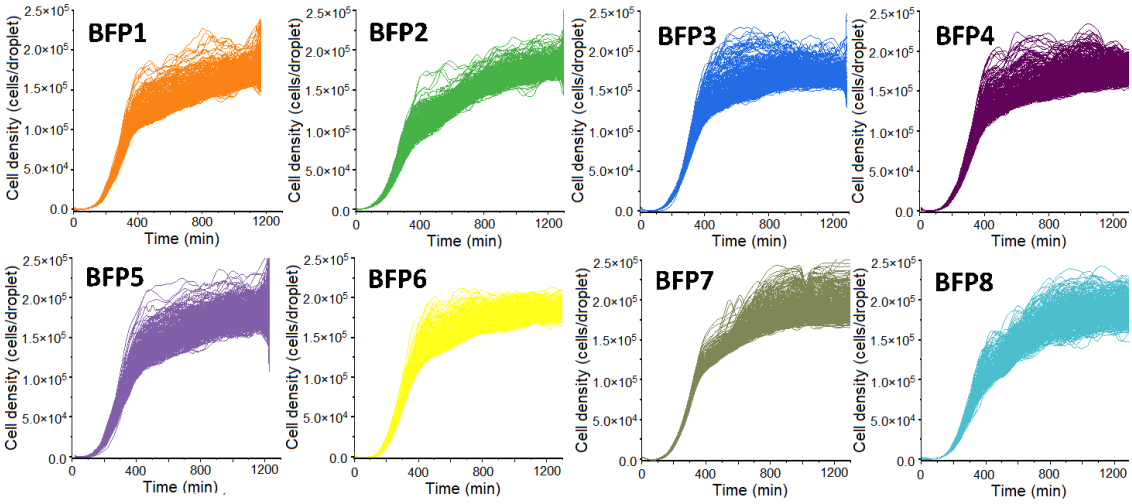

Figure 54: Monoculture growth curves of eight strains of antibiotic-resistant *E. coli* with sufficient nutrients in an environment without antibiotics.

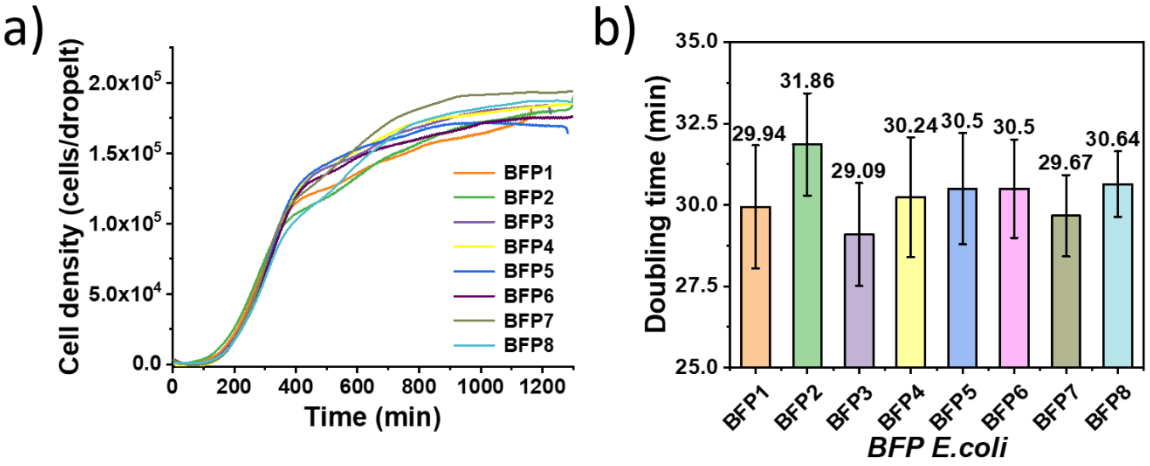

Figure 55: Comparison of eight strains of antibiotic-resistant *E. coli* BFP: **a)** average growth curves and **b)** doubling time.

6.2.2 Reference Monoculture Growth Curves of Antibiotic-Sensitive E. coli YFP

The antibiotic-sensitive strain *E. coli* YFP was taken as the same one used in Chapter 5. Reference growth curves and doubling time obtained by millifluidic devices are displayed in **Figure 56**.

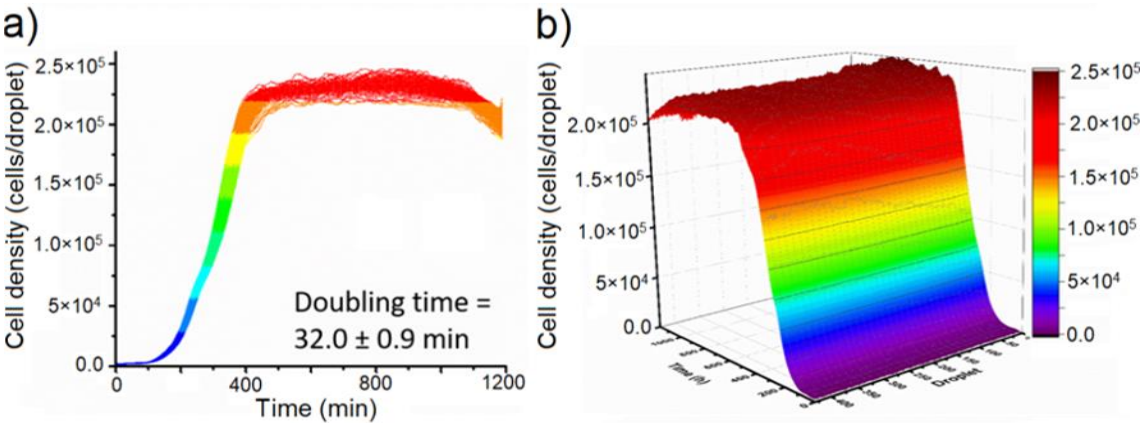

Figure 56: Monoculture growth curves of antibiotic-sensitive *E. coli* YFP with an initial cell density of 1000 cells/droplet: **a)** 2D growth curves with doubling time and **b)** 3D growth curves.

6.2.3 Fluorescence Heat Map of E. coli BFP and E. coli YFP

The fluorescence change with bacteria culture time can be observed more clearly in the fluorescence heat map, as shown in **Figure 57**. All bacterial strains enter the exponential phase at a similar time point, around 200 min. But the Cmax of *E. coli* YFP is greater than *E. coli* BFP strains.

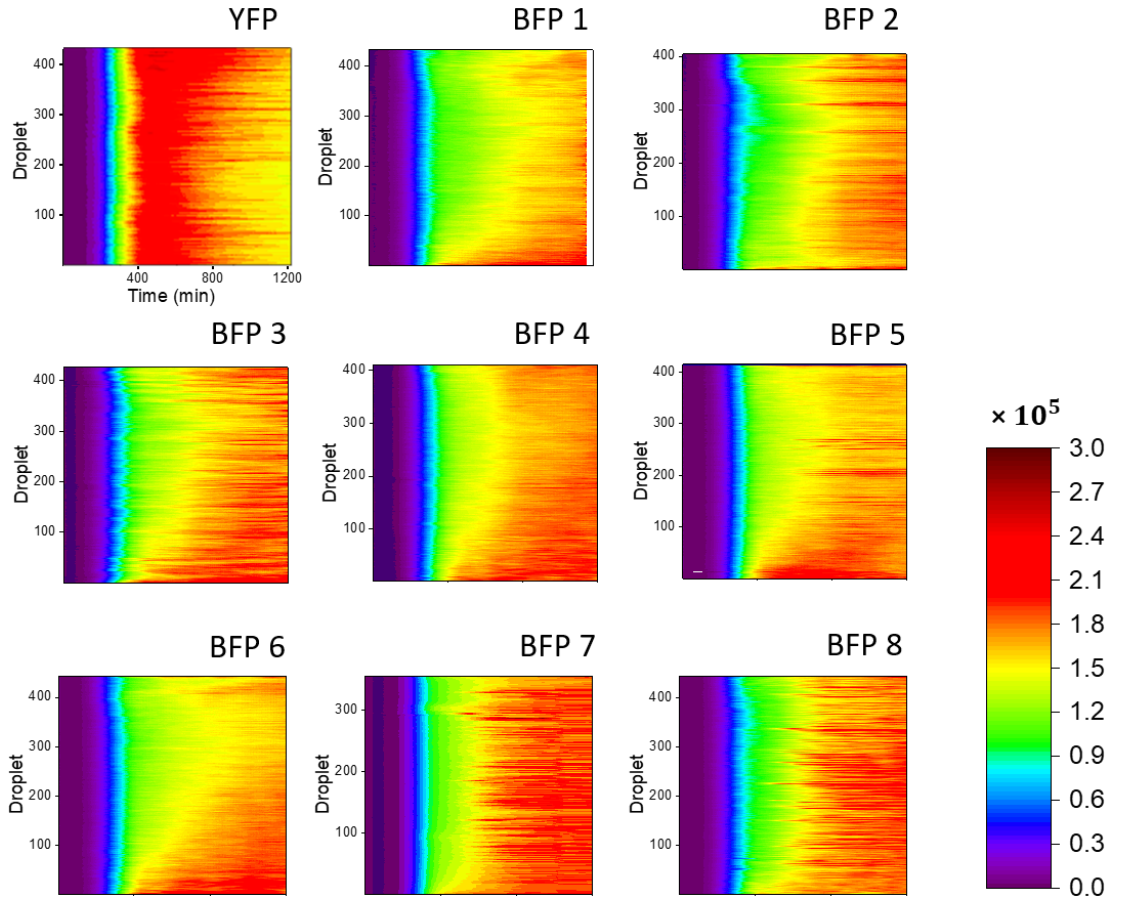

Figure 57: Fluorescence heat map of monoculture *E. coli* YFP and *E. coli* BFP group 1-8. All strains were monoculture with an initial cell density of 1000 cells/droplet. The time scale is from 0 to 1200 min. The fluorescence intensity scale is from 0.0-3.0 × 10^5 a.u. as shown at the right bottom.

6.3 Detection of MIC

In principle, inserting TEM-1 or its mutants into bacteria will help it release β-lactamase to hydrolysis the β-lactam ring; therefore, bacteria can survive in the antibiotic environment. Depends on the mutants type, bacteria will have different abilities against antibiotics. It can be verified by measuring the MICs of antibiotics to each strain.[111]

Based on the protocol in Chapter 3.3.7, the MIC of CTX to eight strains of antibiotic-resistant *E. coli* BFP and antibiotic-sensitive strain *E. coli* YFP were tested. As shown in **Figure 58**, after incubating *E. coli* YFP in the antibiotic environment for 24 hours (with antibiotic CTX gradients starts from 1 μg/mL in 96 well plates), the dividing line of transparent wells and turbid wells indicates the MIC, 0.0625 μg/mL.

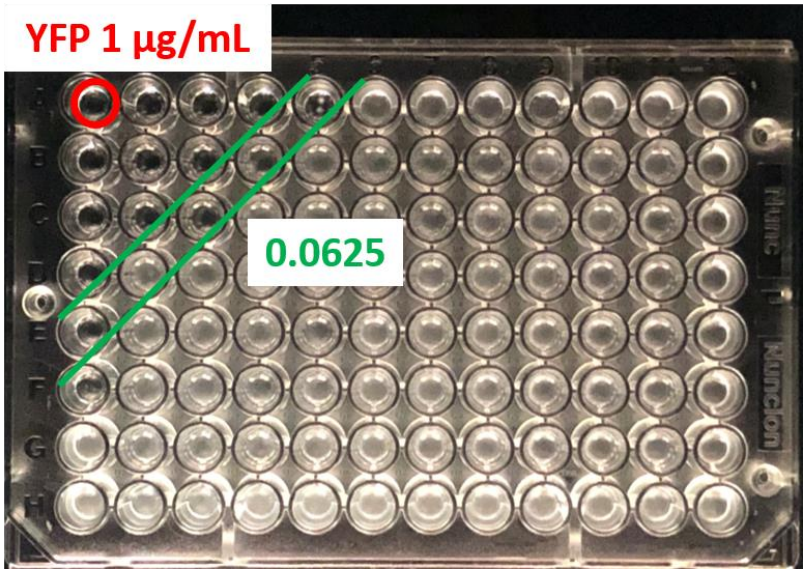

Figure 58: *E. coli* YFP incubated in the antibiotic environment for 24 hours (with antibiotic CTX gradients starts from 1 μg/mL in 96 well plates).

Following the same protocol, the MIC of CTX to all *E. coli* strains were tested, and the results are listed in **Table 14**.

Table 14: The MIC of *E. coli* strains with different types of β-lactamase genes.

Type	Strain	Gene (β-lactamase)	MIC (μg/mL)
antibiotic -sensitive	*E. coli* YFP	No	0.0625
antibiotic -resistant	*E. coli* BFP 1	TEM1	0.1
	E. coli BFP 2	TEM1 M182T	0.15

E. coli BFP 3	TEM1 E104K	1.6
E. coli BFP 4	TEM1 G238S	4
E. coli BFP 5	TEM1 E104K M182	4.8
E. coli BFP 6	TEM1 E104K G238S	6.4
E. coli BFP 7	TEM1 M182T G238S	8
E. coli BFP 8	TEM1 E104K M182T G238S	512

6.4 Tuning Antibiotic Concentration in Droplet Sequence

In this paragraph, the millifluidic device was utilized to generate droplet sequences with a gradient of antibiotic concentrations. Different strains of *E. coli* BFP were monoculture in ampicillin or CTX (containing a gradient concentration).

6.4.1 Tuning the Dye Concentration During Droplets Generation

To confirm the possibility of obtaining the concentration gradient of the substrate, we used the Nemesys pump to control the flow rate of DI water and dye solution during droplets generation and measured the fluorescence intensities of the droplets. From the results of **Figure 59**, the concentration gradient was successfully obtained.

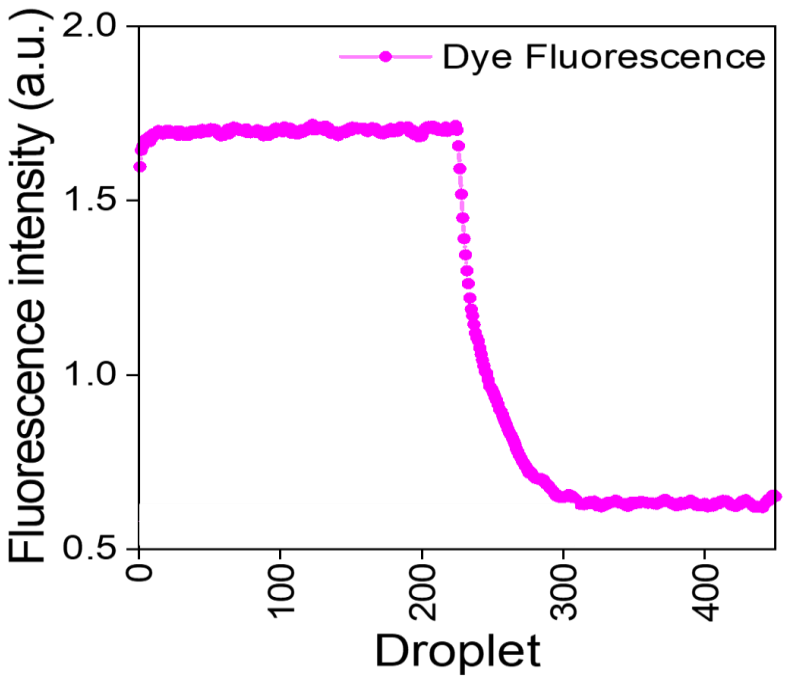

Figure 59: A concentration gradient of dye generated by tuning the DI water and dye solution flow rate ratio from 2:3 to 4:1.

6.4.2 Monoculture E. coli BFP 1 with Tuning the Ampicillin Concentrations

6. Reveal Bacterial Interaction in Antibiotic Environment by Millifluidic System

In this section, the *E. coli* BFP 1 (MIC = 0.1 µg/mL CTX) was first chosen for checking the influence of the β-lactam antibiotic. The concentrations of ampicillin were tuning while generating the droplets by controlling the antibiotic and M9 media flow rate. Two concentration gradient groups were generated and compared to the control group (without antibiotics), as shown in **Figure 60**. At the time point of 200 min, it is clear that the control group reached the exponential phase from the lag phase. Compared to the control group, the droplet sequence with ampicillin gradient from 10-90 µg/mL shows the lower fluorescence signal. This signal decrease is positively correlated to the increase of ampicillin concentration. The signal declined even sharper in the third group of ampicillin gradients from 360-2880 µg/mL. From the time point of 200 min to 300 min and later to 400 min, the positive correlation between signal drop-down and ampicillin concentration rise became obvious. It indicates that adding the β-lactam antibiotic such as ampicillin inhibits the bacteria growth. Besides, it also proves that the millifluidic device can monitor bacteria growth in an antibiotic environment.

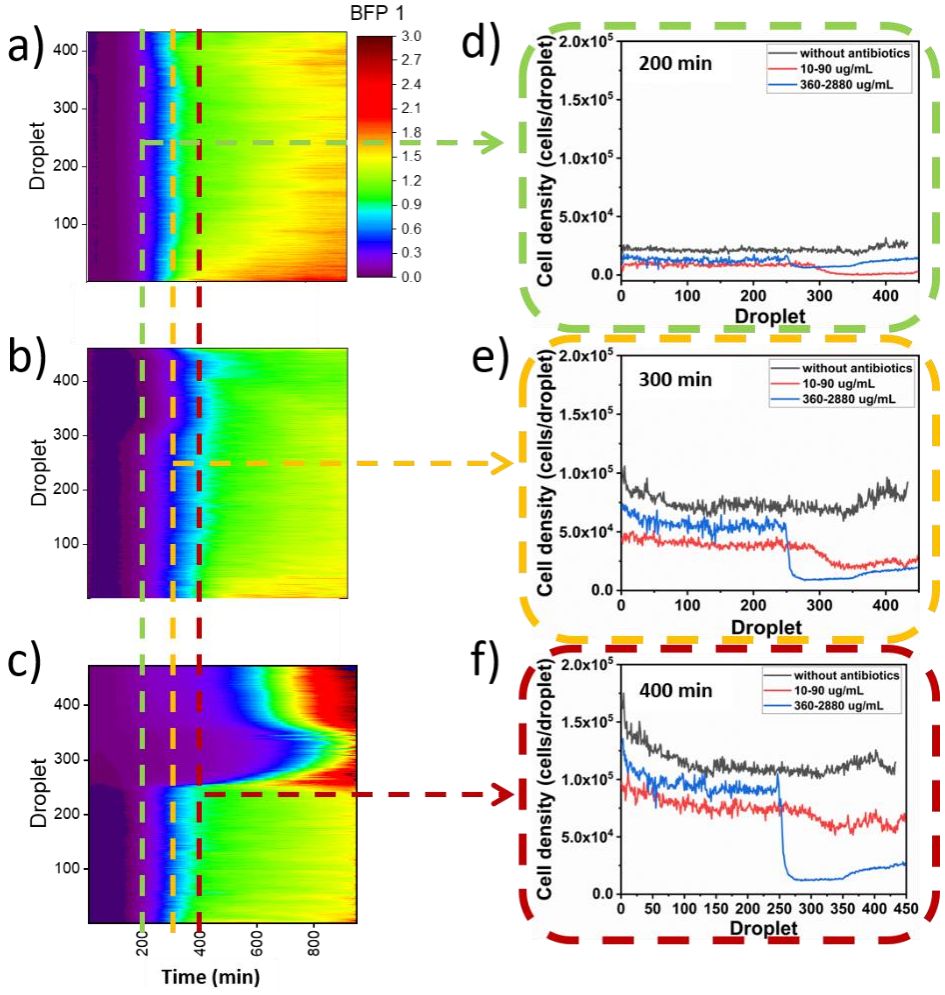

Figure 60: Monoculture *E. coli* BFP 1 in concentration gradients of ampicillin: **a)** 0 µg/mL; **b)** 10-90 µg/mL; **c)** 360-2880 µg/mL, and the selected time point for analysis: **d)** 200 min, **e)** 300 min, and **f)** 400 min.

6.4.3 Monoculture E. coli BFP with Tuning the CTX Concentrations

After checking ampicillin, CTX concentration gradients were also used to check the resistance of different *E. coli* BFP strains. The gradient concentration of CTX was generated similar to the dye dilution method. The maximum concentration is three times the minimum concentration (flow rate ratio of antibiotic solution to M9 media is tuned from 3:2 to 1:4). Fluorescence heat map of monoculture *E. coli* BFP group 2, 3, 4, 6, and 7 without antibiotic (left side) and with gradient concentration of CTX are shown in **Figure 61**.

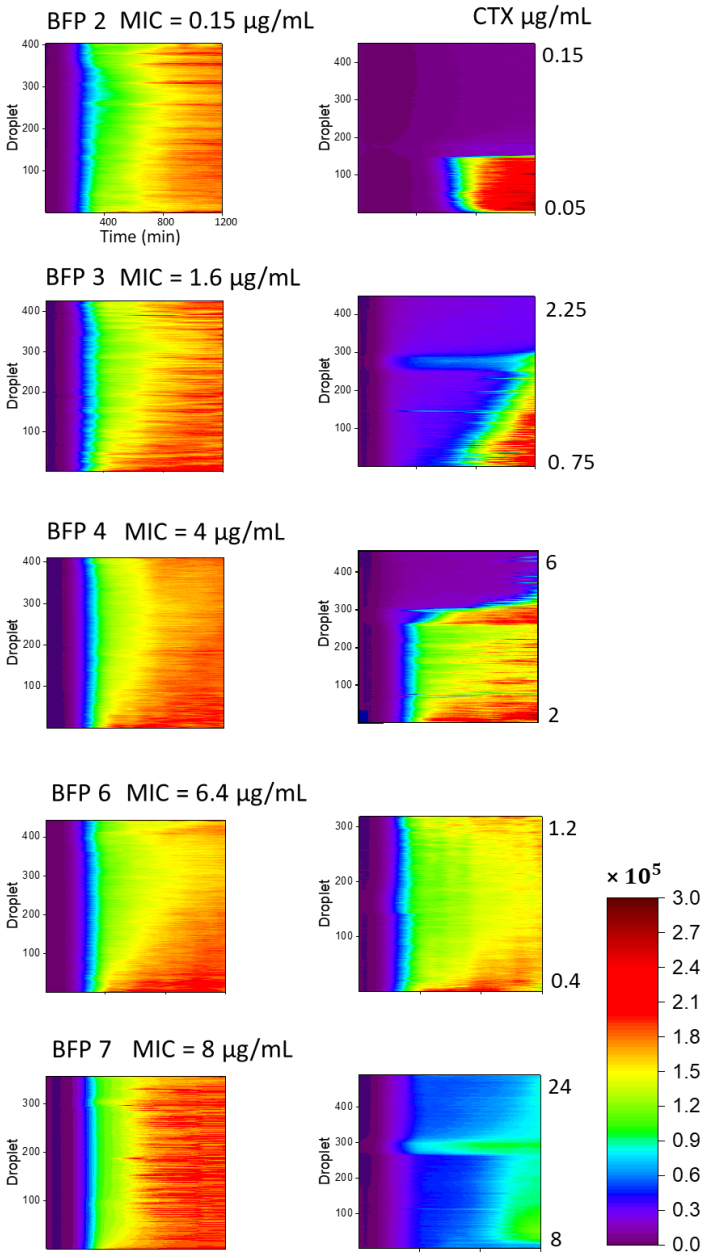

Figure 61: Fluorescence heat maps of monoculture *E. coli* BFP group 2, 3, 4, 6, and 7 without antibiotic (left side) and with gradient concentration of CTX. All strains were monoculture with an initial cell density of 1000 cells/droplet. The time scale is from 0 to 1200 min. The fluorescence intensity scale is from 0.0-3.0 × 10^5 a.u. as shown at the right bottom.

Compared to the environment free from antibiotic stress, the fluorescence intensity of *E. coli* BFP with antibiotic stress decrease in varying degrees. When the MIC is in the middle of the CTX concentration gradient, fluorescence intensity sharply declines in the middle of the heat map, such as *E. coli* BFP groups 2, 3, and 4. When the CTX concentration gradient is below the MIC, fluorescence intensity slightly decreases. For example, *E. coli* BFP 6 was incubated in the CTX concentration gradient environment (from 0.4 to 1.2 μg/mL), below its MIC (6.4 μg/mL). In *E. coli* BFP group 8, since the gradient of CTX concentration is greater than its MIC, it has the most obvious fluorescence decrease. This method of generating antibiotic concentration gradients can be further used for verifying the MIC of antibiotics to bacteria.

6.5 Selection of Antibiotic-Resistant *E. coli* BFP with Millifluidic Device

According to the MIC of CTX to eight strains of antibiotic-resistant *E. coli* BFP and one antibiotic-sensitive strain of *E. coli* YFP, four strains of *E. coli* BFP were chosen due to their clear gradient of MIC. They are *E. coli* BFP 1, *E. coli* BFP 4, *E. coli* BFP 7, and *E. coli* BFP 8, which have the MIC of 0.1, 4, 8, 512 μg/mL separately.

6.5.1 Monoculture E. coli BFP and E. coli YFP with 5 μg/mL CTX

As to the MIC detection results, the MICs of antibiotic-resistant *E. coli* BFP strains have a clear gradient. 5 μg/mL CTX was chosen and added to all selected *E. coli* BFP strains and *E. coli* YFP.

In **Figure 62**, the CTX effect on different strains can be observed clearly with fluorescence heat maps. For the *E. coli* YFP and *E. coli* BFP 1, 5 μg/mL CTX almost completely inhibited their growth. In *E. coli* BFP groups 4 to 7, and 8, the antibiotic effect constantly decreased. Strikingly, even the inhibition effect became weaker and weaker, adding the antibiotic still affected bacterial growth.

To verify this inhibition effect is permanent or temporary, we extended the incubation time for monoculture *E. coli* YFP and *E. coli* BFP 1 until the fluorescence intensity increase. In **Figure 63**, the fluorescence of *E. coli* BFP 1 started to increase after incubating for 1300 min, and *E. coli* YFP also showed a slight fluorescence signal rise after incubating for 2000 min. One of the reasons might be due to the CTX degradation.[158]

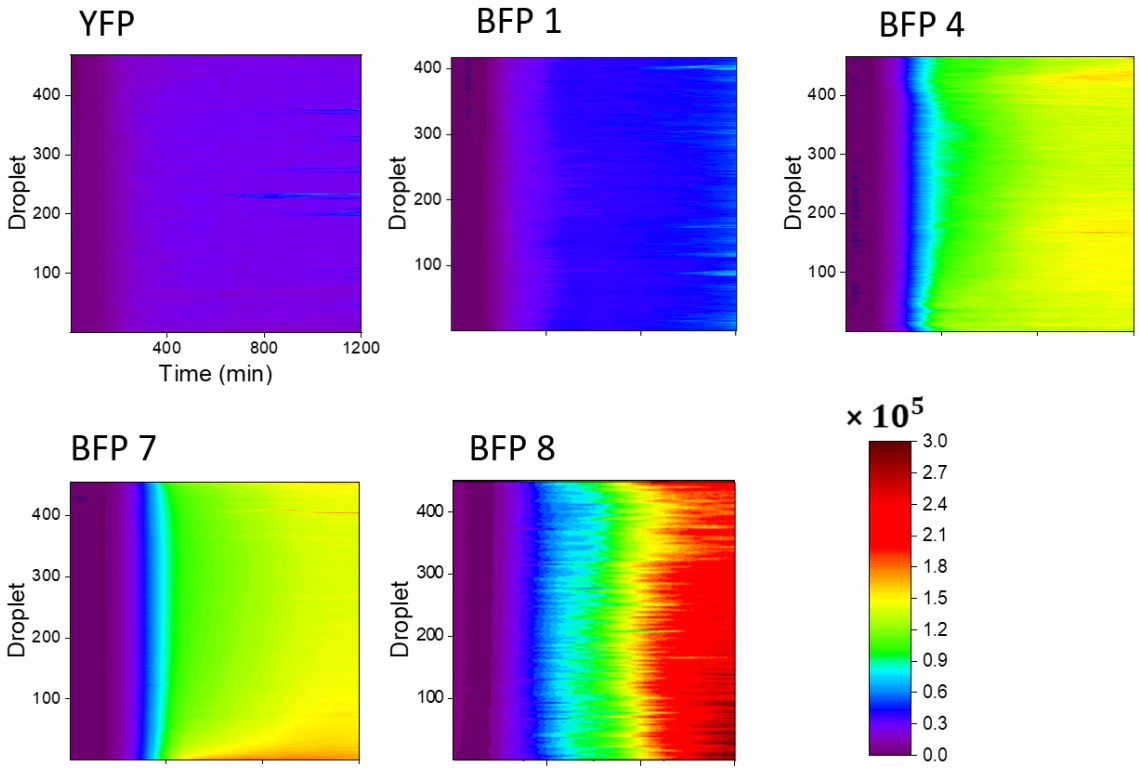

Figure 62: Fluorescence heat maps of monoculture *E. coli* BFP group 1, 4, 7, and 8 and *E. coli* YFP with 5 µg/mL CTX. All strains were monoculture with an initial cell density of 1000 cells/droplet. The time scale is from 0 to 1200 min. The fluorescence intensity scale is from 0.0-3.0 × 10^5 a.u. as shown at the right bottom.

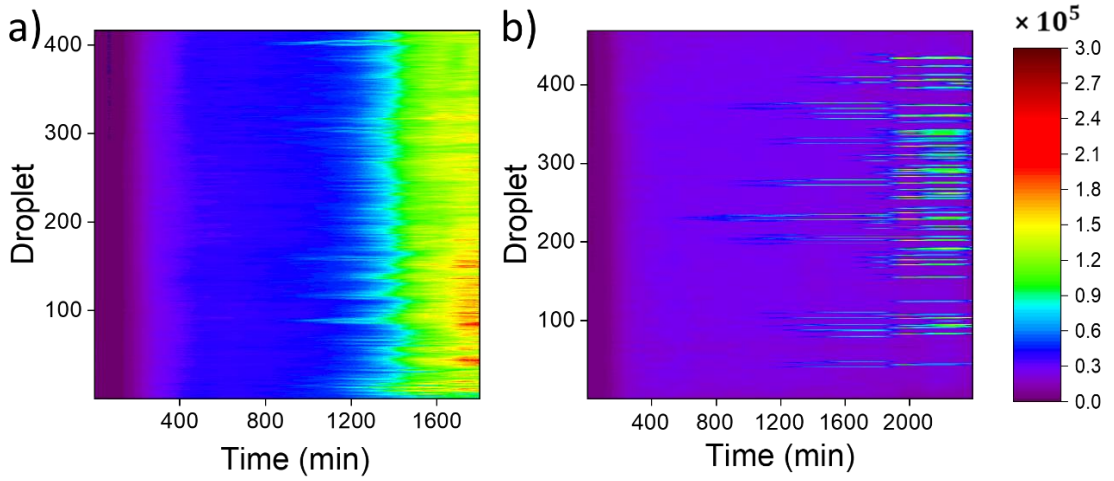

Figure 63: Fluorescence heat maps of monoculture **a)** *E. coli* BFP 1 and **b)** *E. coli* YFP with 5 µg/mL CTX. All strains were monoculture with an initial cell density of 1000 cells/droplet. The fluorescence intensity scale is from 0.0-3.0 × 10^5 a.u. as shown at the right bottom.

6.5.2 Co-culture E. coli BFP and E. coli YFP with 5 µg/mL CTX

To check the antibiotic effect on co-culture strains (*E. coli* BFP and *E. coli* YFP), one of the *E. coli* BFP strains was encapsulated with *E. coli* YFP in droplets; the initial biomass ratio between the two strains was set as 1000: 1000 cells/droplet. Fluorescence heat maps

were still used to compare the fluorescence expressed from bacteria change with incubation time, as shown in **Figure 64**.

Similar to the results of *E. coli* BFP monoculture with CTX, the fluorescence intensity of co-culture *E. coli* BFP decreased in different degrees among four strains of *E. coli* BFP. Since the *E. coli* BFP 8 strain has the highest MIC, it has the least influence from CTX and *E. coli* YFP. However, adding the *E. coli* YFP reduced the fluorescence intensity of all groups of *E. coli* BFP to different degrees. The *E. coli* YFP still had no significant signs of active growth in all co-culture groups. Compared to the monoculture case and co-culture with *E. coli* BFP 1, 4, and 7 groups, co-culture with *E. coli* BFP 8 strain made *E. coli* YFP has a slight increase in fluorescence intensity, heralds cross-protection phenomenon might occur (between *E. coli* BFP 8 strain and *E. coli* YFP).

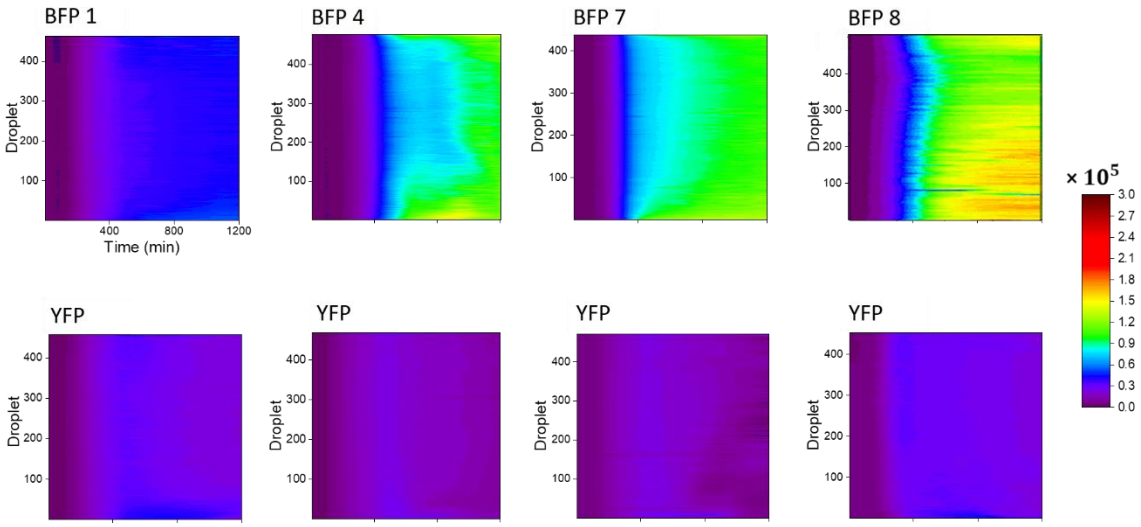

Figure 64: Fluorescence heat map of co-culture *E. coli* BFP group 1, 4, 7, and 8 and *E. coli* YFP with 5 µg/mL CTX. All co-culture groups were encapsulated with an initial cell biomass ratio of 1000: 1000 cells/droplet. The time scale is from 0 to 1200 min. The fluorescence intensity scale is from 0.0-3.0 × 10^5 a.u. as shown at the right bottom.

6.6 Monoculture Bacteria with Various Concentrations of Antibiotic

In the previous paragraph, we selected *E. coli* BFP 8 and *E. coli* YFP to study bacteria co-culture in antibiotics. Before monitoring their growth in co-culture or antibiotics environments, we first observed their reference growth behavior in monoculture.

We incubated the bacteria in approximately 450 droplets were monitored from 0 hours to 20 hours, and for each parallel experiment, we added different concentrations of CTX to the bacterial medium. The fluorescence signal emitted from bacteria was recorded and shown in the fluorescence heat map, as shown in **Figure 65** (*E. coli* BFP 8) and **Figure 66** (*E. coli* YFP).

In the group of *E. coli* BFP 8 incubated without CTX, the fluorescence intensity increase with time, indicates the bacterial grow well without the stress from antibiotics. When CTX concentration rose from 0.05 µg/mL to 5 µg/mL, the influence from the antibiotic became more and more clear; with the increase of CTX, the lag phase of *E. coli* BFP 8 shifted. In this case, the growth was delayed but not completely inhibited. But once CTX concentrations increased to around 50 µg/mL, the fluorescence detected from the droplet remained at almost the same level in the first 15 hours. Interestingly, after 15 hours, a fluorescence burst appeared, as shown in **Figure 65 f-h**.

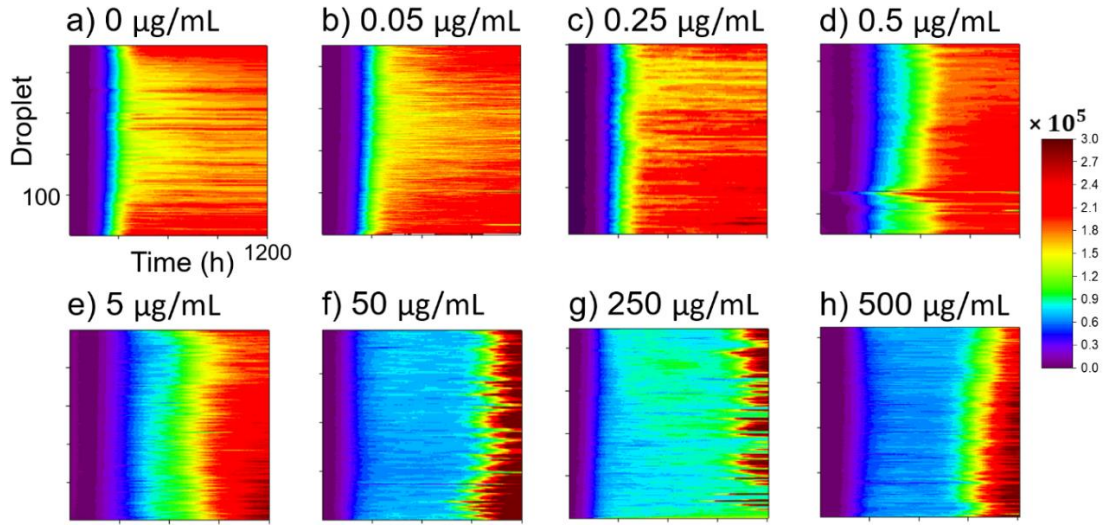

Figure 65: Monoculture of *E. coli* BFP 8 with different CTX concentrations: **a)** 0 µg/mL, **b)** 0.05 µg/mL, **c)** 0.25 µg/mL, **d)** 0.5 µg/mL, **e)** 5 µg/mL, **f)** 50 µg/mL, **g)** 250 µg/mL and **h)** 500 µg/mL. All groups were monoculture with an initial cell density of 1000 cells/droplet. The fluorescence intensity scale is from 0.0-3.0 × 10^5 a.u. as shown at the right bottom.

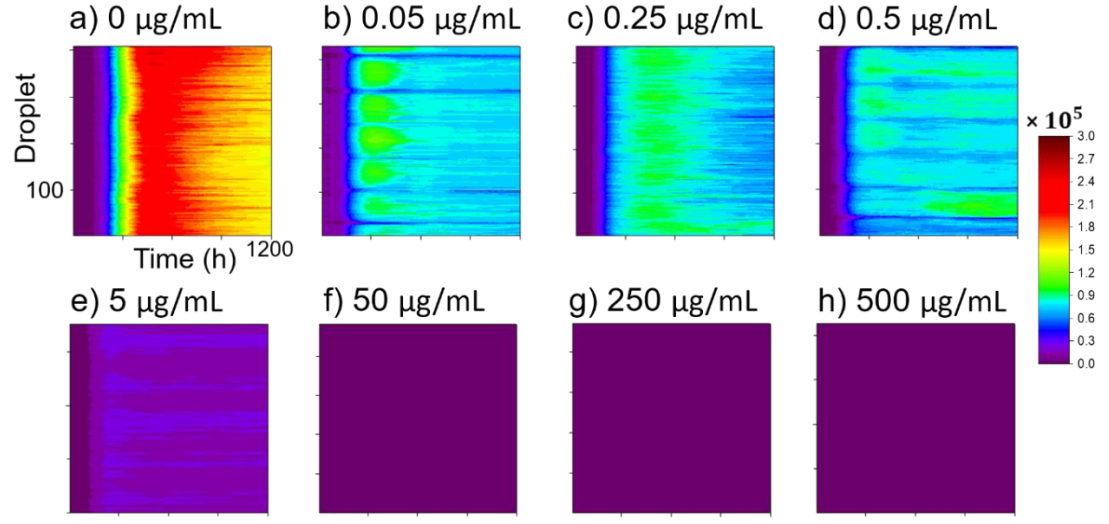

Figure 66: Monoculture of *E. coli* YFP with different CTX concentrations: **a)** 0 µg/mL, **b)** 0.05 µg/mL, **c)** 0.25 µg/mL, **d)** 0.5 µg/mL, **e)** 5 µg/mL, **f)** 50 µg/mL, **g)** 250 µg/mL and **h)** 500 µg/mL. All groups were monoculture with an initial cell density of 1000 cells/droplet. The fluorescence intensity scale is from 0.0-3.0 × 10^5 a.u. as shown at the right bottom.

Compared to the *E. coli* BFP 8, *E. coli* YFP is more sensitive to the antibiotics, which can also be proven in the droplet-reactor, as shown in **Figure 66**. In a case without antibiotic stress, *E. coli* YFP grew well. But when more than 0.05 µg/mL (which is close to its MIC) of CTX was added, *E. coli* YFP was impacted much greater than *E. coli* BFP 8. Notably, the fluorescence intensity of the groups with CTX concentrations of 0.25 µg/mL (5 times of MIC) and 0.5 µg/mL (10 times of MIC) still had a similar value as the 0.05 µg/mL group. Besides, the fluorescence heat map results also show that after employing CTX up to 5 µg/mL, the fluorescence intensity detected from droplets is considered no obvious bacteria growth.

6.7 Co-culture Bacteria with Various Concentrations of Antibiotic

After understanding the growth behavior of bacteria monoculture with various concentrations of CTX, two strains of *E. coli* were incubated together in droplet reactors. The fluorescence heat maps were also used to describe the different growth behavior in the co-culture cases.

Compared to the *E. coli* BFP 8 monoculture with antibiotics, *E. coli* BFP 8 (co-culture with *E. coli* YFP with 1000: 1000 cell initial cell density ratio) got affection slightly from *E. coli* YFP due to its antibiotics resistance, as shown in **Figure 67 b-h**. In no antibiotic stress case, the growth of both *E. coli* BFP 8 and *E. coli* YFP was impacted by each other because of the competition of nutrients and space, as shown in **Figure 67 a** and **Figure 68 a**.

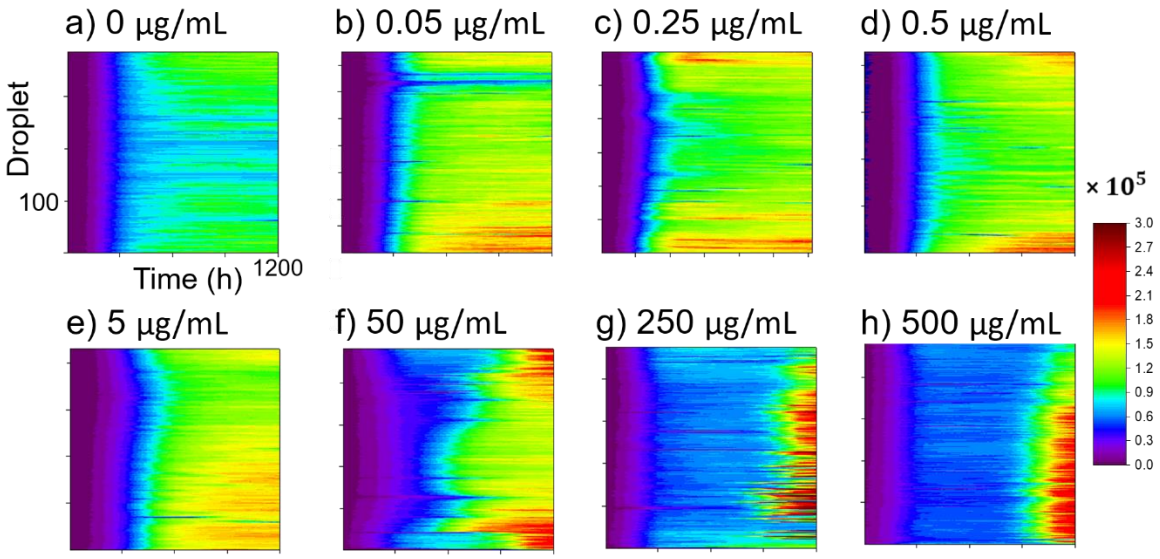

Figure 67: Co-culture of *E. coli* BFP 8 (with *E. coli* YFP of the initial cell density ratio 1:1) with different CTX concentrations: **a)** 0 µg/mL, **b)** 0.05 µg/mL, **c)** 0.25 µg/mL, **d)** 0.5 µg/mL, **e)** 5 µg/mL, **f)** 50 µg/mL, **g)** 250 µg/mL and **h)** 500 µg/mL. The time scale is from 0 to 1200 min. The fluorescence intensity scale is from 0.0-3.0 × 10^5 a.u. as shown at the right bottom.

Unlike antibiotic-resistant strain *E. coli* BFP 8, the antibiotic-sensitive strain *E. coli* YFP was relatively more influenced by the other co-existent strain in the antibiotic environment, as shown in **Figure 68 b-h**.

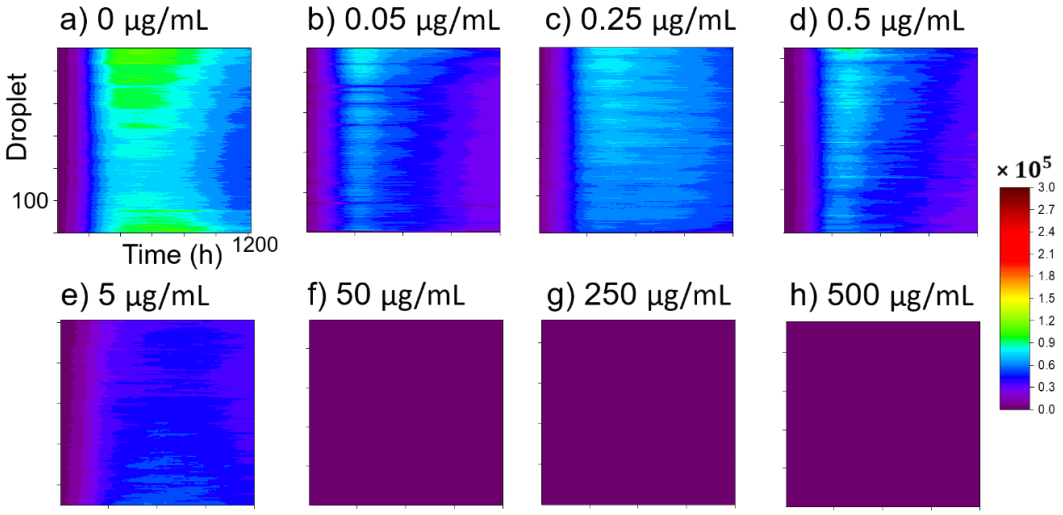

Figure 68: Co-culture of *E. coli* YFP (with *E. coli* BFP 8 of the initial cell density ratio 1:1) with different CTX concentrations: **a)** 0 µg/mL, **b)** 0.05 µg/mL, **c)** 0.25 µg/mL, **d)** 0.5 µg/mL, **e)** 5 µg/mL, **f)** 50 µg/mL, **g)** 250 µg/mL and **h)** 500 µg/mL. The time scale is from 0 to 1200 min. The fluorescence intensity scale is from 0.0-3.0 × 10^5 a.u. as shown at the right bottom.

From its MIC to 10 times the MIC, the fluorescence intensity of *E. coli* YFP decreased compared to the monoculture case. Whether this phenomenon is due to the competition or other interaction between two strains has to be checked with further verification tests. But for now, the millifluidic droplet-reactor achieved monitor two strains of bacteria individually and together. It can high-throughput and quick scan the bacterial growth behavior, which helps to overview the response of bacterial strains to the antibiotics efficiently.

6.8 Verification of Relationship between Cell Density and Fluorescence Signal

The fluorescence heat map results obtained by the millifluidic device clearly show that adding a certain amount of antibiotics inhibited the bacteria growth. However, at the late stage of the fluorescence heat map, the intensity dramatically increased and even showed stronger fluorescence than the control group (without antibiotics). In order to certificate the relationship between cell density and fluorescence intensity, the plate reader was used to record the bacterial growth in optical density and fluorescence intensity. In addition, fluorescence cytometry and fluorescence microscopy were utilized to check the cell size,

shape, and fluorescence. Further verification was done by checking the fluorescence from cell-free media and cells, CTX degradation rate, viable cell rate, and β-lactamase activity.

In this paragraph, *E. coli* BFP 8 and *E. coli* YFP monoculture and co-culture in microplates with various concentrations of CTX. Since the bacteria were incubated in a microplate at 37° C overnight, a membrane was attached to the microplate to avoid media evaporation, as shown in **Figure 69 b**. All the bacterial culture experiments used the same membrane, and there was no significant signal difference observed between with and without membrane. However, using membranes efficiently reduced the influence of evaporation, as shown in **Figure 69 a** and **c**. Transparent microplates were used to detect optical density, and black microplates were used to detect fluorescence intensity.

Figure 69: OD_{600} of monoculture *E. coli* YFP incubated and measured in transparent microplates in various CTX with and without membrane, **a)** growth curves monitored with membrane, **b)** transparent microplate attached with membrane and **c)** growth curves monitored without membrane.

6.8.1 Monitor Bacterial Growth in Antibiotic by Detecting Fluorescence Intensity by Plate Reader

To determine the correlation between the cell density and fluorescence density, calibration curves of cell density-fluorescence intensity were first obtained by detecting the fluorescence densities of bacteria with different cell densities.

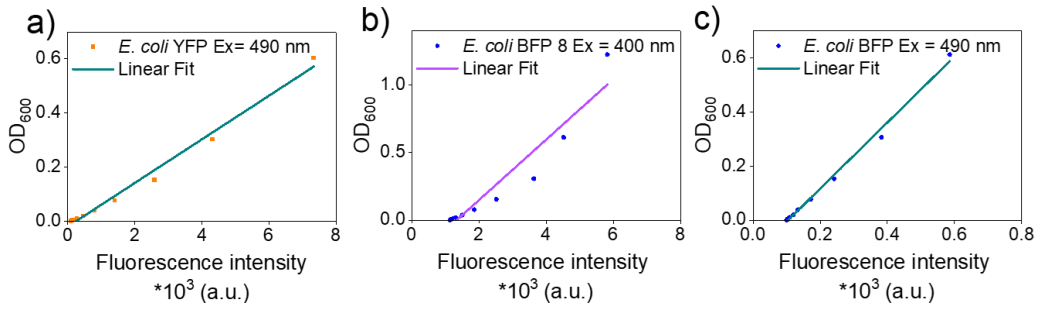

Figure 70: Calibration curves of fluorescence intensity-OD_{600}, **a)** *E. coli* YFP detected with an excitation wavelength of 490 nm; **b)** *E. coli* BFP detected with an excitation wavelength of 400 nm, and **c)** *E. coli* BFP detected with an excitation wavelength of 490 nm.

Calibration curves of *E. coli* BFP 8 and *E. coli* YFP were separately measured by the plate reader and shown in **Figure 70 a** and **b**. Notably, the *E. coli* BFP showed a slight fluorescence under an excitation wavelength at 490 nm, as shown in **Figure 70 c**. It was used to remove the cross-signal emitted from BFP in co-culture cases.

In the results of fluorescence intensity change with incubation time in **Figure 71**, a similar phenomenon was found that at a certain concentration of CTX, the fluorescence intensity dramatically increased. It indicates the fluorescence burst is not caused by the methods we used. For the *E. coli* BFP 8 strain, an extremely strong signal was found in the group of 10, 15, 25, 50, 250, and 500 µg/mL CTX in both monoculture and co-culture cases. For *E. coli* YFP, the signal dramatically increased only in the monoculture case with CTX concentrations of 0.25 and 0.5 µg/mL.

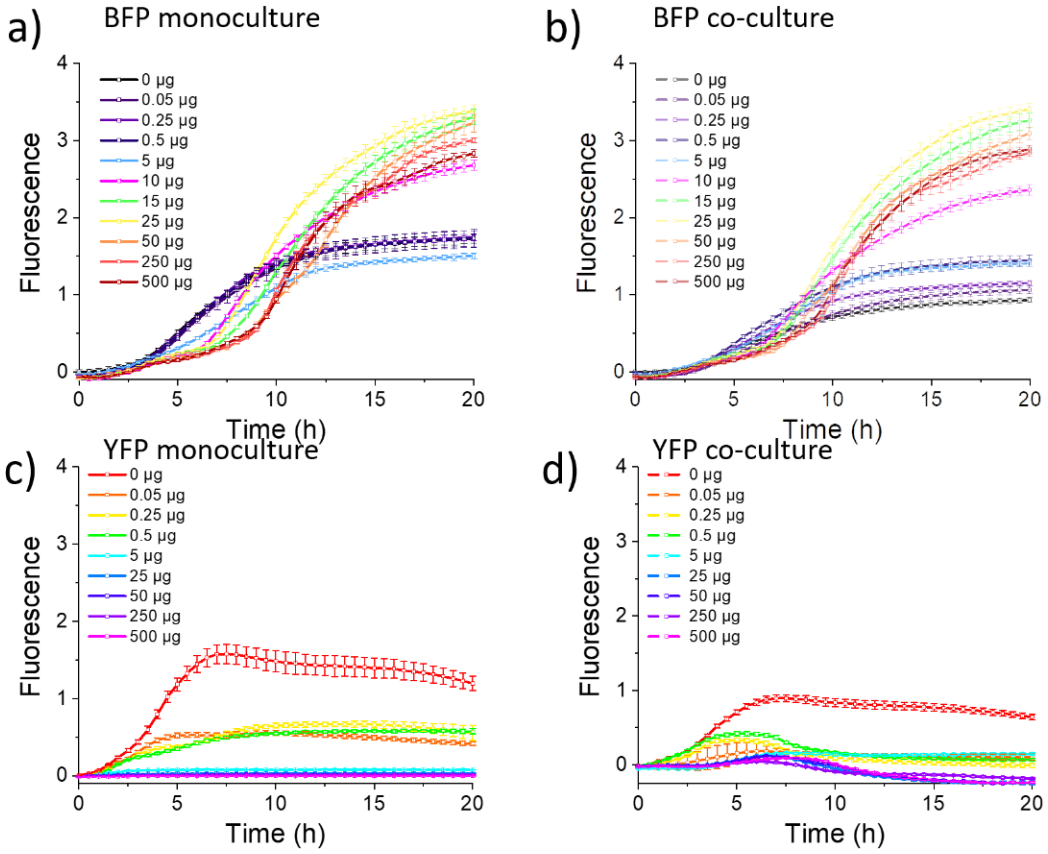

Figure 71: Fluorescence intensity change with incubation time with various CTX concentrations of **a)** *E. coli* BFP 8 monoculture; **b)** *E. coli* BFP 8 co-culture with *E. coli* YFP; **c)** *E. coli* YFP monoculture; **d)** *E. coli* YFP co-culture with *E. coli* BFP 8. All monoculture groups were prepared with an initial cell density of 1000 cells/droplet in the droplet (200 nL). All co-culture groups were prepared with an initial cell biomass ratio of 1000:1000 cells/droplet. The time scale is from 0 to 20 hours.

6.8.2 CTX Degradation Rate Detection

One possible reason that makes the fluorescence of bacteria increased sharply might be the chemicals degradation. When antibiotics are kept at a temperature of 37 °C overnight, their medicinal effect might reduce. To verify the possibility of degradation, CTX concentrations were measured with a UV-Vis spectrometer, and the strongest absorption peak was found at the wavelength of 229 nm, as shown in **Figure 72 a**.[159]

From 15 µg/mL to 25 µg/mL, a linear relationship between CTX concentration and absorption rate was found. So, the CTX with gradient concentration from 15 µg/mL to 25 µg/mL was measured and analyzed at absorption wavelength 229 nm to obtain the calibration curve **Figure 72 b** and **c**. Afterward, CTX concentrations were constantly measured during the incubation. No concentration change was observed in 8 hours, but until 48 hours, there was a slightly drop-down (**Figure 72 d**). It indicates the CTX chemical degradation was not the main reason that caused fluorescence increase.

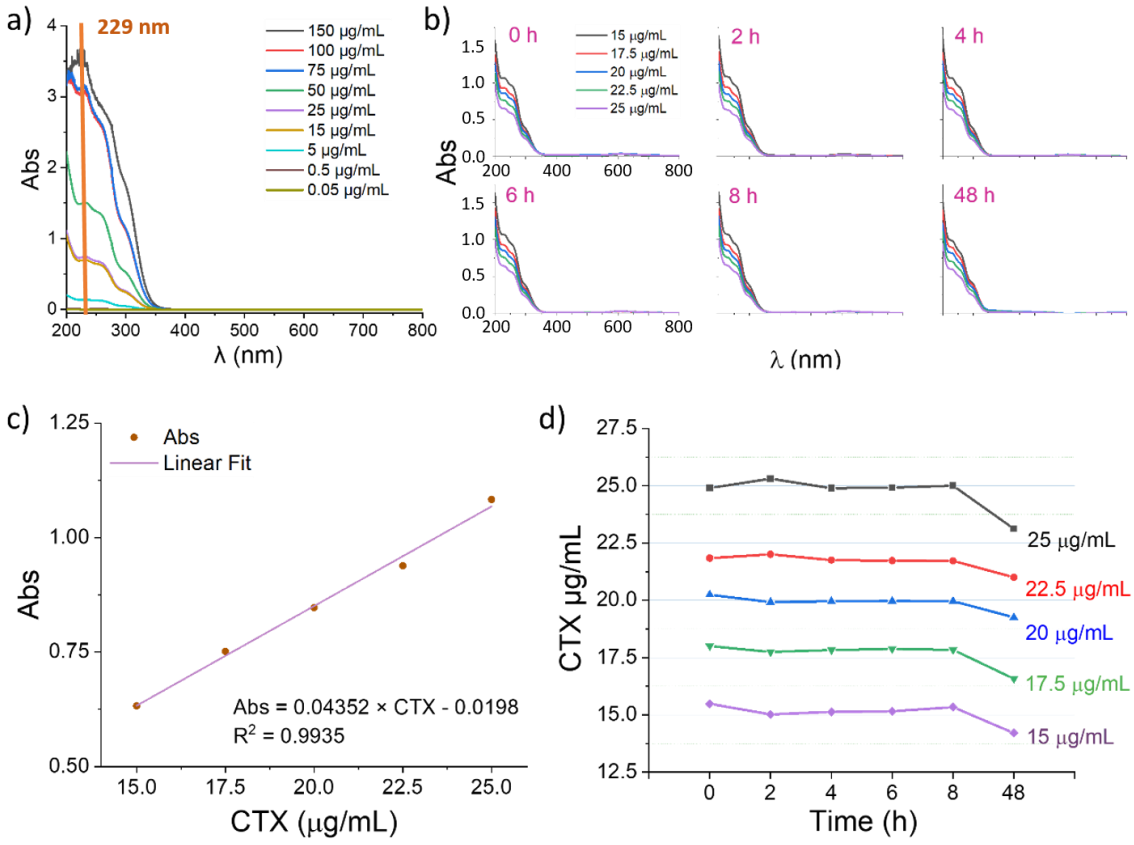

Figure 72: CTX absorption rate at different wavelength measured by a UV-Vis spectrometer, **a)** absorption rate of CTX with different concentrations; **b)** absorption rate of CTX with gradient concentration from 15 µg/mL to 25 µg/mL measured during incubation at 37 °C; **c)** calibration curve of absorption rate-CTX concentration (at 229 nm wavelength); **d)** CTX concentrations change during the incubation time.

6.8.3 Monitor Bacterial Growth with Antibiotic by Detecting OD_{600} by Plate Reader

In parallel, the optical density of the bacterial growth was also measured by a plate reader during incubation and shown in **Figure 73**.

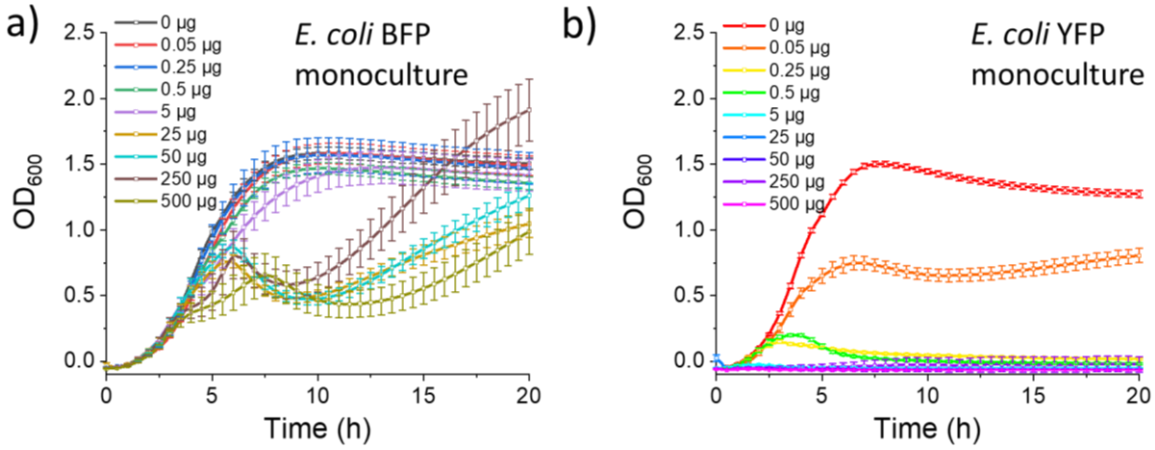

Figure 73: Monoculture growth curves with different concentrations of CTX measured by a plate reader (OD_{600}): **a)** *E. coli* BFP 8 and **b)** *E. coli* YFP.

Likewise, the OD_{600} results of monoculture *E. coli* BFP 8 also showed interesting changes at certain CTX concentrations. For *E. coli* BFP 8 culture in 50, 250, 500 µg/mL CTX, the growth curves first increased slowly compared to the lower CTX concentrations, then dropped down and dramatically increased again. However, this dramatic increase was still in the reasonable range. In contrast, *E. coli* YFP did not show a dramatic increase after declining for all the groups with different concentrations of CTX. So far, we have observed an interesting change in fluorescence and optical density of bacteria in antibiotics; we are looking forward to finding out the reasons that cause this phenomenon.

6.8.4 Cell Filamentary Observation by Fluorescence Microscopy

Based on the difference of fluorescence and optical density change during incubation, fluorescence microscopy was used to check the reason that cause of the discrepancy. The monoculture and co-culture of *E. coli* BFP 8 and *E. coli* YFP in different concentrations of CTX incubated for 0 and 20 hours were observed with fluorescence microscopy and shown in **Figure 74** and **Figure 75** separately.

After adding the CTX to the bacteria culture, the cell media was immediately dropped on the glass slides for observation (0-hour data) with microscopy. In **Figure 74**, the bacteria culture with CTX concentrations from 0 µg/mL to 5 µg/mL had similar cell shape, size, and fluorescence intensity. However, after increasing CTX concentration to 50 µg/mL, the cell length of *E. coli* BFP increased, and the cell shape of *E. coli* YFP became longer first, then to a dot shape with a bulge. It indicates even after a short time, the high concentration of CTX already influenced the bacteria.

Figure 74: Monoculture and co-culture of *E. coli* BFP 8 and *E. coli* YFP with different concentrations of CTX observed with fluorescence microscopy (0 hours incubation) with 100 × magnification. B mono means *E. coli* BFP monoculture, Y mono represents *E. coli* YFP monoculture, and B+Y means the co-culture of *E. coli* BFP and *E. coli* YFP; CTX concentrations are shown as 0, 0.05, 0.25, 0.5, 5, 50, 250, 500 µg/mL

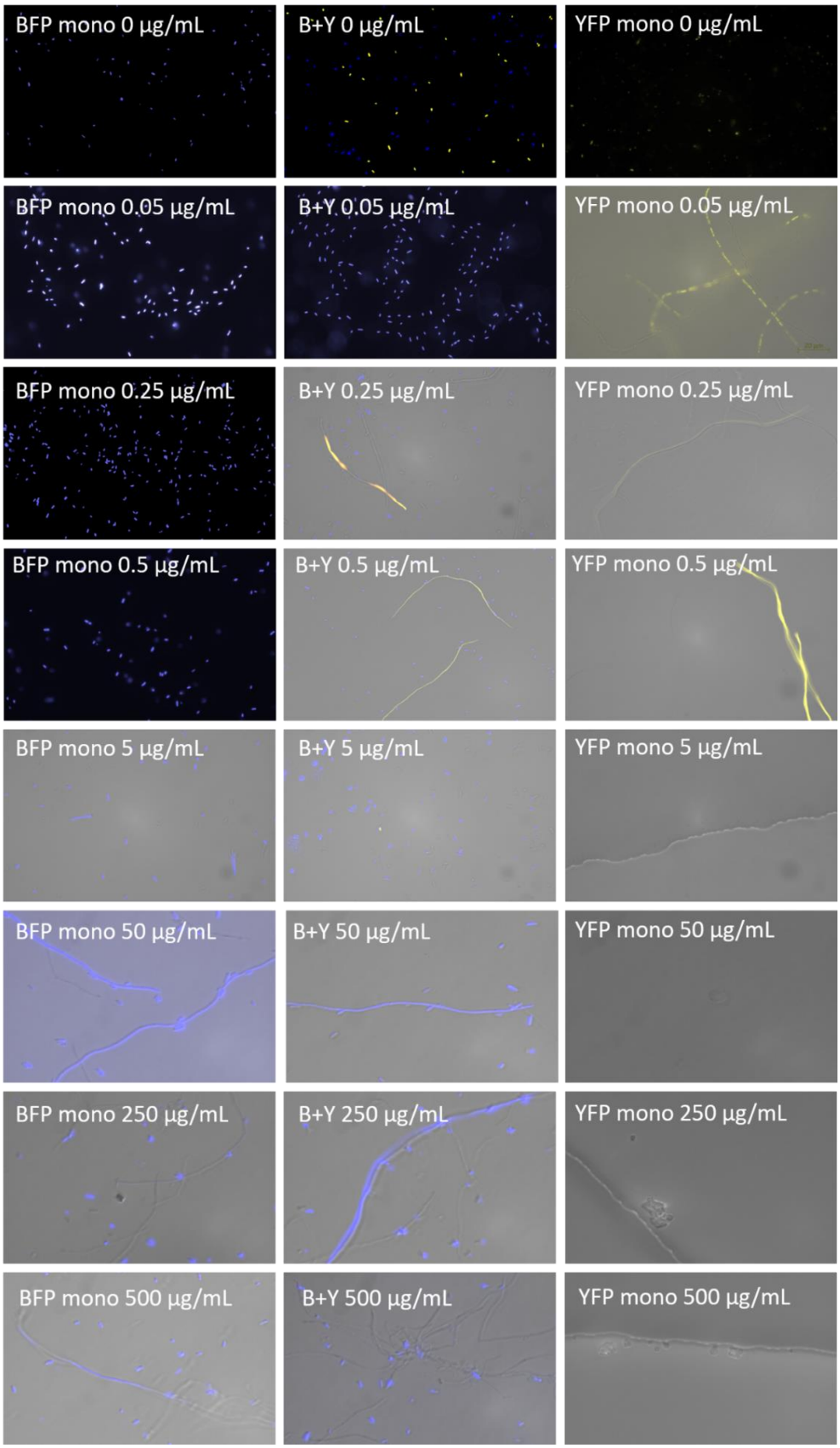

Figure 75: Monoculture and co-culture of *E. coli* BFP 8 and *E. coli* YFP with different concentrations of CTX observed with fluorescence microscopy (20 hours incubation) with 100 × magnification. B mono means *E. coli* BFP monoculture, Y mono represents *E. coli* YFP monoculture, and B+Y means the co-culture of *E. coli* BFP and *E. coli* YFP; CTX concentrations are shown as 0, 0.05, 0.25, 0.5, 5, 50, 250, 500 µg/mL. Pictures with a grey background are the results merged with a bright field to show the lysis cells.

After incubating for 20 hours, as shown in **Figure 75**, cell filamentation was observed. For *E. coli* BFP 8, the cell length became longer once the CTX was more than 5 µg/mL, and the filamentation happened when the CTX concentration was greater than 50 µg/mL. Besides, the fluorescence intensity of some filamentary cells was much stronger than the normal shape cells. Interestingly, these filamentary cells either had strong fluorescence or did not have any fluorescence, which can be clearly observed in **Figure 76**. We speculate that when the CTX concentration is above 250 µg/mL, cells (for *E. coli* BFP 8) start lysis, releasing the fluorescence protein from the cell to the bacterial media. This matched the dramatic fluorescence increase found in the results of the plate reader.

Differently, the filamentation occurred to *E. coli* YFP once the CTX concentration is more than 0.005 µg/mL. Filamentary cell elongated with CTX concentration increase from 0.005 µg/mL to 0.025 µg/mL, as shown in **Figure 77**.

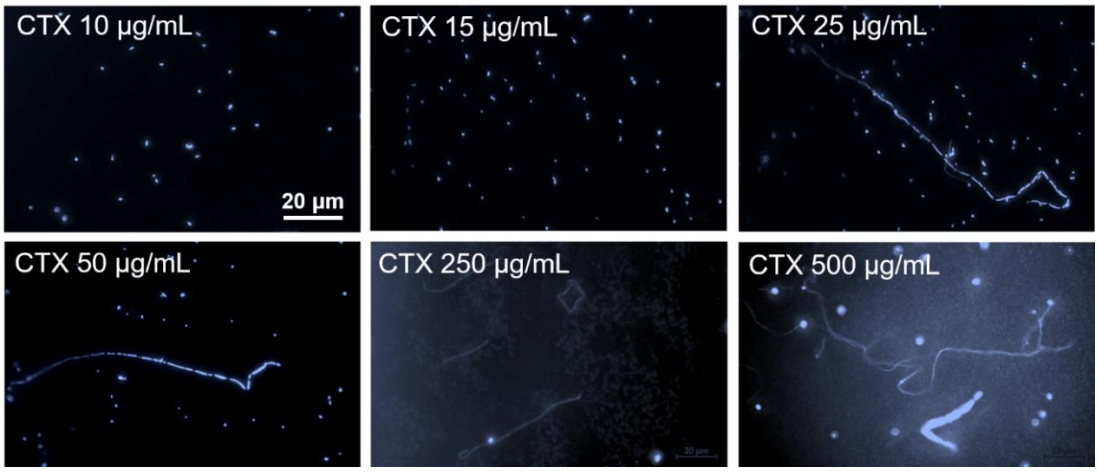

Figure 76: Monoculture of *E. coli* BFP 8 with different concentrations of CTX observed with fluorescence microscopy (20 hours incubation) with 100 × magnification under blue light.

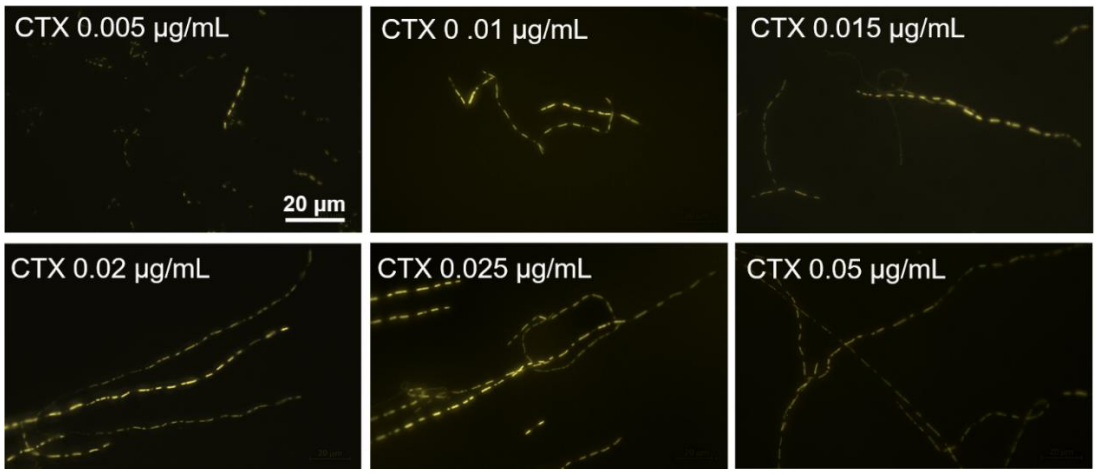

Figure 77: Monoculture of *E. coli* YFP with different concentrations of CTX observed with fluorescence microscopy (20 hours incubation) with 100 × magnification under blue light.

Conspicuously, the *E. coli* YFP grew with the CTX concentration of 0.25 µg/mL or 0.5 µg/mL show strong fluorescence in the filamentary cells. Above the concentration of 5 µg/mL, bacterial cell wreckage was gathered at the media boundary; interestingly, only some still had weak fluorescence. So far, the cell filamentation and cell fluorescence intensity observed by fluorescence microscopy match the results of fluorescence and optical density detected by the plate reader. Hence, we speculate the dramatic cell fluorescence increase is caused by fluorescence protein released from the lysis of bacterial filamentation.

6.8.5 Fluorescence of Cell-Free Media and Cell

According to the cell filamentation observed with microscopy, some filamentary cells have strong fluorescence; some have no fluorescence anymore. The lysis of the cell presumably caused the release of the fluorescence proteins through the cell wall to the bacterial extracellular media. To verify this surmise, the whole-cell media were collected and centrifuged after incubating for 20 hours. The supernatant was sterile filtered for measuring the fluorescence intensity. Sedimentation cells were resuspended to M9 media for fluorescence intensity measurement. The fluorescence results of monoculture and co-culture *E. coli* BFP are presented in **Table 15** and **Figure 78 a, c, and e**; the results of *E. coli* YFP are shown in **Table 16** and **Figure 78 b, d, and f**.

Table 15: *E. coli* BFP monoculture and co-culture fluorescence intensity detection of whole media, cell-free media, and resuspended cell.

***E. coli* BFP 8 monoculture fluorescence intensity**						
CTX (µg/mL)	**0**	**0.05**	**0.25**	**0.5**	**5**	**10**
whole media	1.750	1.710	1.729	1.739	1.507	2.680
cell-free media	0.255	0.305	0.307	0.343	0.547	1.961
resuspended cell	1.525	1.334	0.964	0.845	1.395	2.719
CTX (µg/mL)	**15**	**25**	**50**	**250**	**500**	
whole media	3.309	3.386	3.222	3.007	2.833	
cell-free media	3.927	3.237	2.722	2.758	2.380	
resuspended cell	2.136	1.806	1.877	1.367	1.746	
***E. coli* BFP 8 co-culture fluorescence intensity (with *E. coli* YFP)**						
CTX (µg/mL)	**0**	**0.05**	**0.25**	**0.5**	**5**	**10**
whole media	0.707	0.919	0.946	0.961	1.570	2.355
cell-free media	0.286	0.242	0.308	0.281	0.439	2.208

resuspended cell	0.261	0.359	0.792	1.036	2.044	2.795
CTX (μg/mL)	**15**	**25**	**50**	**250**	**500**	
whole media	3.259	3.401	2.508	2.573	2.006	
cell-free media	3.512	3.263	2.089	2.384	1.974	
resuspended cell	2.454	1.624	2.373	1.934	1.590	

Table 16: *E. coli* YFP monoculture and co-culture fluorescence intensity detection of whole media, cell-free media, and resuspended cell.

***E. coli* YFP monoculture fluorescence intensity**						
CTX (μg/mL)	**0**	**0.05**	**0.25**	**0.5**	**5**	**10**
whole media	1.198	0.409	0.569	0.562	0.070	0.020
cell-free media	0.547	0.396	0.584	0.550	0.063	0.022
resuspended cell	1.219	0.120	0.004	0	0	0
CTX (μg/mL)	15	**25**	**50**	**250**	**500**	
whole media	0.014	0.031	0.025	0.026	0.022	
cell-free media	0.013	0.031	0.013	0.016	0	
resuspended cell	0	0	0	0	0	
***E. coli* YFP co-culture fluorescence intenisty (with *E. coli* BFP 8)**						
CTX (μg/mL)	**0**	**0.05**	**0.25**	**0.5**	**5**	**10**
whole media	0.495	0.158	0.145	0.138	0.097	0
cell-free media	0.125	0.155	0.150	0.160	0.216	0.01
resuspended cell	0.222	0.102	0.157	0.083	0	0
CTX (μg/mL)	15	**25**	**50**	**250**	**500**	
whole media	0	0	0	0	0	
cell-free media	0	0	0	0	0	
resuspended cell	0	0	0	0	0	

For the *E. coli* BFP, below the CTX concentration of 10 μg/mL, most of the fluorescence was from the suspended cells, indicates that the cell wall was still completed. However, when the CTX concentration was above 10 μg/mL, the fluorescence was not only from

the resuspended cell but also cell-free media. It is speculated due to the cell lysis caused by antibiotics.

Likewise, in *E. coli* YFP, fluorescence distribution also reversed mainly from resuspended cells to cell-free media. Notably, the reversion of the fluorescence source happened once the low concentration of CTX was added (0.05 µg/mL) in both monoculture and co-culture cases. Interestingly, the dramatic fluorescence increase disappeared in the co-culture case, and the fluorescence was from not only cell-free media but also resuspended cells. Besides, at the range of the CTX concentration was from 0.05 µg/mL to 0.5 µg/mL, the fluorescence of resuspended cells in co-culture was higher than that of monoculture, which might be caused by cross-protection.

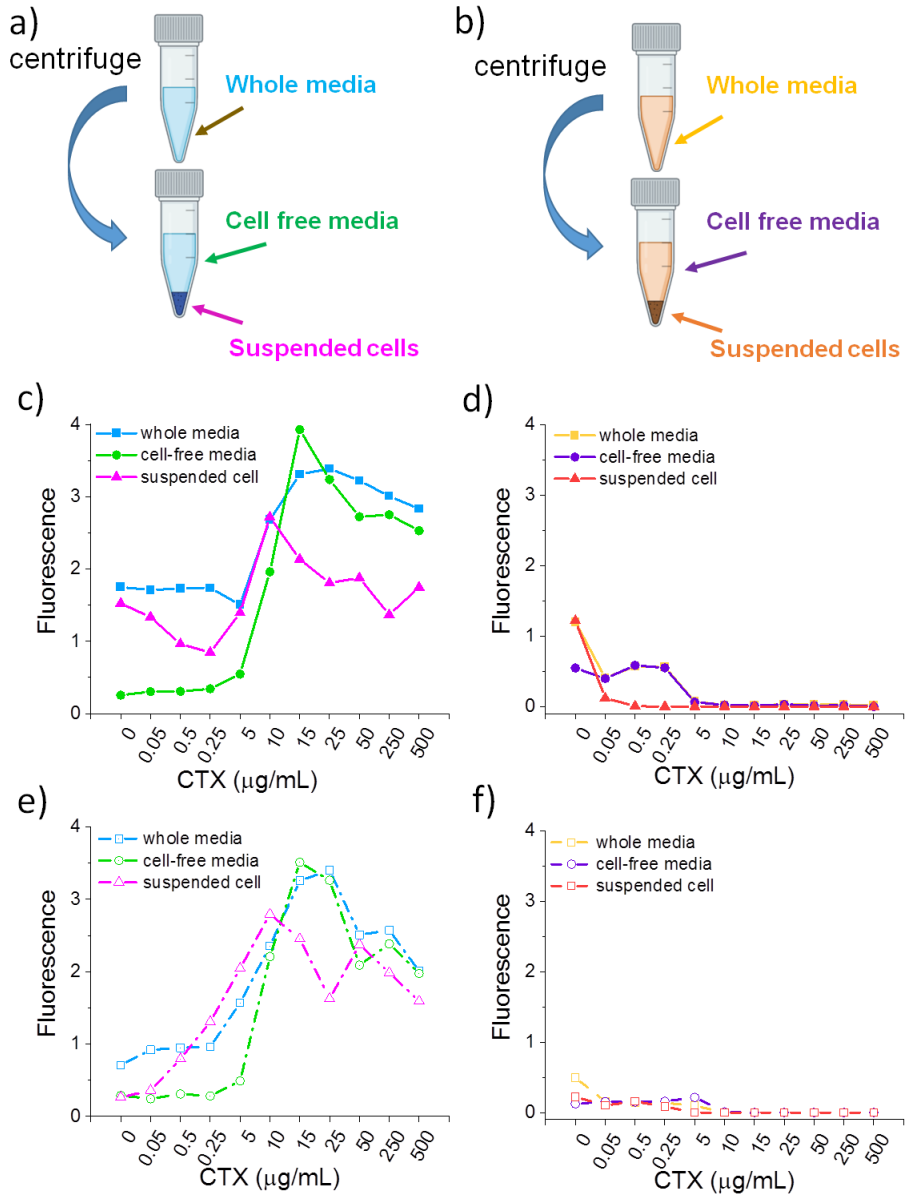

Figure 78: Fluorescence detection of whole media, cell-free media, and resuspended cell of **a)** and **b)** the preparation steps, **c)** *E. coli* BFP monoculture, **d)** *E. coli* YFP monoculture, **e)** *E. coli* BFP co-culture, and **f)** *E. coli* YFP co-culture.

6.8.6 Viable Cell Rate

In a stressful environment, for example, antibiotics and starvation, bacterial cell filamentation happens and helps bacteria tolerate stress damage.[160] Since the β-lactam antibiotic inhibits the cell wall synthesis, filamentary response helps bacteria adjust to the antibiotic environment by stopping bacterial division and copying DNA. From the OD_{600} results, the filamentation cells are still recognized as viable cells. However, whether the cell still has the reproduction ability or restoration has to be proven by testing the viable cell rates. The viable cell rates are done according to the protocol in **Chapter 3.3.9** Cell Viability Detection.

In **Figure 79**, the viable cell rates of *E. coli* BFP decline with increasing antibiotic concentrations. Notably, at a high CTX concentration of 500 µg/mL, half of the bacterial cells are still alive.

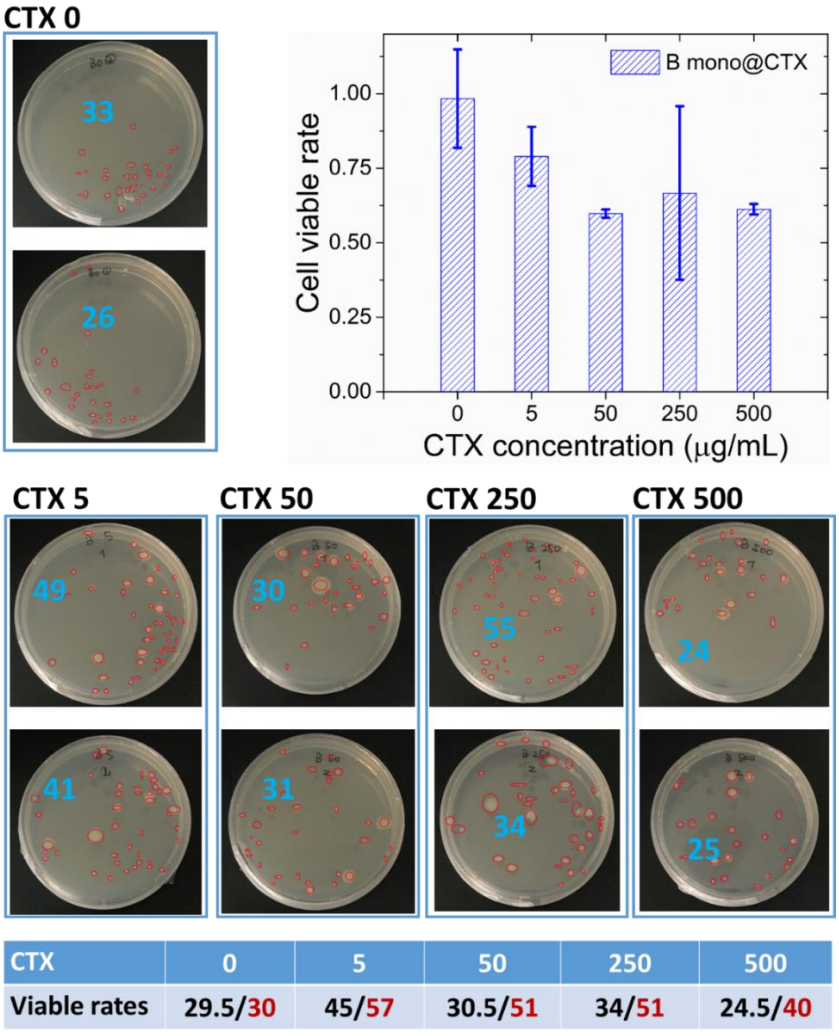

CTX	0	5	50	250	500
Viable rates	29.5/30	45/57	30.5/51	34/51	24.5/40

Figure 79: Cell viable rates of *E. coli* BFP without CTX and with 5, 50, 250, and 500 µg/mL CTX. Blue numbers show the counted colony number. Black numbers represent the average number of the colony (counted) and red numbers are the expected cell numbers measured by OD_{600}.

In contrast, the viable cell rates of *E. coli* YFP sharply dropped once the CTX was used in the culture, as shown in **Figure 80**. It is speculated that the lysis filamentary cells have no reproductive ability to form a colony anymore. In *E. coli* BFP cases, there were still normal cells in the media when cell filamentation happened, so the colony still formed.

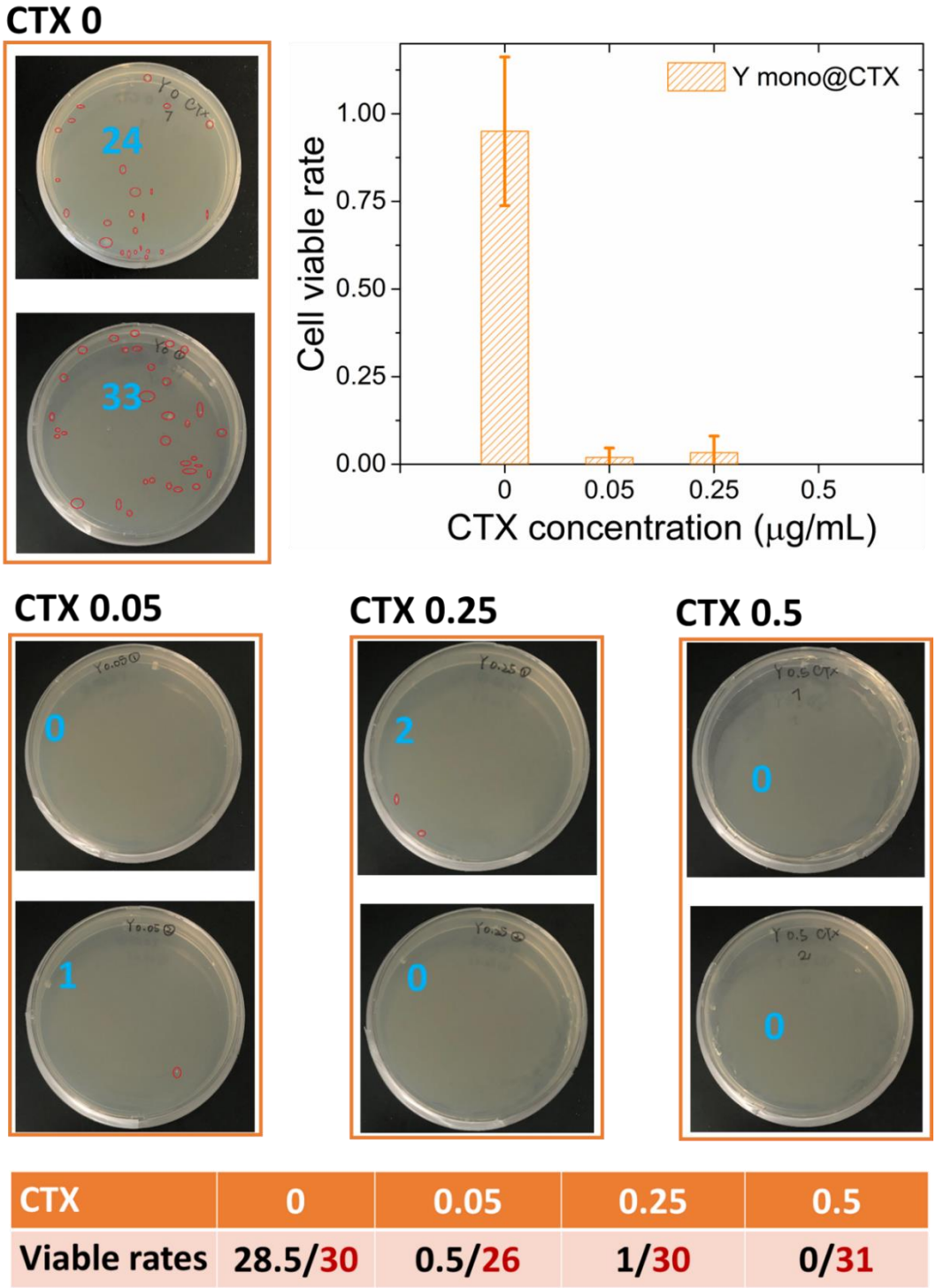

CTX	0	0.05	0.25	0.5
Viable rates	28.5/30	0.5/26	1/30	0/31

Figure 80: Cell viable rates of *E. coli* YFP without CTX and with 0.05, 0.25, and 0.5 μg/mL CTX. Blue numbers show the counted colony number. Black numbers represent the average number of the colony (counted) and red numbers are the expected cell numbers measured by OD_{600}.

6.8.7 Cell Shape Detected by Fluorescence Flow Cytometry

The cell size and shape of the two *E. coli* strains were also detected by flow cytometer to confirm the filamentation appearance and the different MIC of the two strains. In **Figure 81**, *E. coli* BFP 8 and *E. coli* YFP with and without the antibiotic treatment (CTX 0.05 µg/mL) were detected by fluorescence flow cytometry before incubating and after for 20 hours are shown. It clearly shows that after the antibiotic treatment, the cell size and shape of *E. coli* BFP 8 remained. However, the roundness of *E. coli* YFP decreased, indicates that in the CTX 0.05 µg/mL, *E. coli* YFP shows filamentation. Due to *E. coli* BFP 8 has the antibiotic-resistant gene, it still grows well.

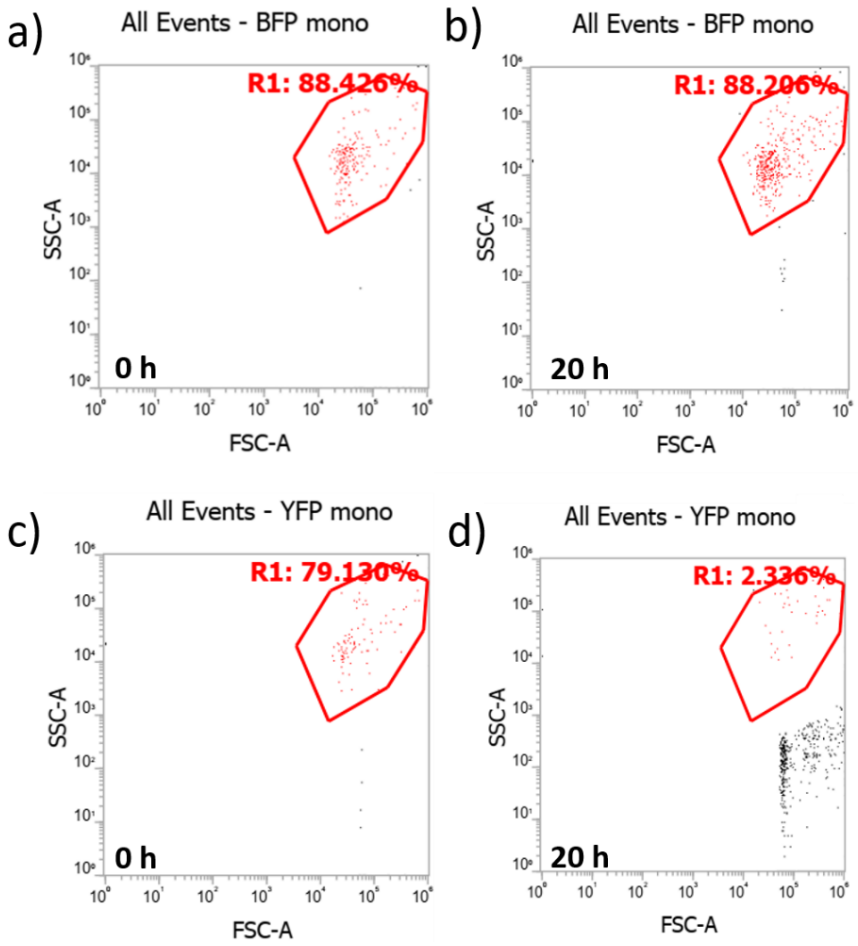

Figure 81: Cell size and shape of the two *E. coli* strains detected by flow cytometer: *E. coli* BFP 8 **a)** without and **b)** with the antibiotic treatment (CTX 0.05 µg/mL) and *E. coli* YFP **c)** without and **d)** with the antibiotic treatment (CTX 0.05 µg/mL).

6.8.8 Detection of β-lactamase Activity

The β-lactamase activity was detected by using nitrocefin. It is a chromogenic β-lactamase substrate that undergoes distinctive color change from yellow as the amide bond in the β-lactam ring is hydrolyzed by β-lactamase. Its quantitative is determined by measuring the red absorption (OD_{490}) in a plate reader.

The monoculture groups of *E. coli* BFP 8 and *E. coli* YFP, which had dramatic fluorescence increases, were first checked. For monoculture *E. coli* BFP 8, groups with 25, 50, 250, 500 μg/mL CTX were tested (M9 media, *E. coli* BFP in M9, and *E. coli* BFP in M9 with IPTG are control groups). It is clear that the groups with CTX finally show the color changed in both the **Figure 82** and OD_{490} detection results (as shown in **Figure 83 a**).

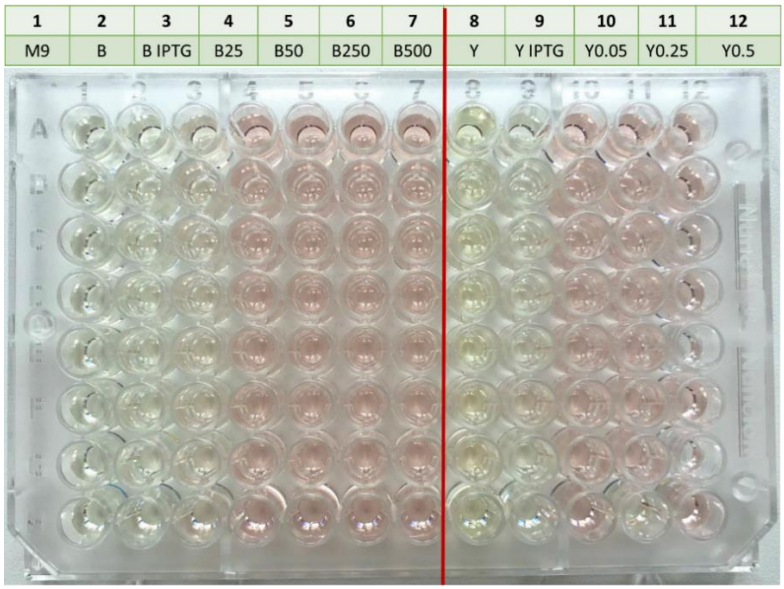

Figure 82: β-lactamase activity testing of monoculture *E. coli* BFP 8 and *E. coli* YFP in 96 well plates with various concentrations of CTX.

The β-lactamase activity testing results of *E. coli* YFP monoculture (in **Figure 83 b)** show high β-lactamase activity in the group with CTX of 0.05, 0.25, and 0.5 μg/mL. 0.05 μg/mL group was lower than the other two groups, which also matches the results of fluorescence intensity. It shows that both the fluorescence protein and β-lactamase were released from the lysis cell under antibiotic stress.

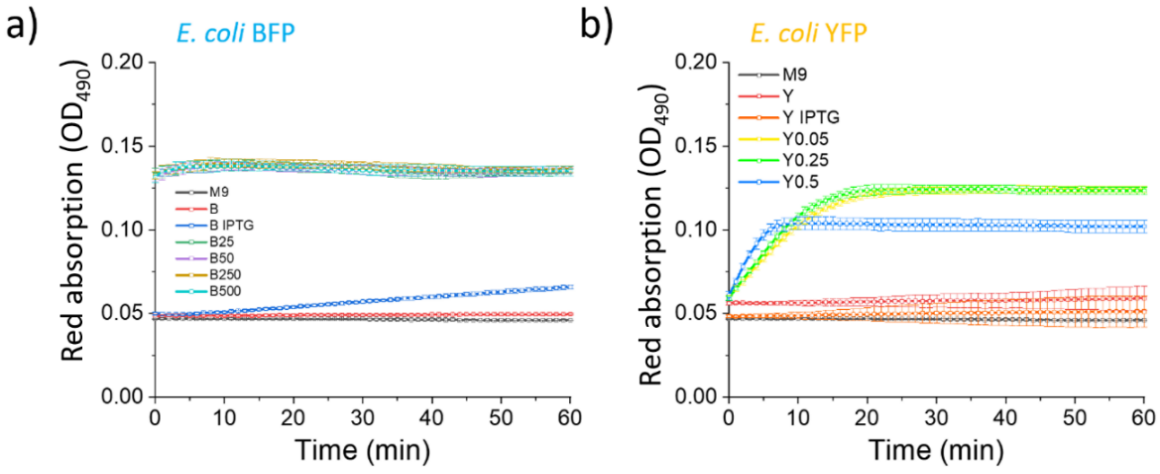

Figure 83: Measurement of red absorption (OD_{490}) of **a)** *E. coli* BFP 8 and **b)** *E. coli* YFP in a plate reader every minute for 1 hour as the nitrocefin is hydrolyzed.

In the β-lactamase activity results of monoculture *E. coli* BFP 8, OD_{490} signal is relatively high, which means the β-lactamase with high concentration quickly consumed the nitrocefin. To accurately evaluate the β-lactamase activity, the cell-free samples were diluted ten times before nitrocefin assay. Besides, more groups with different concentrations of CTX were added and compared in **Figure 84**. We found the groups with higher β-lactamase activity (*E. coli* YFP with 0.05, 0.25 and 0.5 µg/mL CTX; *E. coli* BFP with 10, 15, 25, 50, 250, and 500 µg/mL CTX) showed a dramatic increase in fluorescence intensity. This indicates that both proteins (β-lactamase and fluorescence protein) were released simultaneously from the lysed bacteria and positively correlated with the amount released.

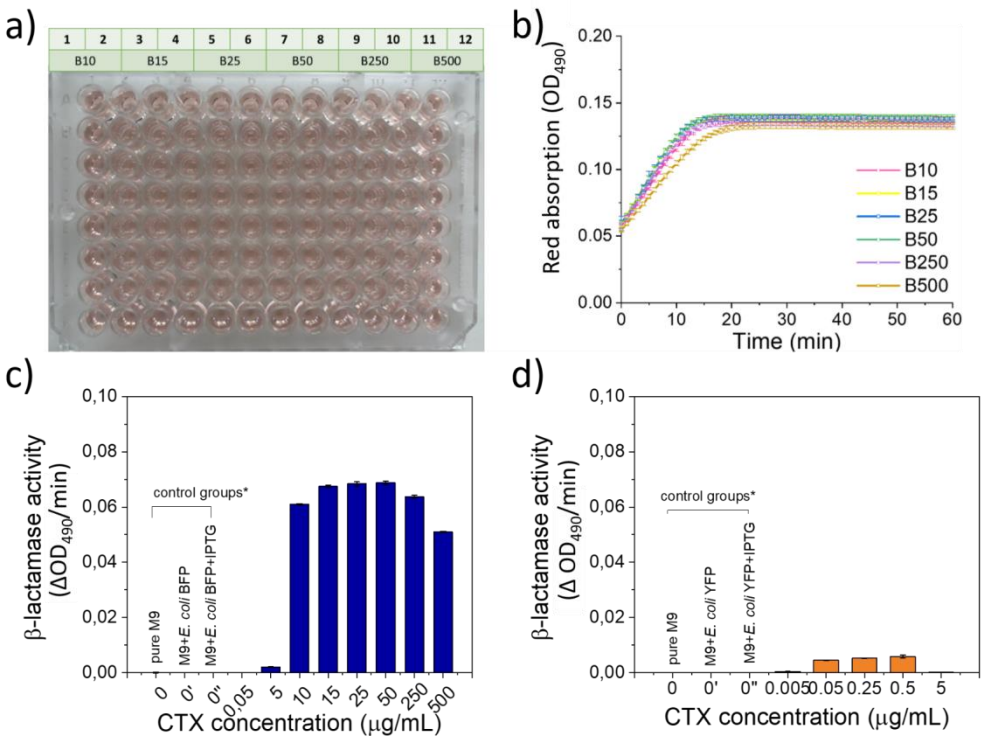

Figure 84: β-lactamase activity testing of monoculture *E. coli* BFP 8 and *E. coli* YFP in 96 well plates with various concentrations of CTX: **a)** *E. coli* BFP 8 color change after 1 hour, **b)** *E. coli* BFP 8 measurement of red absorption (OD_{490}) in a plate reader every minute for 1 hour with the nitrocefin is hydrolyzed; β-lactamase activity of c) *E. coli* BFP 8 (red absorption change per time) and d) *E. coli* YFP (red absorption change per time).

6.9 Conclusion

This chapter mainly focuses on revealing the interaction between the antibiotic-sensitive bacterial strain *E. coli* YFP and antibiotic-resistant strains *E. coli* BFP 8 co-culture in the antibiotic environment. Firstly, the MICs of antibiotics to all *E. coli* groups were detected. Then, by tuning the antibiotic concentration in the droplet sequences, the MICs of antibiotics to different strains were further confirmed. Next, different groups of *E. coli*

BFP were separately co-cultured with *E. coli* YFP in a low concentration of CTX. *E. coli* BFP 8 strain was selected due to its highest MIC, which has ability to produce more β-lactamase to inactivate antibiotics.

Then, the *E. coli* BFP 8 and *E. coli* YFP were monocultured and co-cultured in millifluidic droplet reactors to monitor the microbial co-existence in various concentrations of CTX. All results were further verified with microscopy, flow cytometer, and plate reader. Both strains grew well in the monoculture cases without antibiotic stress and showed a competitive relationship in the co-culture cases.

In monoculture cases, when antibiotic stress was added to the system, the two strains showed different responses to the various antibiotic concentrations. The growth of *E. coli* YFP was influenced by CTX down to 0.05 μg/mL and completely inhibited at 5 μg/mL. Above 5 μg/mL CTX, the growth of *E. coli* BFP 8 showed a slight delay. A further increase in antibiotic concentration caused a flourescence burst in the late stage of the growth curves. This dramatic fluorescence increase was observed around the MIC of both strains in the monoculture cases. This fluorescence burst was speculated to be filamentary cell lysis, which was confirmed by fluorescence microscopy.

In co-culture, with the stress of antibiotics, the growth behavior of *E. coli* BFP was barely impacted. However, the fluorescence burst in the *E. coli* YFP co-culture case was weaker than in the monoculture case.

Moreover, the speculation that the fluorescence burst was related to cell filamentation lysis was also proven by detecting fluorescence from cell-free media (filtered out from the cells) and β-lactamase activity. The results pointed out that the cell wall structure changed after filamentation. Cell viability rates show that the antibiotic effect may lead to cell lysis and death. It is speculated that before the cell wall breaks, the filamentation phenomenon increases the antibiotic tolerance, allowing bacterial survival in the environment with a higher amount of antibiotic doses than its MIC.[160] However, this tolerance disappears when the antibiotic dose is far over the MIC; in this case, both fluorescence proteins and β-lactamase were released from the lysis cells.

Lastly, compared to the *E. coli* YFP monoculture results, the *E. coli* YFP co-culture with *E. coli* BFP 8 can reduce the fluorescence release from cell filamentation, which may occur due to the cross-protection.

7. Summary and Outlook

The main goal of this thesis is to analyze bacterial communities by using a millifluidic droplet-based device. We achieved studying this complex process of bacterial coexistence by successfully developing a system with the properties of high throughput, automatic real-time detection and multi-signal monitoring. This excellent system allows culturing and monitoring two microbial strains in liquid media over an extended period. It also allows sample retrieval without affecting bacterial growth and observing up to 1000 droplets at one time.

In the first part, we used millifluidic droplet-based reactors to analyze the growth curves of *E. coli* BFP and *E. coli* YFP in monoculture and co-culture cases and explained the interaction and relationship between them. Focusing on analyzing the two coexisting strains, the *E. coli* YFP growth was demonstrated to be slightly faster than *E. coli* BFP in monoculture cases and sustains the advantage in co-culture cases when the initial ratio $R_0 < 2$. The 2D doubling time distribution map intuitively showed the growth status of two bacterial strains in each droplet. By combining the modeling results with the experimental data, we found a trade-off between growth rate and relative biomass yield caused by the competition.

In the second part, the antibiotic-sensitive bacterial strain *E. coli* YFP and antibiotic-resistant strains *E. coli* BFP 1-8 groups were separately mono-cultured and co-cultured in the millifluidic droplet-based reactors. Both optical density and fluorescence intensity were measured and compared to quantify the *E. coli* growth in an antibiotic environment with various CTX concentrations. A dramatic fluorescence increase was observed and confirmed to be filamentary cell lysis by fluorescence microscopy. The cell viability rate results showed that the antibiotic effect might lead to cell lysis and death. The results of detecting fluorescence from cell-free media (filtered from the cells) and β-lactamase activity pointed out that the cell wall structure changed after filamentation. It is speculated that before the cell wall breaks, the filamentation phenomenon increases the antibiotic tolerance, allowing bacterial survival in environments with a higher dose of antibiotics than its MIC. However, this tolerance disappears when the antibiotic dose is far over the MIC; in this case, both fluorescence proteins and β-lactamase release from the lysis cells. Moreover, compared to the *E. coli* YFP monoculture results, the *E. coli* YFP co-culture with *E. coli* BFP 8 can reduce the fluorescence release from filamentary cells, which may occur due to cross-protection.

In summary, compared to traditional bacterial detection equipment (such as Biophotometer, fluorescent microscopy, plate reader, and flow cytometry), droplet-based millifluidics have shown advantages in coexistence studies even in a complex environment. It is a reliable and low-cost device and can achieve high-throughput, near real-time and long-term detection. Moreover, it allows automatic real-time detection and multi-signal monitoring. This system has the potential to miniaturize microbial coexistence assays, allowing a controlled single-cell inoculum size. However, due to the LODs, accurate single-cell detection in millifluidic devices is still not possible. To improve it, we need a better optical wavelength filter to as much as possible filter out the light that can influence fluorescence detection. At the same time, we need to be able to remove the signal noises from the black box (*eg.*, the light reflection and diffraction from the other components) as much as possible.

In the future, we expect to gelled droplets by combining millifluidics with solid agar. By seeding the bacteria into the droplets before they are gelled (agarose), the bacteria will be encapsulated in a solid medium environment as the droplet jellifies. The Brownian motion of bacteria grown in a gelatinized droplet will be limited compared to the well-mixed environment in which bacteria are cultured in aqueous droplets. As a result, the bacteria will occupy different areas and form colonies. By comparing bacteria in different culture environments (liquid droplets and gel droplets) with the same antibiotic concentration, we expect to find out the effect of spatial structure on bacterial culture in the antibiotic environment. In addition, we also expect to update the system to contain the feature of droplet sorting. The droplet with different fluorescence signal will be located and sorted out of the system by automatically switching the valves. The droplet sorted out can be further studied to find out the reason for showing the different signals. Besides, this platform is envisioned to succeed in further practical applications of multispecies studies, including drug resistance at the clinical research level.

Publications

Publications in peer review journals

X. Zhao, R. Illing, P. Ruelens, M. Bachmann, J. A. G. M. de Visser, G. Cuniberti and L. Baraban, *Coexistence of the E.coli strains in millfluidic droplets reactors*, Lab on a Chip, **2021**, 21(8), pp 1492-1502.

T. A. Nguyen Le, **X. Zhao (co-first author)**, M. Bachmann, G. Cuniberti and L. Baraban, *Bacterial coexistence in jelly beads*, in preparation.

X. Zhao, P. Ruelens, M. Bachmann, J. A. G. M. de Visser, G. Cuniberti and L. Baraban, *Reveal Bacterial Interaction in Antibiotic Environments*, in preparation.

Oral Presentations in conference

X. Zhao, R. Illing., G. Cuniberti and L. Baraban, *Co-survival and competition relationship between bacteria analyzed in millifluidic droplet sequence,* DPG Frühjahrstagung, **2019**, Regensburg, Germany.

X. Zhao, P. Ruelens, J. A. G. M., de Visser and L. Baraban, *Microfluidic Droplet Reactors to Reveal the Bacterial Interaction in an Antibiotic Environment*, Lab-on-a-Chip and Microfluidics Europe, **2021**, Rotterdam, The Netherlands.

Acknowledgments

First and foremost, I would like to express my sincere thanks to Prof. Cuniberti for offering me the precious opportunity to be a member of this remarkable group.

I am extremely grateful to my supervisor, Dr. Baraban, for her invaluable advice, continuous support, and patience during my Ph.D. study. Her immense knowledge and plentiful experience have encouraged me in all the time of my academic research.

My gratitude extends to Prof. Bachmann for offering me the opportunity to undertake my studies at the Institute of Radiopharmaceutical Cancer Research, Helmholtz-Zentrum Dresden-Rossendorf.

I also appreciate all the support I received from my group members at the chair of materials science and nanotechnology and the Nano-Microsystems research group for Life Sciences at Helmholtz-Zentrum Dresden-Rossendorf.

I want to thank Prof. Arjan de Visser and Dr. Ruelens for supplying the modified bacteria and technical support.

My appreciation also goes out to my family and friends for their encouragement and support through my studies, especially to my mother, who supports my decisions all the time.

Lastly, I would like to thank the China Scholarship Council for the studentship that allowed me to conduct this thesis.

References

1. Holt, R. D., Spatial Heterogeneity, Indirect Interactions, and the Coexistence of Prey Species. Am. Nat, Vol. 124, (1984).
2. Das, P., Ji, B., Kovatcheva-Datchary, P., et al., In vitro co-cultures of human gut bacterial species as predicted from co-occurrence network analysis. *PLoS One* **13**, e0195161 (2018).
3. Keller, L. and Surette, M. G., Communication in bacteria: an ecological and evolutionary perspective. *Nat Rev Microbiol* **4**, 249-58 (2006).
4. Hibbing, M. E., Fuqua, C., Parsek, M. R., et al., Bacterial competition: surviving and thriving in the microbial jungle. *Nat Rev Microbiol* **8**, 15-25 (2010).
5. Savage, D. C., Microbial ecology of the gastrointestinal tract. *Ann. Rev. Microbiol* **31**, 107-133 (1977).
6. Luckey, T. D., Introduction to the Ecology of the Intestinal Flora. *Am. J. Clin. Nutr. AM J CLIN NUTR* **23**, 1430–1432 (1970).
7. Quigley, E. M. M., Gut Bacteria in Health and Disease. *Gastroenterol Hepatol* **9**, 560-569 (2013).
8. Huang, T. T., Lai, J. B., Du, Y. L., et al., Current Understanding of Gut Microbiota in Mood Disorders: An Update of Human Studies. *Front Genet* **10**, 98 (2019).
9. Iida, N., Dzutsev, A., Stewart, C. A., et al., Commensal bacteria control cancer response to therapy by modulating the tumor microenvironment. *Science* **342**, 967-70 (2013).
10. Armstrong, R. A. and Mcgrhee, R., Coexistence of Species Competing for Shared Resources. *Theor. Popul. Biol.* **9**, 317-328 (1976).
11. Cornforth, D. M. and Foster, K. R., Competition sensing: the social side of bacterial stress responses. *Nat Rev Microbiol* **11**, 285-93 (2013).
12. Danku, Z., Perc, M. and Szolnoki, A., Knowing the past improves cooperation in the future. *Sci Rep* **9**, 262 (2019).
13. Murray, C. J. L., Ikuta, K. S., Sharara, F., et al., Global burden of bacterial antimicrobial resistance in 2019: a systematic analysis. *The Lancet* **399**, 629-655 (2022).
14. Vos, T., Lim, S. S., Abbafati, C., et al., Global burden of 369 diseases and injuries in 204 countries and territories, 1990–2019: a systematic analysis for the Global Burden of Disease Study 2019. *The Lancet* **396**, 1204-1222 (2020).
15. Martinez, J. L. and Baquero, F., Interactions among strategies associated with bacterial infection: pathogenicity, epidemicity, and antibiotic resistance. *Clin Microbiol Rev* **15**, 647-79 (2002).
16. Geyrhofer, L. and Brenner, N., Coexistence and cooperation in structured habitats. *BMC Ecol* **20**, (2020).
17. Tilman, D., Isbell, F. and Cowles, J. M., Biodiversity and Ecosystem Functioning. *Annu Rev Ecol Evol Syst* **45**, 471-493 (2014).
18. Kerr, B., Riley, M. A., Feldman, M. W., et al., Local dispersal promotes biodiversity in a real-life game of rock–paper–scissors. *Nature* **418**, 171-174 (2002).
19. Kaji, H., Camci-Unal, G., Langer, R., et al., Engineering systems for the generation of patterned co-cultures for controlling cell–cell interactions. *Biochim Biophys Acta Gen Subj* **1810**, 239-250 (2011).
20. Cairns, J., Jokela, R., Hultman, J., et al., Construction and Characterization of Synthetic Bacterial Community for Experimental Ecology and Evolution. *Front Genet* **9**, 312 (2018).
21. Goers, L., Freemont, P. and Polizzi, K. M., Co-culture systems and technologies: taking synthetic biology to the next level. *J R Soc Interface* **11**, 20140065 (2014).
22. Ahern, H., Microbiology: A Laboratory Experience. State University of New York OER Services: State University of New York at Geneseo, (2018).
23. Lopez, D. and Kolter, R., Extracellular signals that define distinct and coexisting cell fates in Bacillus subtilis. *FEMS Microbiol Rev* **34**, 134-49 (2010).
24. Bogdanowicz, D. R. and Lu, H. H., Studying cell-cell communication in co-culture. *Biotechnol J* **8**, 395-6 (2013).
25. Iwadate, H., Yamada, M., Kimura, N., et al., PDMS microstencil plate-supported fabrication of ultra-thin, condensed ECM membranes for separated cell coculture on both surfaces.

Sens. Actuators B Chem. **287**, 486-495 (2019).
26. Thogersen, M. S., Melchiorsen, J., Ingham, C., et al., A Novel Microbial Culture Chamber Co-cultivation System to Study Algal-Bacteria Interactions Using Emiliania huxleyi and Phaeobacter inhibens as Model Organisms. *Front Microbiol* **9**, 1705 (2018).
27. Fenn, K., Strandwitz, P., Stewart, E. J., et al., Quinones are growth factors for the human gut microbiota. *Microbiome* **5**, 161 (2017).
28. Acai, P., Medved'ova, A., Mancuskova, T., et al., Growth prediction of two bacterial populations in co-culture with lactic acid bacteria. *Food Sci Technol Int* **25**, 692-700 (2019).
29. Stephens, K., Pozo, M., Tsao, C. Y., et al., Bacterial co-culture with cell signaling translator and growth controller modules for autonomously regulated culture composition. *Nat Commun* **10**, 4129 (2019).
30. Jones, J. A. and Wang, X., Use of bacterial co-cultures for the efficient production of chemicals. *Curr Opin Biotechnol* **53**, 33-38 (2018).
31. Moutinho, T. J., Jr., Panagides, J. C., Biggs, M. B., et al., Novel co-culture plate enables growth dynamic-based assessment of contact-independent microbial interactions. *PLoS One* **12**, e0182163 (2017).
32. Osmekhina, E., Jonkergouw, C., Schmidt, G., et al., Controlled communication between physically separated bacterial populations in a microfluidic device. *Commun Biol* **1**, 97 (2018).
33. Kremers, G. J., Gilbert, S. G., Cranfill, P. J., et al., Fluorescent proteins at a glance. *J Cell Sci* **124**, 157-60 (2011).
34. Surette, C. M. S. a. M. G., The dynamic microbe: green fluorescent protein brings bacteria to light. *Mol. Microbiol.* **45**, 1191–1196 (2002).
35. Kaushal, D., Ma, L., Zhang, G., et al., Green Fluorescent Protein Labeling of Listeria, Salmonella, and Escherichia coli O157:H7 for Safety-Related Studies. *PLoS ONE* **6**, (2011).
36. Guo, X., Silva, K. P. T. and Boedicker, J. Q., Single-cell variability of growth interactions within a two-species bacterial community. *Phys Biol* **16**, 036001 (2019).
37. Terekhov, S. S., Smirnov, I. V., Stepanova, A. V., et al., Microfluidic droplet platform for ultrahigh-throughput single-cell screening of biodiversity. *Proc. Natl. Acad. Sci. U.S.A.* **114**, 2550-2555 (2017).
38. Cottinet, D., Condamine, F., Bremond, N., et al., Lineage Tracking for Probing Heritable Phenotypes at Single-Cell Resolution. *PLoS One* **11**, e0152395 (2016).
39. Baraban, L., Bertholle, F., Salverda, M. L. M., et al., Millifluidic droplet analyser for microbiology. *Lab Chip* **11**, (2011).
40. Illing, R., Burkart, C., Pfitzner, D., et al., Ecotoxicity assessment using ciliate cells in millifluidic droplets. *Biomicrofluidics* **10**, 024115 (2016).
41. DeMello, A. J., Control and detection of chemical reactions in microfluidic systems. *Nature* **442**, 394-402 (2006).
42. Bhatia, S. N. and Ingber, D. E., Microfluidic organs-on-chips. *Nat Biotechnol* **32**, 760-72 (2014).
43. Yeo, L. Y., Chang, H. C., Chan, P. P., et al., Microfluidic devices for bioapplications. *Small* **7**, 12-48 (2011).
44. Elvira, K. S., Casadevall i Solvas, X., Wootton, R. C., et al., The past, present and potential for microfluidic reactor technology in chemical synthesis. *Nat Chem* **5**, 905-15 (2013).
45. Guijt, R. M., Dodge, A., van Dedem, G. W., et al., Chemical and physical processes for integrated temperature control in microfluidic devices. *Lab Chip* **3**, 1-4 (2003).
46. Mehling, M. and Tay, S., Microfluidic cell culture. *Curr Opin Biotechnol* **25**, 95-102 (2014).
47. Becker, H. and Locascio, L. E., Polymer microfluidic devices. *Talanta* **56**, 267-287 (2002).
48. Todd Thorsen, S. J. M. a. S. R. Q., Microfluidic Large-Scale Integration. *Science* **298**, 580-584 (2002).
49. Schutt, J., Ibarlucea, B., Illing, R., et al., Compact Nanowire Sensors Probe Microdroplets. *Nano Lett* **16**, 4991-5000 (2016).
50. Boitard, L., Cottinet, D., Bremond, N., et al., Growing microbes in millifluidic droplets. *Eng. Life Sci.* **15**, 318-326 (2015).
51. Tsuda, S., Jaffery, H., Doran, D., et al., Customizable 3D Printed 'Plug and Play' Millifluidic Devices for Programmable Fluidics. *PLoS One* **10**, e0141640 (2015).
52. Kitson, P. J., Rosnes, M. H., Sans, V., et al., Configurable 3D-Printed millifluidic and

microfluidic 'lab on a chip' reactionware devices. *Lab Chip* **12**, 3267-71 (2012).
53. Sai Krishna, K., Navin, C. V., Biswas, S., et al., Millifluidics for time-resolved mapping of the growth of gold nanostructures. *J Am Chem Soc* **135**, 5450-6 (2013).
54. Lam, P., Wynne, K. J. and Wnek, G. E., Surface-Tension-Confined Microfluidics. *Langmuir* **18**, 948-951 (2002).
55. Atencia, J. and Beebe, D. J., Controlled microfluidic interfaces. *Nature* **437**, 648-55 (2005).
56. Lee, C. Y., Chang, C. L., Wang, Y. N., et al., Microfluidic mixing: a review. *Int J Mol Sci* **12**, 3263-87 (2011).
57. Ward, K. and Fan, Z. H., Mixing in microfluidic devices and enhancement methods. *J Micromech Microeng* **25**, (2015).
58. Teh, S. Y., Lin, R., Hung, L. H., et al., Droplet microfluidics. *Lab Chip* **8**, 198-220 (2008).
59. Garstecki, P., Fuerstman, M. J., Stone, H. A., et al., Formation of droplets and bubbles in a microfluidic T-junction-scaling and mechanism of break-up. *Lab Chip* **6**, 437-46 (2006).
60. Liu, H. and Zhang, Y., Droplet formation in microfluidic cross-junctions. *Phys. Fluids* **23**, (2011).
61. Yu, W., Liu, X., Zhao, Y., et al., Droplet generation hydrodynamics in the microfluidic cross-junction with different junction angles. *Chem. Eng. Sci.* **203**, 259-284 (2019).
62. Trivedi, V., Doshi, A., Kurup, G. K., et al., A modular approach for the generation, storage, mixing, and detection of droplet libraries for high throughput screening. *Lab Chip* **10**, 2433-42 (2010).
63. Sugiura, S., Nakajima, M., Yamamoto, K., et al., Preparation characteristics of water-in-oil-in-water multiple emulsions using microchannel emulsification. *J Colloid Interface Sci* **270**, 221-8 (2004).
64. Bridson, E. Y., Brecker, A., Design and Formulation of Microbial Culture Media. In *Methods in Microbiology*, Elsevier: London, England, 1970; Vol. 3, Part A, pp 229-295.
65. Laupland, K. B. and Valiquette, L., The changing culture of the microbiology laboratory. *Can J Infect Dis Med Microbiol* **24**, 125-128 (2013).
66. Braga, P. A. C., Tata, A., Gonçalves dos Santos, V., et al., Bacterial identification: from the agar plate to the mass spectrometer. *RSC Adv.* **3**, 994-1008 (2013).
67. Abayasekara, L. M., Perera, J., Chandrasekharan, V., et al., Detection of bacterial pathogens from clinical specimens using conventional microbial culture and 16S metagenomics: a comparative study. *BMC Infect Dis* **17**, 631 (2017).
68. A Rouf, V. K., HR Naik, Bazilla Naseer and Tahiya Qadri, An overview of microbial cell culture. *Journal of Pharmacognosy and Phytochemistry* **6**, 1923-1928 (2017).
69. Lagier, J. C., Edouard, S., Pagnier, I., et al., Current and past strategies for bacterial culture in clinical microbiology. *Clin Microbiol Rev* **28**, 208-36 (2015).
70. Ochsner, M., Dusseiller, M. R., Grandin, H. M., et al., Micro-well arrays for 3D shape control and high resolution analysis of single cells. *Lab Chip* **7**, 1074-7 (2007).
71. Shiloh, M. U., Ruan, J. and Nathan, C., Evaluation of Bacterial Survival and Phagocyte Functionwith a Fluorescence-Based Microplate Assay. *Infect. Immun.* **65**, 3193–3198 (1997).
72. Au, S. H., Shih, S. C. and Wheeler, A. R., Integrated microbioreactor for culture and analysis of bacteria, algae and yeast. *Biomed Microdevices* **13**, 41-50 (2011).
73. Gawad, S., Schild, L., and Renaud, P. H., Micromachined impedance spectroscopy flow cytometer for cell analysis and particle sizing. *Lab Chip* **1**, 76-82 (2001).
74. Mazutis, L., Gilbert, J., Ung, W. L., et al., Single-cell analysis and sorting using droplet-based microfluidics. *Nat Protoc* **8**, 870-91 (2013).
75. Jiang, L., Boitard, L., Broyer, P., et al., Digital antimicrobial susceptibility testing using the MilliDrop technology. *Eur J Clin Microbiol Infect Dis* **35**, 415-22 (2016).
76. Lohse, S. E., Size and shape control of metal nanoparticles in millifluidic reactors. *Phys. Sci. Rev.* **3**, (2018).
77. Lohse, S. E., Eller, J. R., Sivapalan, S. T., et al., A Simple Millifluidic Benchtop Reactor System for the High-Throughput Synthesis and Functionalization of Gold Nanoparticles with Different Sizes and Shapes. *ACS Nano* **7**, 4135–4150 (2013).
78. Seaberg, J., Kaabipour, S., Hemmati, S., et al., A rapid millifluidic synthesis of tunable polymer-protein nanoparticles. *Eur J Pharm Biopharm* **154**, 127-135 (2020).
79. Niehaus, L., Boland, I., Liu, M., et al., Microbial coexistence through chemical-mediated

interactions. *Nat Commun* **10**, 2052 (2019).
80. Wagg, C., Schlaeppi, K., Banerjee, S., et al., Fungal-bacterial diversity and microbiome complexity predict ecosystem functioning. *Nat. Commun.* **10**, 4841 (2019).
81. Monod, J., The growth of bacterial cultures. *Ann. Rev. Microbiol.* **3**, 371-394 (1949).
82. Butler, D., Goel, N., Goodnight, L., et al., Detection of bacterial metabolism in lag-phase using impedance spectroscopy of agar-integrated 3D microelectrodes. *Biosens Bioelectron* **129**, 269-276 (2019).
83. Swain, P. S., Stevenson, K., Leary, A., et al., Inferring time derivatives including cell growth rates using Gaussian processes. *Nat. Commun.* **7**, (2016).
84. Al-Qadiri, H. M., Al-Alami, N. I., Lin, M., et al., Studying of the Bacterial Growth Phases Using Fourier Transform Infrared Spectroscopy and Multivariate Analysis. *Journal of Rapid Methods & Automation in Microbiology* **16**, 73-89 (2008).
85. Baranyi, J. and Roberts, T. A., A dynamic approach to predicting bacterial growth in food. *Int. J. Food Microbiol.* **23**, 277-294 (1994).
86. Zwietering, M. H., Jongenburger, I., Rombouts, F. M., et al., Modeling of the Bacterial Growth Curve. *Appl. Environ. Microbiol.* **56**, 1875-1881 (1990).
87. Gopalsamy, K., Exchange of equilibria in two species Lotka-Volterra competition models. *J. Aust. Math. Soc.* **24**, 160-170 (2009).
88. Dantas, G., Sommer, M. O. A., Oluwasegun, R. D., et al., Bacteria Subsisting on Antibiotics. *Science* **320**, 100-103 (2008).
89. Vidal, L., Paul, M., Ben dor, I., et al., Oral versus intravenous antibiotic treatment for febrile neutropenia in cancer patients: a systematic review and meta-analysis of randomized trials. *J Antimicrob Chemother* **54**, 29-37 (2004).
90. Adamu, B., Abdu, A., Abba, A. A., et al., Antibiotic prophylaxis for preventing post solid organ transplant tuberculosis. *Cochrane Database Syst Rev*, CD008597 (2014).
91. Bell, M., Antibiotic misuse: a global crisis. *JAMA Intern Med* **174**, 1920-1 (2014).
92. Hutchings, M. I., Truman, A. W. and Wilkinson, B., Antibiotics: past, present and future. *Curr Opin Microbiol* **51**, 72-80 (2019).
93. Lewis, K., Platforms for antibiotic discovery. *Nat Rev Drug Discov* **12**, 371-87 (2013).
94. Aminov, R. I., A brief history of the antibiotic era: lessons learned and challenges for the future. *Front Microbiol* **1**, 134 (2010).
95. O'Rourke, A., Beyhan, S., Choi, Y., et al., Mechanism-of-Action Classification of Antibiotics by Global Transcriptome Profiling. *Antimicrob Agents Chemother* **64**, (2020).
96. Stokes, J. M., Lopatkin, A. J., Lobritz, M. A., et al., Bacterial Metabolism and Antibiotic Efficacy. *Cell Metab* **30**, 251-259 (2019).
97. Béahdy, J., Recent Developments of Antibiotic Research and Classification of Antibiotics According to Chemical Structure. In *Advances in Applied Microbiology*, Elsevier: Research Institute for Pihamceutical Chemistry, Budapest, Hungary, 1974; Vol. 18, pp 309-406.
98. Walsh, M. A. F. a. C. T., Antibiotics for Emerging Pathogens. *Science* **325**, 1089-1093 (2009).
99. Ventola, C. L., The Antibiotic Resistance Crisis. *Pharmacy and Therapeutics* **40**, 227-283 (2015).
100. Lee, D., Das, S., Dawson, N. L., et al., Novel Computational Protocols for Functionally Classifying and Characterising Serine Beta-Lactamases. *PLoS Comput Biol* **12**, e1004926 (2016).
101. Demain, A. L. and Elander, R. P., The β-lactam antibiotics: past, present, and future. *Antonie van Leeuwenhoek* **75**, 5-19 (1999).
102. Lam, T., Brennan, M. D., Morrison, D. A., et al., Femtoliter droplet confinement of Streptococcus pneumoniae: bacterial genetic transformation by cell-cell interaction in droplets. *Lab Chip* **19**, 682-692 (2019).
103. Collignon, P. J., Antibiotic resistance. *Med. J. Aust.* **177**, 325-329 (2002).
104. Yurtsev, E. A., Conwill, A. and Gore, J., Oscillatory dynamics in a bacterial cross-protection mutualism. *Proc Natl Acad Sci U S A* **113**, 6236-41 (2016).
105. Fisher, J. F., Meroueh, S. O. and Mobashery, S., Bacterial Resistance to β-Lactam Antibiotics: Compelling Opportunism, Compelling Opportunity. *Chem. Rev.* **105**, 395-424 (2005).
106. Poole, K., Resistance to beta-lactam antibiotics. *Cell Mol Life Sci* **61**, 2200-23 (2004).
107. Then, R., Beta-Lactamase. In *xPharm: The Comprehensive Pharmacology Reference*, Bylund, S. J. E. a. D. B., Ed. Elsevier: Allschwil, Switzerland, 2007; pp 1-9.

108. Thorsing, M., Bentin, T., Givskov, M., et al., The bactericidal activity of beta-lactam antibiotics is increased by metabolizable sugar species. *Microbiology (Reading)* **161**, 1999-2007 (2015).
109. Diene, S. M., Pinault, L., Keshri, V., et al., Human metallo-beta-lactamase enzymes degrade penicillin. *Sci Rep* **9**, 12173 (2019).
110. Chantemesse, B., Betelli, L., Solanas, S., et al., A nitrocefin-based amperometric assay for the rapid quantification of extended-spectrum beta-lactamase-producing Escherichia coli in wastewaters. *Water Res* **109**, 375-381 (2017).
111. Andrews, J. M., Determination of minimum inhibitory concentrations. *J. Antimicrob. Chemother.* **48**, 5-16 (2001).
112. Chikezie, I. O., Determination of minimum inhibitory concentration (MIC) and minimum bactericidal concentration (MBC) using a novel dilution tube method. *Afr. J. Microbiol. Res.* **11**, 977-980 (2017).
113. Datsenko, K. A. and Wanner, B. L., One-step inactivation of chromosomal genes in Escherichia coli K-12 using PCR products. *Proc. Natl. Acad. Sci. U.S.A.* **97**, 6640–6645 (2000).
114. Kelly, S. and Kouzmin, A., Reframing strategic thinking: emergence beyond the box. *J. Manag. Dev.* **28**, (2009).
115. Edwards, J. S. and Palsson, B. O., The Escherichia coli MG1655 in silico metabolic genotype: Its definition, characteristics, and capabilities. *Proc. Natl. Acad. Sci. U.S.A.* **97**, 5528–5533 (2000).
116. Lee, S. J., Trostel, A., Le, P., et al., Cellular stress created by intermediary metabolite imbalances. *Proc. Natl. Acad. Sci. U.S.A.* **106**, 19515–19520 (2009).
117. Munita, J. M. and Arias, C. A., Mechanisms of Antibiotic Resistance. *Microbiol Spectr* **4**, (2016).
118. Ruiz, J., Etymologia: TEM. *Emerg. Infect. Dis.* **24**, 709-709 (2018).
119. Palzkill, T., Structural and Mechanistic Basis for Extended-Spectrum Drug-Resistance Mutations in Altering the Specificity of TEM, CTX-M, and KPC beta-lactamases. *Front Mol Biosci* **5**, 16 (2018).
120. Gomes, L., Monteiro, G. and Mergulhao, F., The Impact of IPTG Induction on Plasmid Stability and Heterologous Protein Expression by Escherichia coli Biofilms. *Int J Mol Sci* **21**, (2020).
121. Sanders, E. R., Aseptic laboratory techniques: plating methods. *J Vis Exp*, e3064 (2012).
122. Wei, Y., Wang, X., Liu, J., et al., The population dynamics of bacteria in physically structured habitats and the adaptive virtue of random motility. *Proc Natl Acad Sci U S A* **108**, 4047-52 (2011).
123. Mitchell, J. G. and Kogure, K., Bacterial motility: links to the environment and a driving force for microbial physics. *FEMS Microbiol Ecol* **55**, 3-16 (2006).
124. Wolfe, A. J. and Berg, H. C., Migration of bacteria in semisolid agar. *Proc. NatI. Acad. Sci. USA* **86**, 6973-6977 (1989).
125. Sezonov, G., Joseleau-Petit, D. and D'Ari, R., Escherichia coli physiology in Luria-Bertani broth. *J Bacteriol* **189**, 8746-9 (2007).
126. Dan, Y., Detecting microorganism growth with microfluidic resonance detector. *Master's thesis, TU Dresden*, (2012).
127. Lichtman, J. W. and Conchello, J. A., Fluorescence microscopy. *Nat Methods* **2**, 910-9 (2005).
128. Szymula, K. P., Magaraci, M. S., Patterson, M., et al., An Open-Source Plate Reader. *Biochemistry* **58**, 468-473 (2019).
129. McKinnon, K. M., Flow Cytometry: An Overview. *Curr Protoc Immunol* **120**, 5 1 1-5 1 11 (2018).
130. Renggli, S., Keck, W., Jenal, U., et al., Role of autofluorescence in flow cytometric analysis of Escherichia coli treated with bactericidal antibiotics. *J Bacteriol* **195**, 4067-73 (2013).
131. Bari, M. L. and Yeasmin, S., Microbes Culture Methods. In *Reference Module in Biomedical Sciences*, Elsevier: 2021.
132. Edoo, Z., Arthur, M. and Hugonnet, J. E., Reversible inactivation of a peptidoglycan transpeptidase by a beta-lactam antibiotic mediated by beta-lactam-ring recyclization in the enzyme active site. *Sci Rep* **7**, 9136 (2017).
133. Diene, S. M., Pinault, L., Keshri, V., et al., Human metallo-β-lactamase enzymes degrade

penicillin. *Scientific Reports* **9**, 12173 (2019).
134. Illing, R., Development of a Fluorescent Droplet Analyser for microbiological studies. *Doctoral thesis, TU Dresden*, (2018).
135. Zhao, X., Illing, R., Ruelens, P., et al., Coexistence of fluorescent Escherichia coli strains in millifluidic droplet reactors. *Lab Chip* **21**, 1492-1502 (2021).
136. Huang, L., Optimization of a new mathematical model for bacterial growth. *Food Control* **32**, 283-288 (2013).
137. Zwietering, M. H., Rombouts, F. M. and van 't Riet, K., Comparison of definitions of the lag phase and the exponential phase in bacterial growth. *J. Appl. Bacteriol.* **72**, 139-145 (1992).
138. McAnaney, T. B., Zeng, W., Doe, C. F. E., et al., Protonation, Photobleaching, and Photoactivation of Yellow Fluorescent Protein (YFP 10C): A Unifying Mechanism. *Biochemistry* **44**, 5510-5524 (2005).
139. Karpova, T. S., Baumann, C. T., He, L., et al., Fluorescence resonance energy transfer from cyan to yellow fluorescent protein detected by acceptor photobleaching using confocal microscopy and a single laser. *J. Microsc.* **209**, 56–70 (2003).
140. Yu, Y.-J., Amorim, M., Marques, C., et al., Effects of whey peptide extract on the growth of probiotics and gut microbiota. *Journal of Functional Foods* **21**, 507-516 (2016).
141. Zhang, X., Jiang, X., Yang, Q., et al., Online Monitoring of Bacterial Growth with an Electrical Sensor. *Anal Chem* **90**, 6006-6011 (2018).
142. Russell, J. B., Sharp, W. M. and Baldwin, R. L., The Effect of PH on Maximum Bacterial Growth Rate and its Possible Role as a Determinant of Bacterial Competition in the Rumen. *J Anim Sci.* **48**, 251–255 (1979).
143. Cotter, P. D. and Hill, C., Surviving the acid test: responses of gram-positive bacteria to low pH. *Microbiol Mol Biol Rev* **67**, 429-53, table of contents (2003).
144. Henderson, J. N., Ai, H.-W., Campbell, R. E., et al., Structural basis for reversible photobleaching of a green fluorescent protein homologue. *Proc. Natl. Acad. Sci. U.S.A.* **104**, 6672-6677 (2007).
145. Jach, G. a. W., Jochen, Focus on Fluorescent Proteins. In *Studies in Natural Products Chemistry*, Atta-ur-Rahman, Ed. Elsevier: Germany, 2006; Vol. 33, pp 3-67.
146. Cranfill, P. J., Sell, B. R., Baird, M. A., et al., Quantitative assessment of fluorescent proteins. *Nat Methods* **13**, 557-62 (2016).
147. Spectroscopic Imaging. In *Chemical Imaging Analysis*, Adams Freddy, B. C., Ed. Elsevier: 2015; Vol. 69, pp 339-384.
148. Hall, B. G., Acar, H., Nandipati, A., et al., Growth Rates Made Easy. *Mol. Biol. Evol.* **31**, 232-238 (2013).
149. Powell, E. O., Growth Rate and Generation Time of Bacteria, with Special Reference to Continuous Culture *J. gen. Microbial* **15**, 492-511 (1956).
150. Gullberg, E., Albrecht, L. M., Karlsson, C., et al., Selection of a multidrug resistance plasmid by sublethal levels of antibiotics and heavy metals. *mBio* **5**, e01918-14 (2014).
151. Juergensmeyer, M. A., Nelson, E. S. and Juergensmeyer, E. A., Shaking alone, without concurrent aeration, affects the growth characteristics of Escherichia coli. *Lett Appl Microbiol* **45**, 179-83 (2007).
152. Rama, Y., Dellus-Gura, E., Bibid, M., et al., Predicting microbial growth in a mixed culture from growth curve data. *Proc. Natl. Acad. Sci. U.S.A.* **117**, 13848 (2020).
153. Levin, B. R., Stewart, F. M. and Chao, L., Resource-Limited Growth, Competition, and Predation: A Model and Experimental Studies with Bacteria and Bacteriophage. *Am. Nat.* **111**, 3-24 (1977).
154. Concepcion-Acevedo, J., Weiss, H. N., Chaudhry, W. N., et al., Malthusian Parameters as Estimators of the Fitness of Microbes: A Cautionary Tale about the Low Side of High Throughput. *PLoS One* **10**, e0126915 (2015).
155. von Bronk, B., Schaffer, S. A., Gotz, A., et al., Effects of stochasticity and division of labor in toxin production on two-strain bacterial competition in Escherichia coli. *PLoS Biol* **15**, e2001457 (2017).
156. McKane, A. J. and Newman, T. J., Stochastic models in population biology and their deterministic analogs. *Phys Rev E Stat Nonlin Soft Matter Phys* **70**, 041902 (2004).
157. Andersson, D. I. and Hughes, D., Antibiotic resistance and its cost: is it possible to reverse resistance? *Nat Rev Microbiol* **8**, 260-71 (2010).

158. Gjonbalaj, M., Keith, J. W., Do, M. H., et al., Antibiotic Degradation by Commensal Microbes Shields Pathogens. *Infect Immun* **88**, (2020).
159. Most. Umme Bushra, N. A., Md. Rajib Hassan ,Atikul Islam, Md. Radwan Hossain, Development and Validation of a Simple UV Spectrophotometric Method for the Determination of Cefotaxime Sodium in Bulk And Pharmaceutical Formulation. *IOSR J. Pharm.* **4**, 74-77 (2014).
160. Zahir, T., Wilmaerts, D., Franke, S., et al., Image-Based Dynamic Phenotyping Reveals Genetic Determinants of Filamentation-Mediated beta-Lactam Tolerance. *Front Microbiol* **11**, 374 (2020).

References

Appendix

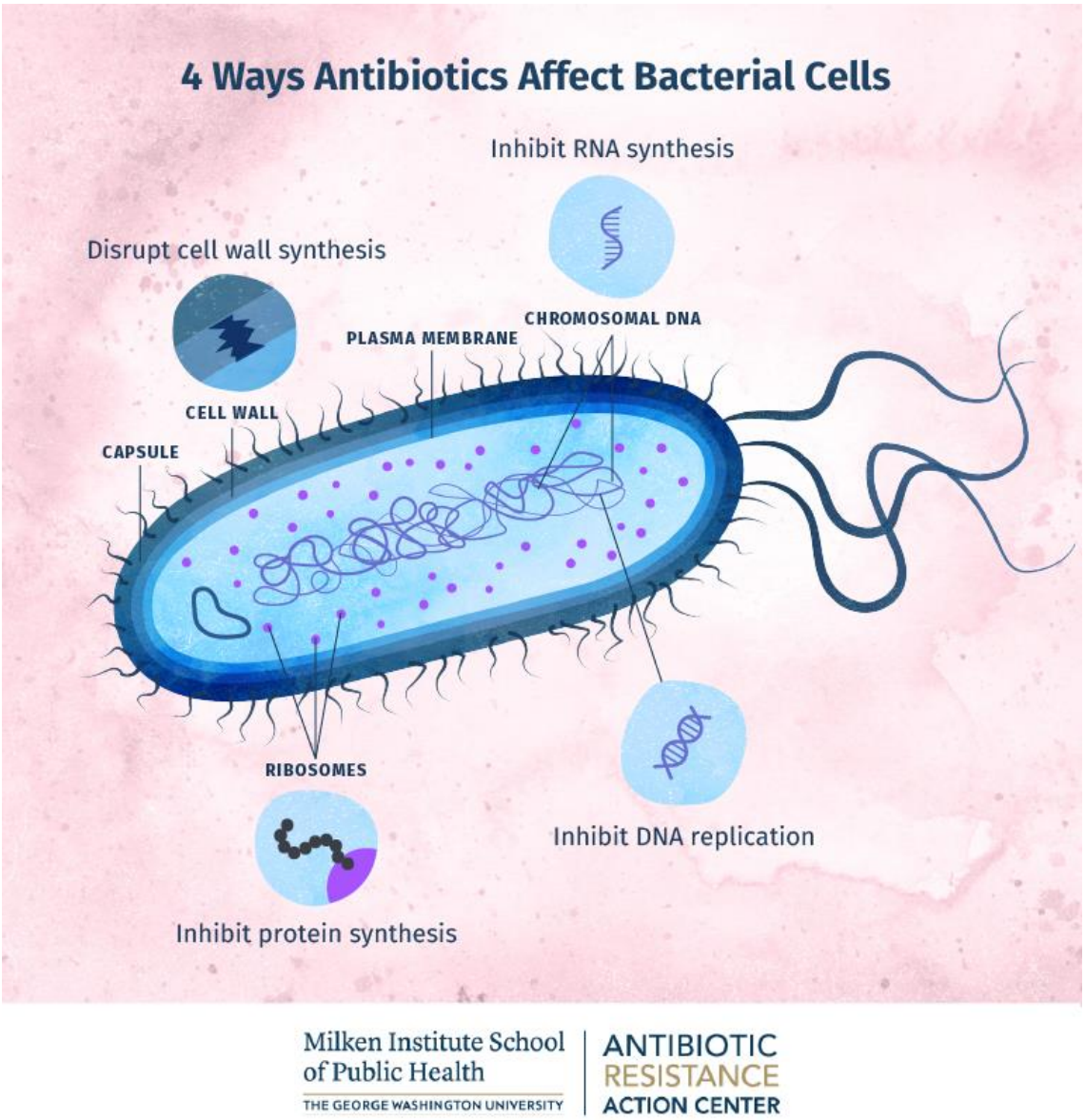

Figure S1: Four ways antibiotics affect bacterial cells: Disrupt cell wall synthesis; Inhibit RNA synthesis; Inhibit protein synthesis; Inhibit DNA replication. Picture produced by Milken Institute School of Public Health, The George Washington University, Antibiotic Resistance Action Center, 2017.

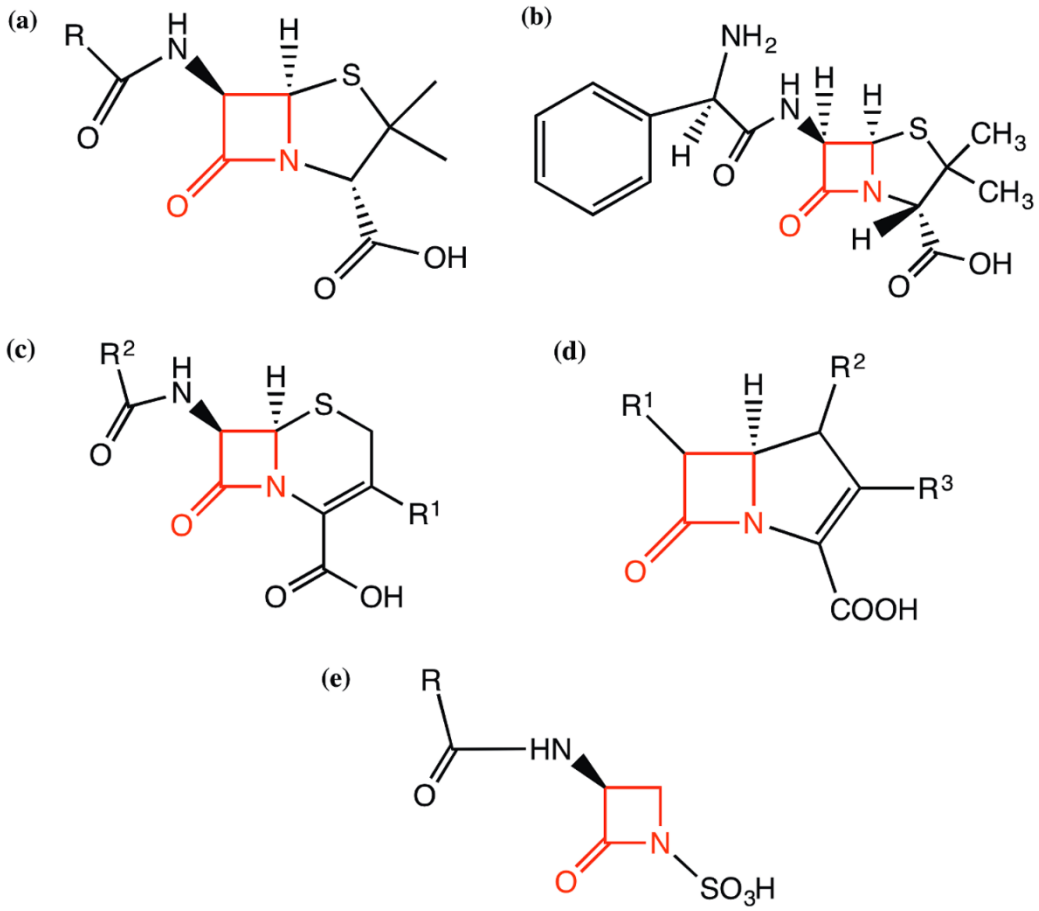

Figure S2: Chemical structures of some β-lactam antibiotics: (a) core structure of penicillins, (b) structure of ampicillin, a broad-spectrum antibiotic in the penicillin group of antibiotics, (c) core structure of cephalosporins, (d) core structure of carbapenems and (e) core structure of monobactams. The β-lactam ring is highlighted in red in all the antibiotics. Picture and description is from Ref[100].

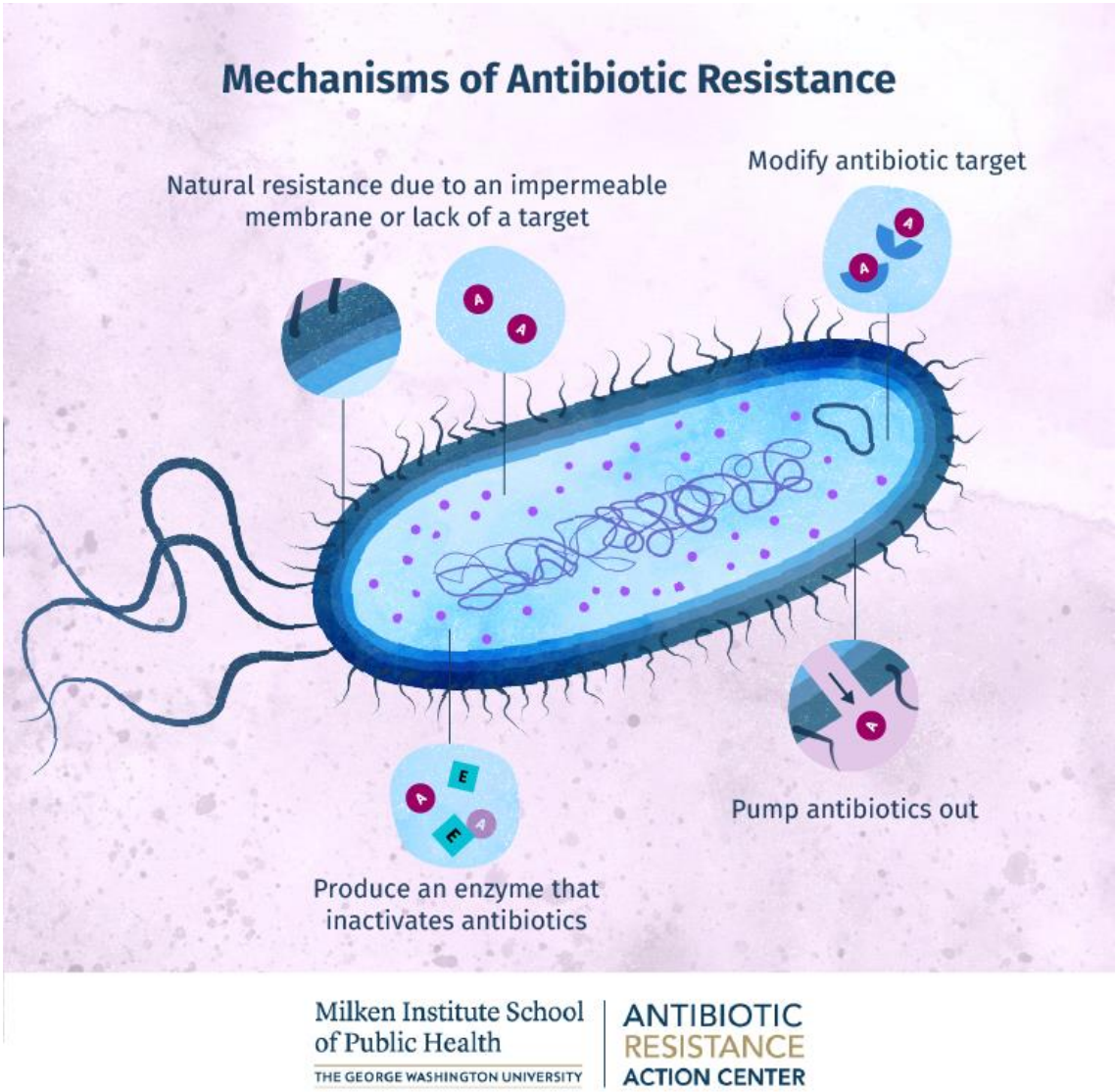

Figure S3: Mechanisms of antibiotic resistance: Natural resistance due to an impermeable membrane or lack of a target; Modify antibiotic target; Produce an enzyme that inactivates antibiotics; Pump antibiotics out. Picture produced by Milken Institute School of Public Health, The George Washington University, Antibiotic Resistance Action Center, 2017.

The total price for the whole system of the millifluidic device is estimated to be 10000 Euros. The items used for assembling the device, their amount, prices, and suppliers are summarized and listed in **Table 17**.

Table 17: Summary of items and their price of the millifluidic device.

Part	Item	amount	total	company
heater	Temperature Sensors / Thermocouples	1	11.81	Allied
	Enclosure Heater	1	66.74	RS
	Thermostat	1	128.93	RS
Spectrometer	CCS100, 350 nm-700 nm	1	1.961.39	Thorlabs
	Core fiber, BFL200HS02	1	257.85	Thorlabs
Fluorescence detector	NI DAQ USB 6002	1	400.50	National Instrument
	Power Supply RoHS conform	1	1227.27	HAMAMASTU
	Photosensor module	1	775.64	HAMAMASTU
Power supply	3-way DC laboratory power supplies	1	418.29	Meilhaus Electronic GmbH
Fluidic	Tubing (FEP), 1.6 mm x 0.5 mm x 10 m	1	229.00	dolomite
	T-connector	3	216.00	
	X-junction	1	72.00	
	2-way in-line valve	2	194.00	
	Tubing connector	5	55.00	
filter switcher	Motorized Filter Flip Mount	1	640.35	Thorlabs
	Lens Mount with Retaining Ring	2	28.52	Thorlabs
Relay card	Relay card	1	58.70	Robotshop
Plug	Plug-in power supply, 12 V / DC	2	15.98	Conrad
	Power connection cable black 1.50 m	2	7.58	Conrad
Light sources, fiber, and filters	Slip Ring, SM1 Lens Tubes	1	22.82	Thorlabs
	SM1 Lens Tube	3	36.33	
	Post-Mountable Ø3.2 mm Ferrule Clamp	1	21.83	
	1x2 Multimode Fiber Optic Coupler	1	312.21	
	Cyan light, 505 nm	1	269.52	
	UV light, 385 nm	1	419.04	
	BFP Excitation Filter, 390 nm (± 18 nm)	1	234.10	

	YFP Excitation Filter, 497 nm (± 16 nm)	1	234.10	
	BFP Emission Filter, 460 nm (± 60 nm)	2	468.20	
	YFP Emission Filter, 535 nm (± 22 nm)	2	468.20	
Objective lens	Objective A-Plan 20x	1	274.89	Zeiss
Post and holder	Ø12.7 mm Pedestal, 34.7 mm	6	135.72	Thorlabs
	Mounting Base, 50 mm x 75 mm x 10 mm	1	6.84	
	Ø12.7 mm Optical Post, L = 20 mm	3	13.32	
	Ø12.7 mm Optical Post, L = 50 mm	2	9.72	
	Ø12.7 mm Optical Post, L = 75 mm	3	15.21	
	SM1-Threaded 30 mm Cage Plate	3	46.05	
	Clamping Fork	2	101.18	
Black box	XE25 25 mm Construction Rails	8	126.64	
	XE25 25 mm Construction Rails	4	59.00	
	Counterbored Construction Rails	12	228.96	
	Breadboard Lifting Handles	1	14.36	
	Hinge for 25 mm Rail Enclosures	2	20.48	
	Lid Stop for 25 mm Rail Enclosures	2	14.28	
	Black Hardboard, 610 mm x 610 mm	1	62.92	
	Aluminum Breadboard, 30 cm x 30 cm	1	145.62	
Others	luster terminal flexible	3	4.56	Conrad
	electricity wire	1	23.41	
	Connectors 15-pin	1	7.44	
	Tubing cutter	1	26.00	dolomite
		Total price		**10588.50**